AD-A031 010 TRW SYSTEMS GROUP REDONDO BEACH CALIF F/G 20/5
ADVANCED LASER CONCEPTS.(U)
JUL 76 J A BETTS, J F FRIICHTENICHT F29601-73-A-0036
UNCLASSIFIED AFWL-TR-75-289 NL

1 OF 2
ADA031010

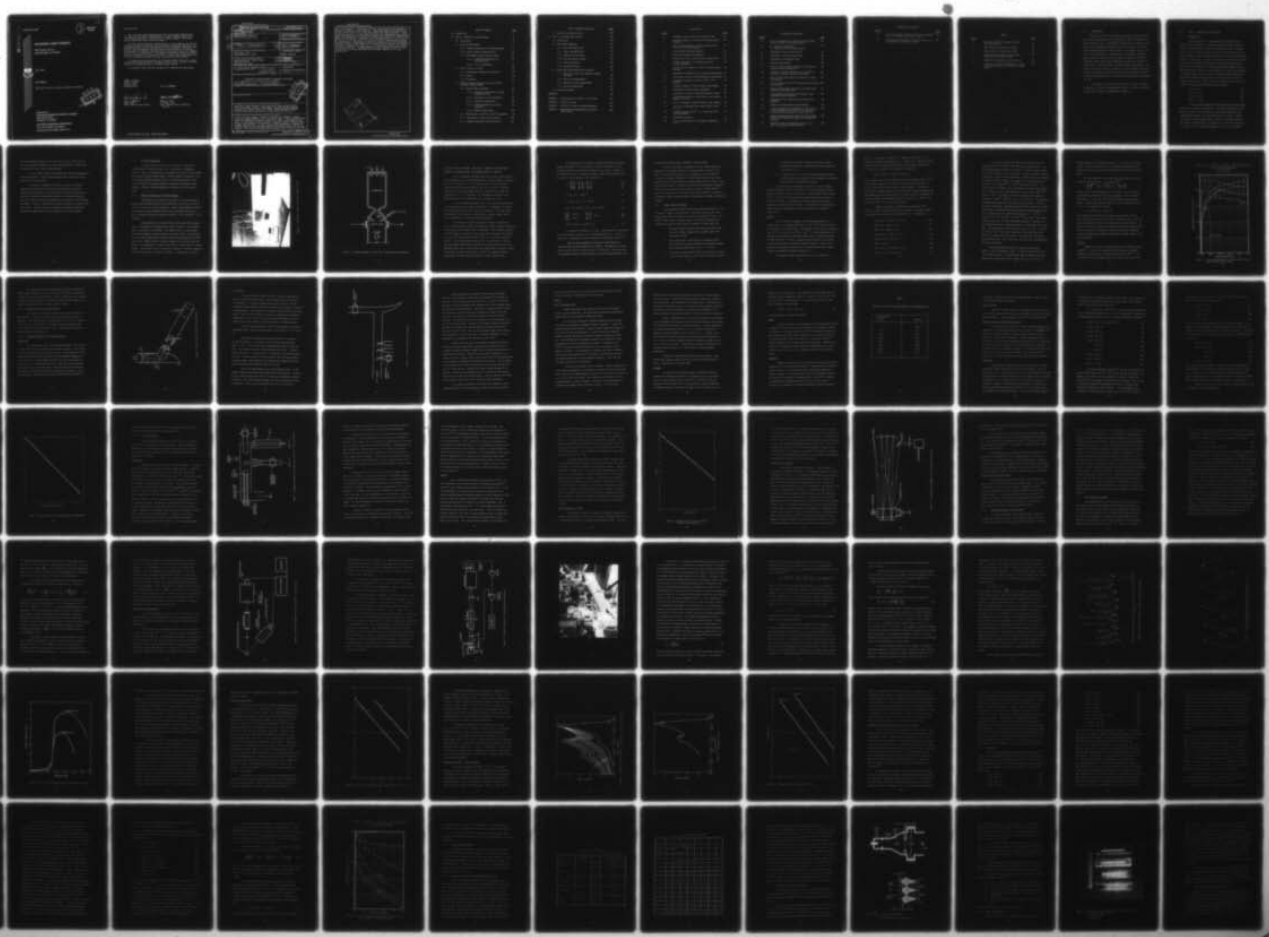

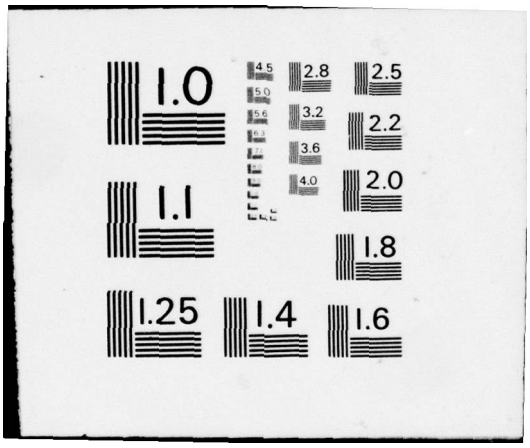
1.0
1.1
1.25
1.4
1.6
1.8
2.0
2.2
2.5
2.8
3.2
3.6
4.0
4.5
5.0
5.6

AFWL-TR-75-289

ADVANCED LASER CONCEPTS

TRW Systems Group
Redondo Beach, CA 90278

July 1976

Final Report

Approved for public release; distribution unlimited.

Prepared for
ADVANCED RESEARCH PROJECTS AGENCY
1400 Wilson Blvd.
Arlington, VA 22209

AIR FORCE WEAPONS LABORATORY
Air Force Systems Command
Kirtland Air Force Base, NM 87117

AFWL-TR-75-289

This final report was prepared by the TRW Systems Group, Redondo Beach, CA, under Contract 729601-73-A-0036-0001, Job Order 12560302, with the Air Force Weapons Laboratory, Kirtland AFB, NM. Captain Steven J. Davis (ALC) was the Laboratory Project Officer-in-Charge.

When US Government drawings, specifications, or other data are used for any purpose other than a definitely related Government procurement operation, the Government thereby incurs no responsibility nor any obligation whatsoever, and the fact that the Government may have formulated, furnished, or in any way supplied the said drawings, specifications, or other data is not to be regarded by implication or otherwise as in any manner licensing the holder or any other person or corporation or conveying any rights or permission to manufacture, use, or sell any patented invention that may in any way be related thereto.

This report has been reviewed by the Information Office (OI) and is releasable to the National Technical Information Service (NTIS). At NTIS, it will be available to the general public, including foreign nations.

This technical report has been reviewed and is approved for publication.

Steven J. Davis
STEVEN J. DAVIS
Captain, USAF
Project Officer

FOR THE COMMANDER

Carl A. Forbrich
CARL A. FORBRICH
Major, USAF
Chief, Chemical Laser Branch

Armand D. Maio
ARMAND D. MAIO
Lt Colonel, USAF
Chief, Advanced Laser Technology Division

DO NOT RETURN THIS COPY. RETAIN OR DESTROY.

UNCLASSIFIED

SECURITY CLASSIFICATION OF THIS PAGE *(When Data Entered)*

(19) REPORT DOCUMENTATION PAGE		READ INSTRUCTIONS BEFORE COMPLETING FORM
1. REPORT NUMBER (18) AFWL-TR-75-289	2. GOVT ACCESSION NO.	3. RECIPIENT'S CATALOG NUMBER
4. TITLE *(and Subtitle)* (6) ADVANCED LASER CONCEPTS.		5. TYPE OF REPORT & PERIOD COVERED (9) Final Report.
		6. PERFORMING ORG. REPORT NUMBER
7. AUTHOR(s) (10) J. A. Betts J. F. Friichtenicht		8. CONTRACT OR GRANT NUMBER(s) (15) F29601-73-A-0036-0001
9. PERFORMING ORGANIZATION NAME AND ADDRESS TRW Systems Group Redondo Beach, CA 90278		10. PROGRAM ELEMENT, PROJECT, TASK AREA & WORK UNIT NUMBERS 62301E; 12560302
11. CONTROLLING OFFICE NAME AND ADDRESS Advanced Research Projects Agency 1400 Wilson Blvd Arlington, VA 22209		(11) 12. REPORT DATE July 1976
		13. NUMBER OF PAGES 186
14. MONITORING AGENCY NAME & ADDRESS *(if different from Controlling Office)* Air Force Weapons Laboratory (ALC) Kirtland AFB, NM 87117 (12) 194 p.		15. SECURITY CLASS. *(of this report)* UNCLASSIFIED
		15a. DECLASSIFICATION/DOWNGRADING SCHEDULE

16. DISTRIBUTION STATEMENT *(of this Report)*

Approved for public release; distribution unlimited.

(16) AF-1256 (17) 125603

17. DISTRIBUTION STATEMENT *(of the abstract entered in Block 20, if different from Report)*

DDC RELEASED OCT 20 1976

18. SUPPLEMENTARY NOTES

19. KEY WORDS *(Continue on reverse side if necessary and identify by block number)*

Chemically pumped electronic state transition laser; Energy transfer; CN radicals; Atomic iodine; Interhalogens; Fluorine-hydrogen-cyanogen compound flame system; Carbon atom stream; Chemiluminescent radiation
Al; B; Ba; Ce; Co; Cr; Fe; Ge; Hv; In; Mn; Mo; Nd; Ni; Sm; Sn; Ti

20. ABSTRACT *(Continue on reverse side if necessary and identify by block number)*

In the first task element, research is described on attempts to produce chemically pumped electronic state transition lasers. Energy transfer experiments from metastable electronic states of NF, which can be produced chemically, to the potential lasing species CN radicals, atomic iodine and interhalogens were performed. In the course of these experiments, a method for chemical production of high number densities of the $A^2\Pi$ state of CN was discovered. This fluorine-hydrogen-cyanogen compound flame system has consider-

DD FORM 1 JAN 73 1473 EDITION OF 1 NOV 65 IS OBSOLETE

UNCLASSIFIED 354 595

SECURITY CLASSIFICATION OF THIS PAGE *(When Data Entered)*

LB

able laser potential. Experiments utilizing energy transfer from metastable states of CO and CS are also described. These experiments were limited by the ability to efficiently mix a carbon atom stream with other reactants. In the second task element, a crossed atomic-molecular beam apparatus has been used to study the characteristics of reactions leading to the formation of chemiexcited metal, oxide molecules. Experiments were conducted with Al, B. Ba, Ce, Co, Cr, Fe, Ge, Hv, In, Mn, Mo, Nd, Ni, Sm, Sn, and Ti atoms interacting with N_2O and NO_2 target gases. Measurements included the intensity of the chemiluminescent radiation relative to the intensity of the metal atom beam pulse, the radiative lifetime of chemiexcited states, and on a limited basis, spectra of the chemiluminescent radiation. The measurements have been combined to yield a figure of merit for the various reactions which provides a measure of the total photon yield.

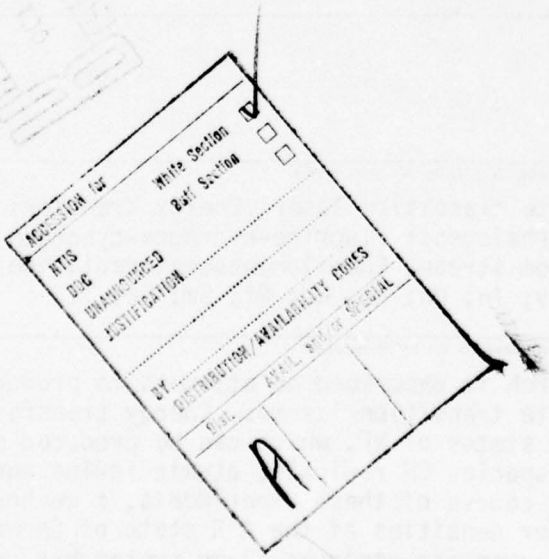

TABLE OF CONTENTS

TABLE OF CONTENTS (Continued)

ILLUSTRATIONS

ILLUSTRATIONS (Continued)

ILLUSTRATIONS (Continued)

TABLES

1.0 INTRODUCTION

The major goal of the Advanced Laser Concepts contract is directed towards the understanding and development of chemically pumped electronic transition lasers. The program is divided into two separate tasks which use two approaches towards achieving the common goal. The first task is entitled Chemistry of Excited States. The approach used for this task is the investigation of the possibility of producing a chemically pumped visible or ultraviolet laser by means of chemically producing a metastable excited species which subsequently transfers its energy to a lasing species. The second task is entitled Molecular Beam Studies. The approach used in this task is to explore and screen a number of species as potential candidates for chemically pumped electronic transition lasers. The central experimental tool is a pulsed, high flux molecular beam apparatus.

This report is divided into two sections. Section 2 contains a description of technical accomplishments of Task I. Section 3 contains a description of technical accomplishments of Task II.

2.0 TASK I. CHEMISTRY OF EXCITED STATES

2.1 Introduction

The major objective of this program was to perform studies leading to the development of a chemically pumped electronic transition laser. The major difficulty posed in meeting this objective is finding either a specific chemical reaction or series of reactions that will selectively produce a given electronically excited state which has properties conducive to laser gain. To date, there has been a notable lack of success in the scientific community in finding a single chemical reaction that meets all the requirements for a successful chemically pumped electronic state laser system. The aim of this program was to avoid being restricted to a single chemical reaction by using an alternate approach which would separate the pumping and lasing steps. The approach used involves an energy transfer scheme. The way in which this scheme works can be illustrated by considering the following reaction sequence:

$$A + B \rightarrow C^* + D \quad (1)$$

$$A + B \rightarrow C + D \quad (2)$$

$$C^* + X \rightarrow C + X^* \quad (3)$$

$$X^* + h\nu \rightarrow X + 2h\nu \quad (4)$$

In this reaction sequence, an electronically excited metastable species C* is produced in reaction (1). The major requirements for this species are that it can be produced in large number densities by some chemical means and that it be long-lived enough to be able to transfer its energy to another molecule before losing it by radiative processes. The species C* then transfers its energy to the laser atom or molecule X via reaction (3). The desirable properties for X are (1) a radiative

2.0 TASK I. CHEMISTRY OF EXCITED STATES

2.1 Introduction

The major objective of this program was to perform studies leading to the development of a chemically pumped electronic transition laser. The major difficulty posed in meeting this objective is finding either a specific chemical reaction or series of reactions that will selectively produce a given electronically excited state which has properties conducive to laser gain. To date, there has been a notable lack of success in the scientific community in finding a single chemical reaction that meets all the requirements for a successful chemically pumped electronic state laser system. The aim of this program was to avoid being restricted to a single chemical reaction by using an alternate approach which would separate the pumping and lasing steps. The approach used involves an energy transfer scheme. The way in which this scheme works can be illustrated by considering the following reaction sequence:

$$A + B \rightarrow C^* + D \quad (1)$$

$$A + B \rightarrow C + D \quad (2)$$

$$C^* + X \rightarrow C + X^* \quad (3)$$

$$X^* + h\nu \rightarrow X + 2h\nu \quad (4)$$

In this reaction sequence, an electronically excited metastable species C* is produced in reaction (1). The major requirements for this species are that it can be produced in large number densities by some chemical means and that it be long-lived enough to be able to transfer its energy to another molecule before losing it by radiative processes. The species C* then transfers its energy to the laser atom or molecule X via reaction (3). The desirable properties for X are (1) a radiative

lifetime commensurate with laser requirements, (2) an energy level in near resonance with that of the donor molecule C*, (3) slow collisional quenching, (4) it has either a 3-level system or a system with displaced potential energy curves so the lower lasing level is not the ground state of X and (5) it is a species that is either stable or easily produced so it can be mixed with the metastable.

The metastable species studied in this program were NF in its $b^1\Sigma^+$ and $a^1\Delta$ states and CO and CS in their $a^3\Pi$ states. The $b^1\Sigma^+$ and $a^1\Delta$ states of NF have energies of 2.42 and 1.5 eV and have lifetimes longer than 0.1 sec. They have been shown to be produced in reasonable number densities in a combustion system with NF_3 and hydrogen-containing compounds. The most suitable acceptor molecule for the $a^1\Delta$ state of NF is the $A^2\Pi$ state of CN. Experiments were performed to demonstrate the transfer from NF($a^1\Delta$) to CN($A^2\Pi$). In the course of these experiments, additional methods of forming large number densities of the $A^2\Pi$ state of CN were discovered. Since this state of CN is a promising laser candidate, this discovery was an added bonus for the program. Acceptor molecules for the $b^1\Sigma^+$ state of NF are various halogen and interhalogen species, Cl_2 and ClF being the most promising. Experiments designed to demonstrate transfer to these acceptors were also performed.

The $a^3\Pi$ state of CO has an energy of 6.02 eV and a radiative lifetime of 7 msec whereas the $a^3\Pi$ state of CS has an energy of 3.42 eV and a radiative lifetime of the order of a millisecond. Both species are produced in carbon atom reactions; the $a^3\Pi$ state of CO being produced from the reaction of carbon atoms with oxygen and the $a^3\Pi$ state of CS being produced from the reaction of carbon atoms with carbonyl sulfide.

The most promising acceptor for the $a^3\Pi$ state of CO is the $B^2\Pi$ state of NO. Arc experiments designed to produce large densities of carbon atoms to allow use of these reactions are described.

For all systems studied, experiments were backed with appropriate theoretical analysis. Several simple computer codes were developed and used to aid in this analysis.

The report is organized as follows: Section 2.2 describes studies of the production of the NF excited states and also study of transfer from these states to excited states of potential lasing species. Section 2.3 describes the chemical production of high number densities of the $A^2\Pi$ state of CN which was discovered in the course of the NF system experiment. Section 2.4 describes the studies involving the excited states of CO and CS. Finally, section 2.5 summarizes conclusions reached and discusses the implication of these conclusions for further research.

2.2 NF System Experiments

The following section presents a discussion of experiments involving the $b^1\Sigma^+$ and $a^1\Delta$ states of NF. The section is arranged as follows. First, is a description of experiments in which NF excited species were formed by purely chemical means. Second, follows a discussion of possible energy transfer acceptors for the NF excited state energy. Third, is a description of flowtube experiments designed to demonstrate energy transfer. Finally, a general appraisal of prospects for this system is given.

2.2.1 Chemical Production of NF Excited Species

The experiment that motivated the study of NF excited species as energy transfer donors was an HF laser experiment in which NF_3 was used as a fuel in place of F_2 in the precombustor. Bright chemiluminescent emission was observed in these experiments which spectral analysis showed to be due to nitrogen first positive emission and $NF(a^1\Delta - X^3\Sigma)$ and $NF(b^1\Sigma^+ - X^3\Sigma)$ emissions.

The experiments were conducted using a small scale HF/DF chemical laser. A photograph of the apparatus is shown in Figure 1. Two different lasers were used in the experiment. The smallest has a 3 cm gain length which allows operation using relatively low reactant flows. The larger one has a 30 cm gain length and can produce 100 watts of continuous wave, HF/DF laser power. Figure 2 shows a schematic diagram of the various laser components. The precombustor is used to burn fuels to produce atomic or radical species. The effluent from the precombustor undergoes a supersonic expansion and is then mixed with an additional reactant. A simple side on injector

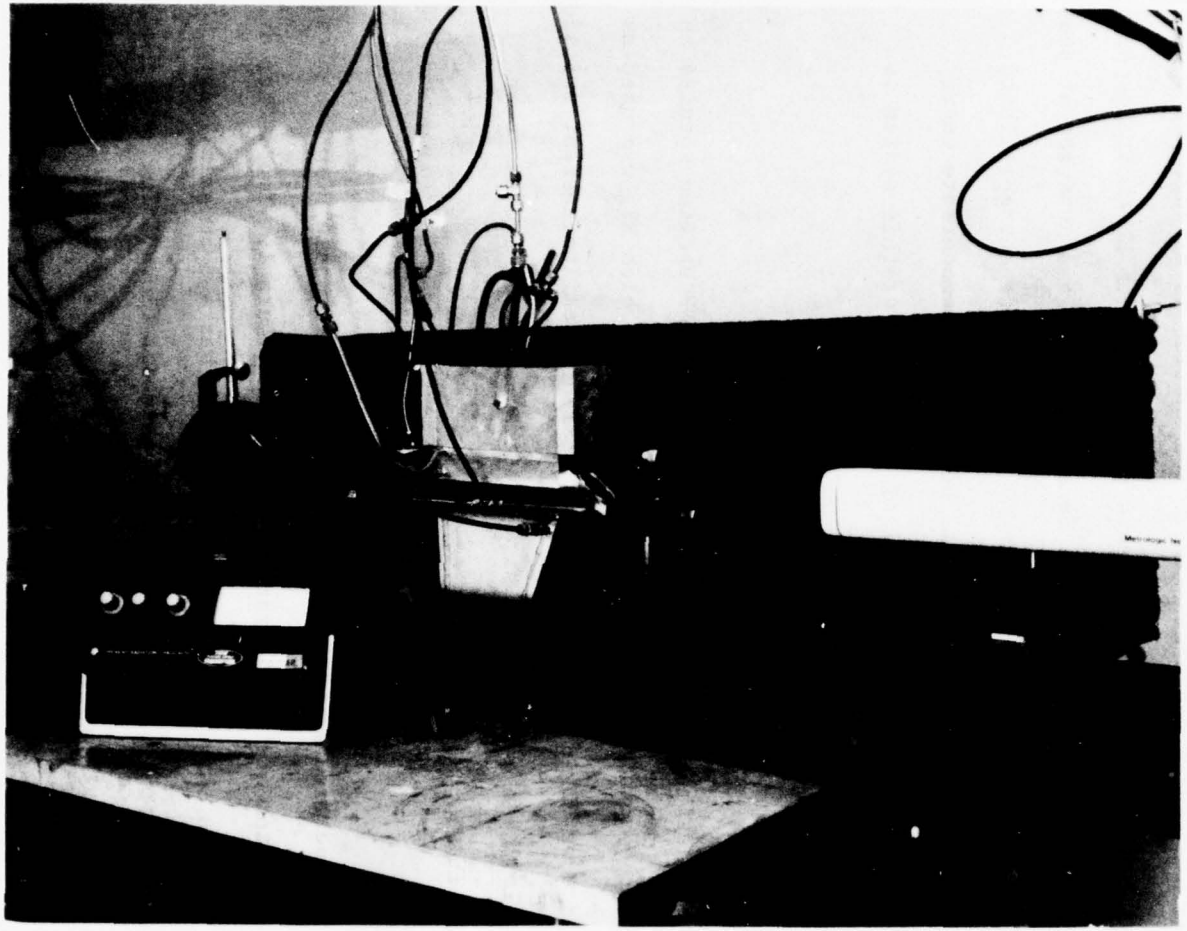

Figure 1. Photograph of small scale HF/DF chemical laser.

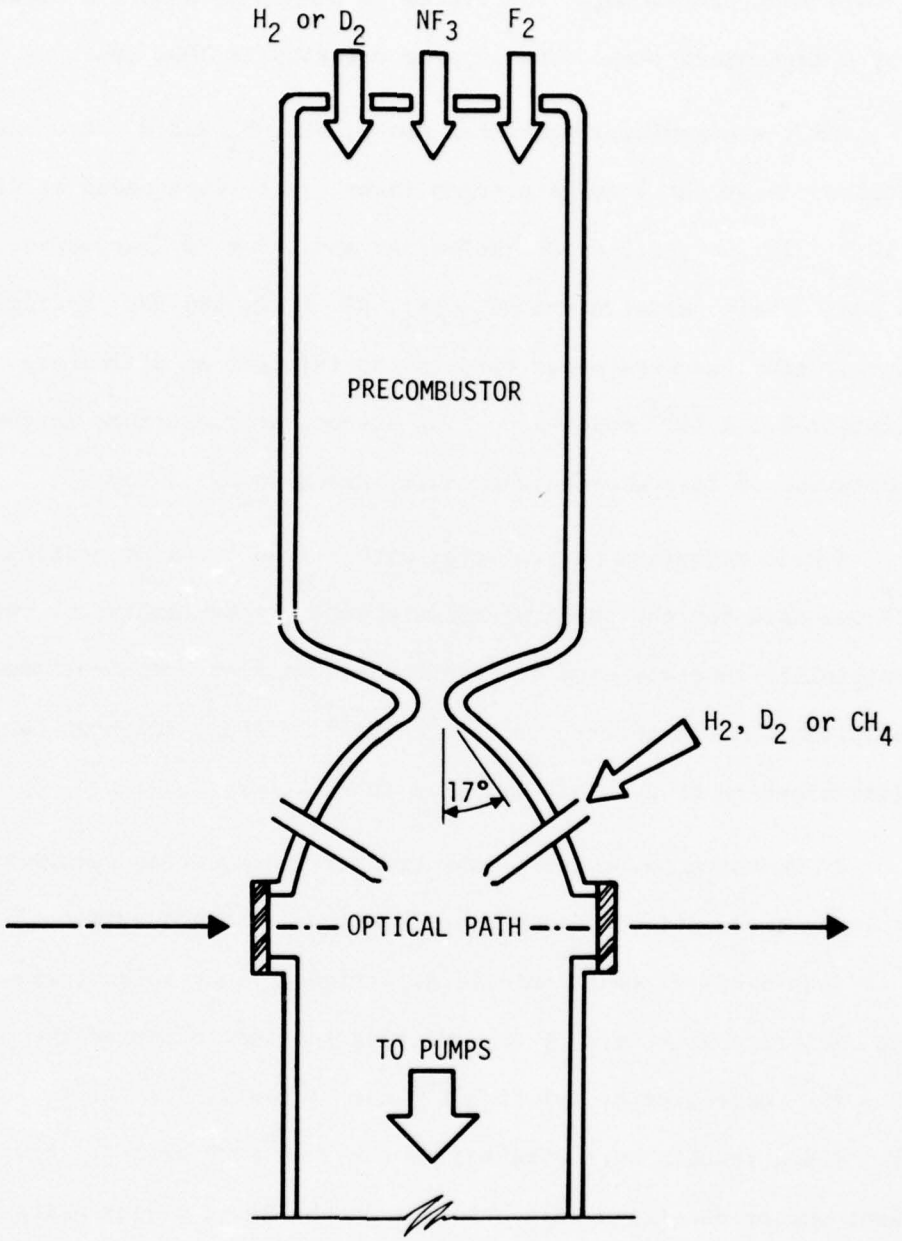

Figure 2. Schematic diagram of laser device showing various components.

is used to effect the mixing. The system is pumped by a Root's blower backed by a mechanical pump. The pumping capacity is 3000 cfm.

For the experiment described above, NF_3, F_2, and H_2 were burned in the precombustor of the 3 cm gainlength laser. They were added at flowrates of 2×10^{-3} moles/sec, 1.5×10^{-3} moles/sec and 1.2×10^{-3} moles/sec. Species most likely produced are NF_3, NF_2, NF, N, F, and HF. Hydrogen, deuterium or ethylene were added through the injector at a flowrate of approximately 0.5×10^{-3} moles/sec. The precombustor pressure in these experiments was 18 torr whereas the cavity pressure was 3 torr.

A 0.3m McPherson spectrometer with a 1200 lines/mm grating blazed at 7500Å was used for the spectral measurements. A Hammamatsu S1 response phototmultiplier tube was used to detect the radiation. The spectrometer-photomuliplier tube setup were calibrated with an Epply filament lamp to allow determination of absolute emission intensities.

By scanning the emission spectrum of the laser and analyzing the resulting intensities using the calibration, absolute emission intensities in the various bands present could be determined. Such an analysis combined with the radiative lifetimes of the emitting species indicated the presence of $\sim 1.5 \times 10^{13}$ molecules/cm^3 of $NF(b^1\Sigma^+)$ and $\sim 4.4 \times 10^{11}$ molecules/cm^3 of $N_2(B^3\Pi)$. These results were obtained in the 3 cm path device. However, equivalent number densities were obtained in the 30 cm device using correspondingly higher flows. When ethylene was added through the nozzle in place of hydrogen, only green emission due to $NF(b^1\Sigma^+)$ is observed visually. Spectroscopic analysis shows the presence of $NF(a^1\Delta)$ emission also.

The emissions can be accounted for using a mechanism proposed by Herbelin and Cohen[1] for an experiment in which the effluent of an RF discharge through NF_3 was mixed with either H_2, D_2, or CH_4. In order for the mechanism to apply in combustion system, F atoms and NF_2 radicals must be formed in the precombustor. The mechanism is:

$$F + \begin{Bmatrix} H_2 \\ D_2 \\ CH_4 \end{Bmatrix} \rightarrow \begin{Bmatrix} HF^{\dagger} \\ DF^{\dagger} \end{Bmatrix} + \begin{Bmatrix} H \\ D \\ CH_3 \end{Bmatrix} \quad \begin{matrix} (1a) \\ (1b) \\ (1c) \end{matrix}$$

$$X + NF_2 \rightarrow XF^{\dagger} + NF(X^3\Sigma^-) \quad (2)$$

$$X + NF_2 \rightarrow XNF_2^{*} \rightarrow XF^{\dagger} + NF(a^1\Delta) \quad (3)$$

$$HF(v \geq 2) + NF(a^1\Delta) \rightarrow HF(v - 2) + NF(b^1\Sigma^+) \quad (4)$$

$$\begin{Bmatrix} H \\ D \end{Bmatrix} + \begin{matrix} NF(X^3\Sigma^-) \\ NF(a^1\Delta) \end{matrix} \rightarrow \begin{Bmatrix} HF^{\dagger} \\ DF^{\dagger} \end{Bmatrix} + N(^2D) \quad \begin{matrix} (5a) \\ (5b) \end{matrix}$$

$$N(^2D) + NF(a^1\Delta) \rightarrow N_2(B^3\pi_g) + F \quad (6)$$

In the above, X denotes H, D or CH_3. Note that $NF(b^1\Sigma^+)$ production can be suppressed by using D_2, thus eliminating reaction (4). $N_2(B^3\pi_g)$ production is suppressed by using a hydrocarbon, eliminating reaction (5).

There was some experimental evidence that high densities of nitrogen atoms were being produced in the system. The endpoint of a nitric oxide titration came at an NO flow equal to the NF_3 flow. Also CN red and blue emissions similar to those observed in active nitrogen reactions could

be produced by adding organic compounds to the gas stream.

The above experiments illustrated a strictly chemical means for production of high number densities of excited states. The NF($a^1\Delta$) and NF($b^1\Sigma^+$) states are quite long-lived. Consequently, for these species to be laser candidates themselves, very high number densities and a long pathlength device would be needed to generate enough gain for lasing. Since these criteria cannot be achieved with the present experimental arrangement, it was felt that best use of these species would be as energy transfer donors. The remainder of this section will address itself to a discussion of potential energy transfer acceptors and experiments intended to demonstrate transfer.

2.2.2 Energy Transfer Acceptors

The preceding subsection described the chemical production of the $a^1\Delta$ and $b^1\Sigma^+$ states of the NF radical. The NF($a^1\Delta$) state is the lowest lying excited state of NF being 1.42 eV above the ground $X^3\Sigma^+$ state. The NF($b^1\Sigma^+$) state is next in energy, being 2.41 eV above the ground state. Criteria for selecting energy transfer acceptors for these states are:

- The chosen acceptor molecule should have an excited state lying at an energy resonant with or slightly lower than the chosen NF state.
- The excited state to which energy is transferred should have a radiative lifetime consistant with properties needed for a chemical laser species, i.e., $\tau > \sim 10$ μsec.
- The acceptor species should present the potential for either a 3-level laser system or in the case of a diatomic molecule,

the energy levels should be displaced so there are high Franck-Condon factors for transitions into other vibrational levels than v" = 0.

- The ground state of the acceptor molecule should be either a stable species or be capable of easy formation to facilitate addition into the metastable gas stream.

A scan was made of non-metallic substances for use as energy transfer acceptors for $NF(a^1\Delta)$ and $NF(b^1\Sigma^+)$. The most promising acceptor species for $NF(a^1\Delta)$ is CN in its $A^2\Pi$ state. Atomic iodine is also a possibility. For $NF(b^1\Sigma)$ the most promising acceptor species are ClF and Cl_2 in their $A^3\Pi$ states. A discussion of why these species are promising acceptors is presented in the following. A description of flowtube experiments performed to demonstrate the transfer mechanism is presented in Section 2.2.3.

$\underline{CN(A^2\Pi)}$

The $A^2\Pi$ state of CN appears a very promising candidate for a chemical laser. Its radiative lifetime of 7 μsec[2] is within the limits of feasibility for a mixing laser. Its potential energy curves are displaced (r_e for $X^2\Sigma^+$ is 1.1798; r_e for $A^2\Pi$ is 1.2332[3]). This combined with the relatively wide spacing of vibrational levels allows favorable transitions to other than the v" = 0 level. Lasing has been achieved in this species in both flash photolysis and electric discharge lasers. Finally, the CN radical can be produced relatively easily in chemical reactions as demonstrated by experiments discussed in Section 2.4.

The transfer scheme is from $NF(a^1\Delta)$ with T_o = 11439 cm^{-1} to

$CN(A^2\Pi_i, v = 0)$ with $T_o = 10021.1\ cm^{-1}$. Transfer to the $CN(A^2\Pi, v = 1)$ state is not energetically possible as $T_1 = 11808.4\ cm^{-1}$. Hence, the energy levels are close to resonant, particularly when rotational levels of the $v = 0$ level are considered. The equation for transfer is:

$$NF(a^1\Delta) + CN(X^2\Sigma^+) \rightleftarrows NF(X^3\Sigma^+) + CN(A^2\Pi_i) \tag{7}$$

Such a transfer does obey the Wigner-Witmer spin conservation rules. Spins of the various species in this scheme are the same as in the $O_2(^1\Delta)$ to $I(^2P_{3/2})$ scheme which has been shown to proceed rapidly. Therefore, on the basis of the near resonance of the transfer and the spin considerations, this transfer should proceed rapidly to the right hand size in Equation (7). The most probable lasing transition would be from the $v' = 0$ level of the $A^2\Pi$ state to the $v'' = 2$ level of the $X^2\Sigma$ state.

A kinetic calculation to determine the feasibility of the $NF(a^1\Delta)$ to $CN(A^2\Pi)$ transfer scheme can be performed. The kinetic steps to be considered are as follows for lasing on the (0 - 2) transition.

$$NF^* + CN(v = 0) \rightleftarrows CN^*\ (v = 0) + NF \tag{8}$$

$$CN^*(v = 0) \rightarrow CN(v = 2) + h\upsilon \tag{9}$$

$$CN^*(v = 0) \rightarrow CN(v \neq 2) + h\upsilon \tag{10}$$

$$CN^*(v = 0) + Q \rightarrow CN(v = 2) + Q \tag{11}$$

$$CN^*(v = 0) + Q \rightarrow CN(v \neq 0) + Q \tag{12}$$

$$NF^* + Q \rightarrow NF + Q \tag{13}$$

$$NF^* + CN(v = 2) \rightleftarrows CN^*(v = 1) + NF \tag{14}$$

$$CN(v = 2) + Q \rightarrow CN(v \neq 2) + Q \tag{15}$$

In the above equations NF* refers to the NF($a^1\Delta$) state and CN* and CN refer to the CN($A^2\Pi$) and CN($X^2\Sigma$) states respectively. Q is any quenching species present in the system. The kinetic rates in most of the above equations are not well known. In order to perform a kinetic calculation to indicate system feasibility, pertinent rates were estimated. The transfer rates k_8 and k_{14} were assumed to be of the same order as for $O_2(^1\Delta)$ to I* transfer[4] or 7×10^{-11} cm^3 $molecule^{-1}$ sec^{-1}. The reverse rates were assumed to be slow because of the large energy difference. Thus k_{-8} and k_{-14} were assumed to be of the order of 10^{-13} cm^3 $molecule^{-1}$ sec^{-1}. k_9 and k_{10} are just the inverse of the radiative lifetime of 7 μsec[2]. Thus, $k_9 = k_{10} = 1.4 \times 10^5$ sec^{-1}. The principal quenching species expected to be present are R-CN, where R is CN, H or Cl; and H_2; HF and NF_n. Quenching rates for the $A^2\Pi$ state of CN by these species were not available when these calculations were performed. However, reaction rates of CN radicals with hydrogen ($< 1 \times 10^{-13}$ cm^3 $molecule^{-1}$ sec^{-1} [5]) and CNCl (2.5×10^{-15} [5]) are slow. Also, unless quenching rates are very rapid, spontaneous emission is expected to be the dominant deexcitation mechanism because of the relatively short lifetime. For these studies, quenching rates of $k_{20} = k_{21} = k_{22} = 1 \times 10^{-12}$ cm^3 $molecule^{-1}$ sec^{-1} were used. Variation of these rates has little effect on the result of the calculation. For the present calculation k_{24} was assumed zero. This is the worst case since this step depopulates the lower lasing level.

Initial concentrations used for a model calculation were [NF*] = 1×10^{15} molecules/cm^3, [CN] = 1×10^{15} molecules/cm^3 and [Q] = 5×10^{15} molecules/cm^3. The computational results using the above rate constants and concentrations with a mixing time, t_m, of 20 μsec are

plotted in Figure 3. The difference CN*(v' = 0) - CN(v" = 2) is plotted as gain. For times shorter than t_m the calculated concentrations were multiplied by t/t_m to give average concentrations over an arbitrary gain length.

The number densities in the upper and lower states of CN can be related to the optical gain α by the equation[6]:

$$\alpha = \left(\frac{\ln 2}{\pi}\right)^{1/2} \frac{g' A}{4\pi} \frac{\lambda^2}{\Delta\nu} \left(\frac{N'_{v', J'}}{g'} - \frac{N''_{v'', J''}}{g''}\right) \qquad [1]$$

where g' and g" are the degeneracies of the levels, A is the Einstein coefficient for spontaneous emission at wavelength λ with an effective line width of $\Delta\nu$, and v and J are vibrational and rotational quantum numbers. Substituting numerical values in the above expression for the v' = 2, v" = 0 transition in CN gives

$$\alpha \approx 6 \times 10^{-16} \, (N_U - 1/2 \, N_L) \ \text{cm}^{-1}$$

This calculation indicates that a concentration difference of only 1.6×10^{12} molecules/cm^3 would be required to produce a gain of 10^{-3} cm^{-1}. Thus, high number densities are not required for lasing on CN($A^2\Pi$). The results of the kinetic calculation above indicate that the transfer mechanism could produce a concentration difference sufficient for lasing. The major problem may be pumping the lasing state rapidly enough to maintain an inversion.

$I(^2P_{1/2})$

Transfer from $O_2(a^1\Delta)$ to atomic iodine has been shown to proceed rapidly[3]. In fact, this transfer has been proposed as a promising mechanism for production of a chemically pumped iodine laser[7]. The $a^1\Delta$ state of NF is isoelectronic with the $a^1\Delta$ state of O_2 and thus may

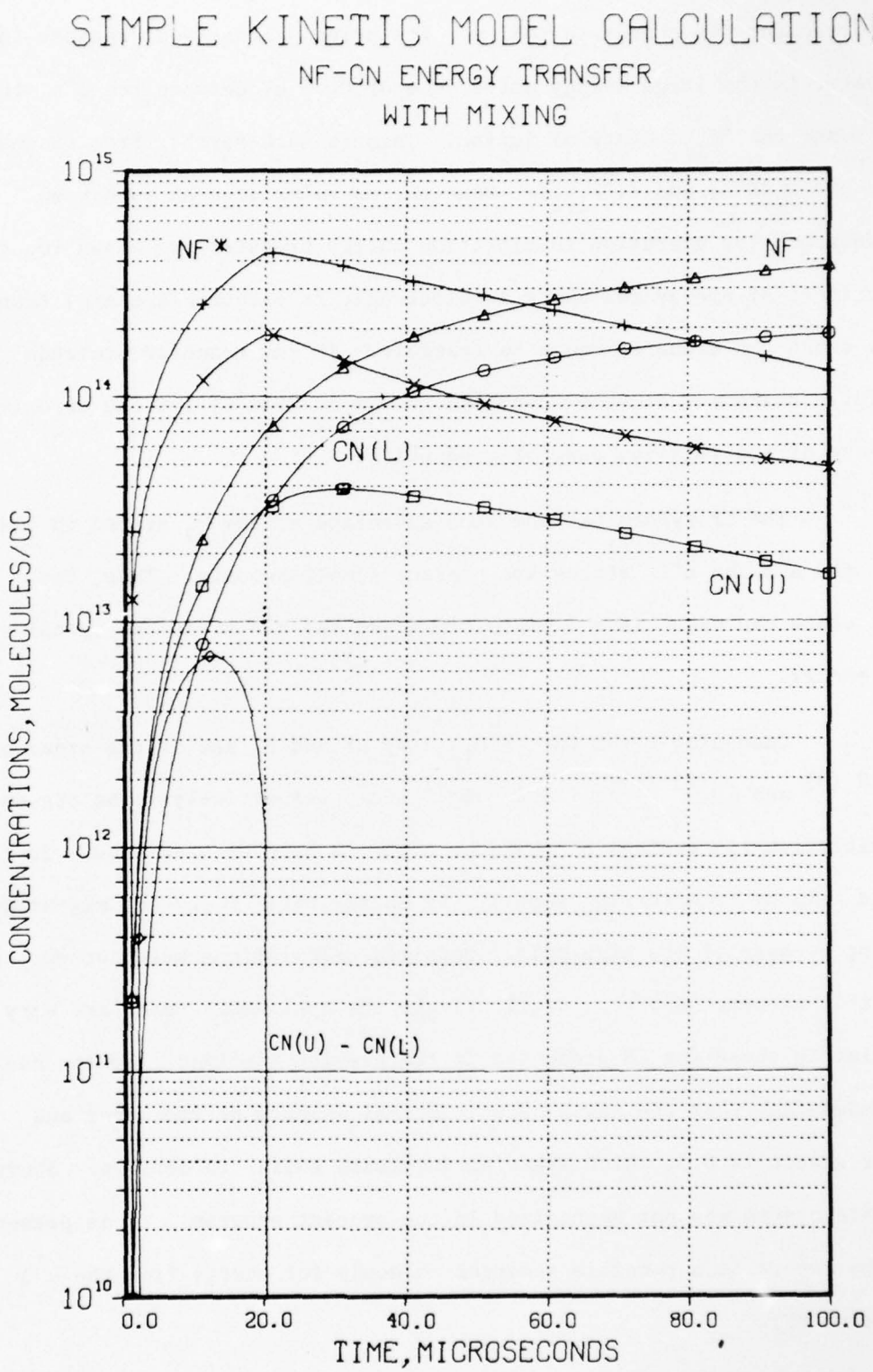

Figure 3. Plots of concentrations of various species versus time for NF-CN energy transfer.

also transfer its energy to iodine. The principal argument against this transfer is the large energy difference of 0.48 eV between the $a^1\Delta$ state of NF and the $^2P_{1/2}$ state of iodine. This is much farther from resonance than are $O_2(a^1\Delta)$ and $I(^2P_{1/2})$. However, no rules such as have been established for vibration to vibration energy transfer are known for the importance of energy resonance in electronic to electronic energy transfer. This means the transfer could be feasible. If the transfer proceeds rapidly, there may be some advantage to use of $NF(a^1\Delta)$ instead of $O_2(a^1\Delta)$ because of the relative ease of production.

The NF system has the same advantage as the O_2 system in that both the $a^1\Delta$ and $b^1\Sigma^+$ states are present simultaneously. Thus, the $b^1\Sigma^+$ state can dissociate I_2 into atoms and the $a^1\Delta$ state can transfer its energy.

Quenching rates for $I(^2P_{1/2})$ by HF and H_2 are of the order of 10^{-12} (8) and 10^{-13} (9) cm^3 $molecule^{-1}$ sec^{-1} respectively. The presence of vibrationally excited HF could be either a help or hindrance. It could help by transferring some of its energy to $I(^2P_{1/2})$ but may hinder lasing because of its high gain. Detailed calculations were not performed for this system. However, qualitatively the applicable rates are very similar to those for CN presented in the previous section. Iodine has the advantage that the ratio of statistical weights of the upper and lower states is 0.5, which makes an inversion easier to achieve. Study of this system was not emphasized in the present program. It is presented in the report as a possible acceptor molecule for energy from the $a^1\Delta$ state of NF.

$ClF(A^3\Pi_{0,1})$, $Cl_2(A^3\Pi_0)$

The low lying triplet states of halogens and interhalogens appear to have lifetimes in a range to make them possible laser candidates. For example, Broida, et al.[10, 11] have measured collision free lifetimes of the $B^3\Pi_0$ states of iodine and bromine to be from 0.28 μsec to 1.2 μsec depending on upper vibrational level. The collision-free lifetime of ICl was measured[12] to be of the order of 100 μsec. ClF and Cl_2 should have longer lifetimes than bromine or iodine since their absorption bands are weaker indicating smaller transition probabilities.

Quenching rates of halogens have been measured to be exceedingly rapid. However, this observation was made when vibrational levels above the dissociation limit of the molecule had been excited, making predissociation a likely path for quenching. However, if levels below the dissociation limit are excited, predissociation is no longer a quenching mechanism. Thus, quenching of these levels may be considerably slower.

There is a reasonable match between the energies of the $NF(a^1\Sigma^+)$ state and the $A^3\Pi$ states of ClF and Cl_2. For $NF(b^1\Sigma)$, T_o is 19473.5 cm^{-1}. For ClF, T_o is 19112 cm^{-1} [10]. The dissociation energy of ClF is 20632 cm^{-1} indicating that there is not enough energy available to decompose the molecule. For Cl_2, T_o is 17938.6 cm^{-1} and the dissociation energy is 20632 cm^{-1}. Again the energy of $NF(b^1\Sigma^+)$ is sufficient to populate the $A^3\Pi$ level without dissociating the molecule. Other halogens and interhalogens could also be of interest although their dissociation energies are slightly lower than the energy, T_o, of the $NF(b^1\Sigma)$ state.

The above species are the nonmetals that look most promising as energy transfer acceptors for the $a^1\Delta$ and the $b^1\Sigma^+$ states of NF based both on energy and lifetime considerations. Metallic systems were not considered in these screening because of difficulties in handling metal vapors in the experimental apparatus used for energy transfer studies.

2.2.3 Experimental Energy Transfer Studies

The majority of the energy transfer studies were conducted in a flow apparatus. However, one experiment was performed in an HF laser apparatus. The flowtube methods of production of the $a^1\Delta$ and $b^1\Sigma^+$ states of NF were: (1) an electrical or microwave discharge through NF_3 and (2) the reaction of hydrogen atoms with NF_2. The experimental details of these studies are presented below.

2.2.3.1 Discharge Production of NF Excited Species

Experimental

Two flowtubes were used for discharge experiments. The first was a flowing hollow cathode discharge system shown in Figure 4. The flowtube is 32 mm in diameter and is constructed of pyrex. The discharge is of the hollow cathode type and can be operated at total pressures ranging from 0.2 to 15 torr at voltages ranging from 200 - 500 volts and currents of from 1 - 200 ma. A right-angle bend with a light trap is placed between the discharge and interaction region. Three mixing ports are available. The first is a pinwheel design with holes spaced on each spoke to provide optimum mixing. The other two are simple injection ports downstream of

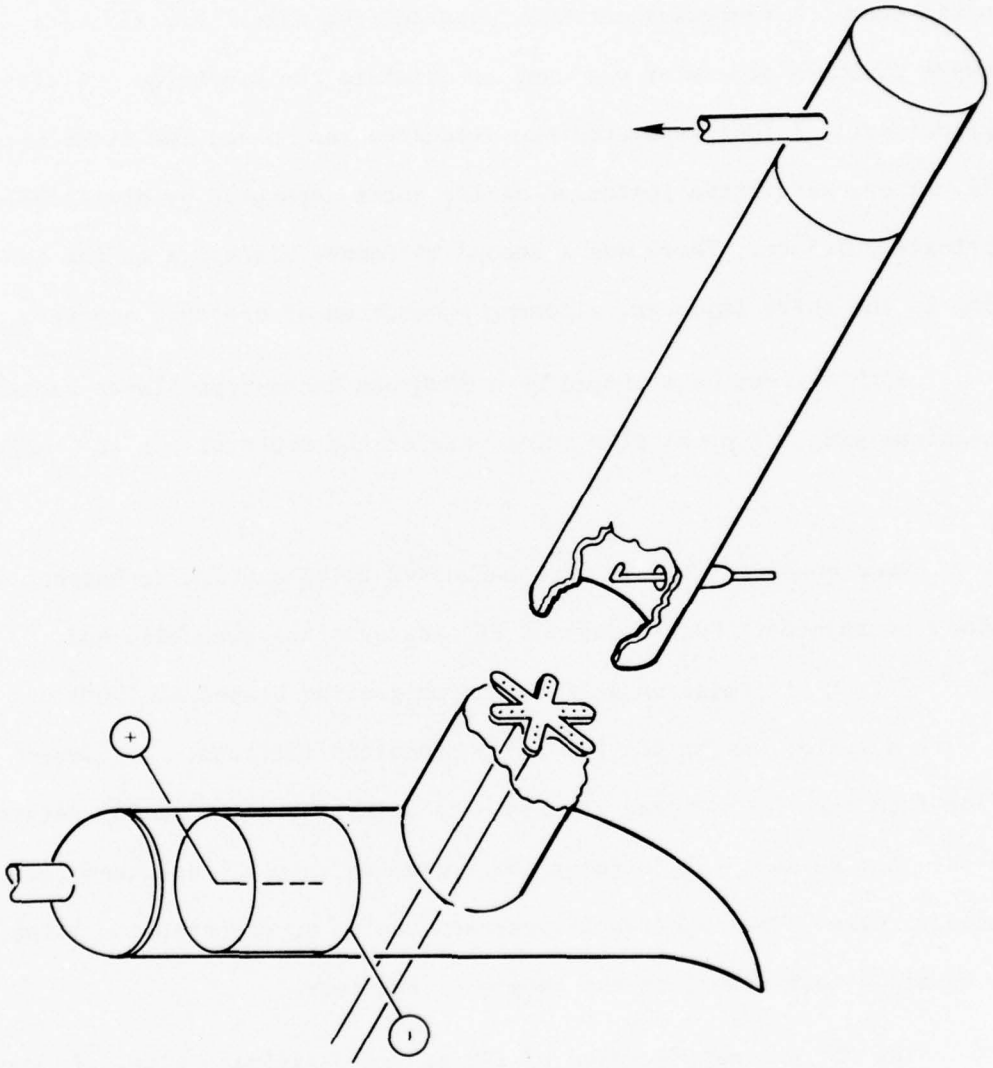

Figure 4. Hollow cathode discharge flow apparatus.

the pinwheel.

The second flowtube shown in Figure 5 utilized a microwave discharge to generate excited species. The flowtube was 120 cm long and 3.7 cm in diameter. A microwave antenna operated from a 2450 Mc, 125 watt microwave diatherm generator was used to maintain the discharge. A distance of approximately 1 foot separated the discharge region and the first mixing nozzle. There were three injection mixing ports separated by distances of approximately 7.5 cm. There was a second microwave discharge on the tube leading to the third injector, allowing production of unstable species.

Both systems were pumped by a 3000 cfm Roots-type blower backed by a mechanical pump. Typical flow rates were of the order of 5×10^{-3} moles/sec.

Spectroscopic studies were conducted using a 0.3 m McPherson 218 VUV spectrometer. For studies of NF excited state quenching and $CN(A^2\Pi - X^2\Sigma, \Delta V > 1)$ emission a 1200 line/mm grating blazed at 7500Å was used. The detector was an RCA C31034A photomultiplier tube. To observe emission from the (0 - 0) band of CN(A - X) emission, a cooled PbS detector was used. A lens was used to focus the radiation into the spectrometer at the proper angle. The spectrometer was mounted on an adjustable milling table to allow movement along the length of the tube.

The NF_3 was manufactured by TRW at the Capistrano site. It was normally diluted with helium before being added to the discharge. Mixtures of NF_3 in helium ranging from .001% to 5% were used depending on discharge conditions. The hollow cathode discharge could not be maintained at high NF_3 pressures. Thus, very dilute mixtures were used in this device.

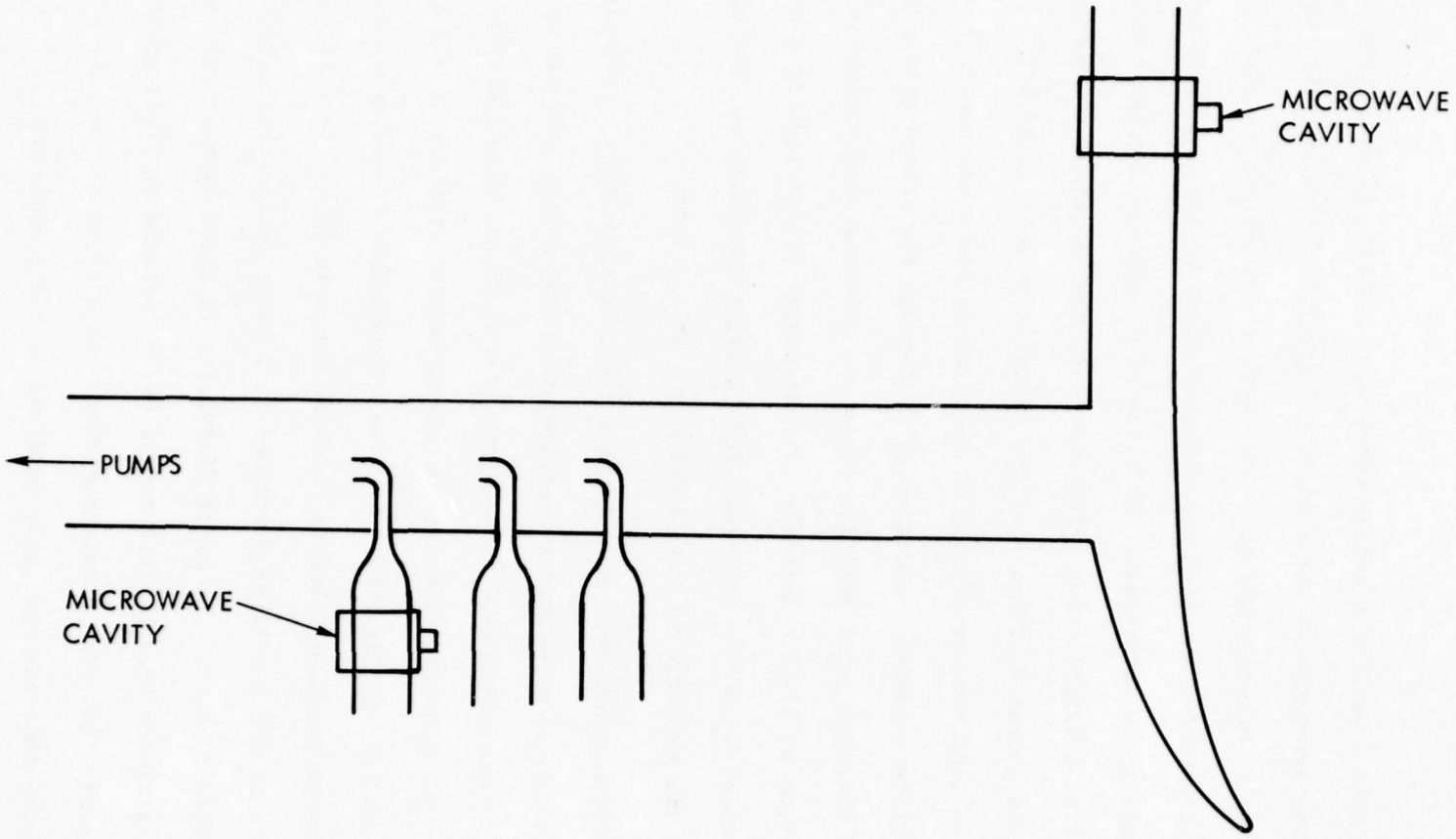

Figure 5. Microwave discharge flow apparatus.

Initial experiments concentrated on optimizing NF emissions. With NF_3 in the discharge, a large amount of green $NF(b^1\Sigma^+)$ emission was observed. $NF(a^1\Delta)$ emission was only one tenth of the $NF(b^1\Sigma^+)$ emission. Nitrogen first positive emission was observed close to the discharge region but became negligible downstream. Addition of D_2 through the first mixing port resulted in a bright orange glow extending the length of the tube. A spectral scan showed N_2 first positive emission as well as $NF(b^1\Sigma^+)$ emission. The region where $NF(a^1\Delta)$ is expected to occur was masked by the N_2 first positive emission. Addition of NO through the second mixing port quenched the nitrogen first positive emission, allowing observation of the $NF(a^1\Delta)$ line at 8742Å. Both the pure discharge stream and the stream after addition of D_2 and NO were used for transfer experiments. For all experiments, the pressure in the flowtube was near 1 torr.

Several means were used in an attempt to generate CN radicals. With this particular experimental configuration the method used was a secondary microwave discharge through either a cyanogen-helium mixture or a methane-nitrogen mixture. Because the mixing nozzle consists of a 3 cm length of 2 mm O.D. tubing, there is some concern that CN radicals generated in the discharge recombined before reaching the main flow. Some CN absorption experiments which will be described in a later section indicate that this is a valid concern. The major difficulty in these systems was to produce a relatively concentrated source of CN radicals in their ground state and to mix them with a second stream. As will be seen in the following discussion, this was not fully achieved in these experiments.

For a typical experiment, NF emissions were adjusted to their optimum values and a mixture expected to produce CN radicals was added

through the third mixing nozzle, having first passed through the secondary microwave discharge. Observations are reported below.

Results

$NF(b^1\Sigma^+)$ Transfer to CN

Initial experiments were conducted with NF_3 in the discharge without D_2 and NO downstream. These experiments produced some interesting results which will be described in some detail below.

In the initial experiment, a methane-nitrogen mixture was added to the main flow through the secondary microwave discharge. A flame that visually appeared white resulted. Spectral analysis showed the presence of both CN red and blue band emissions. A slight increase in CN emission intensity was observed when the secondary microwave discharge was turned off. This indicated that the emission resulted from interaction of something produced in the NF_3 discharge with methane. Observation of the $NF(b^1\Sigma^+)$ and $NF(a^1\Delta)$ emissions showed that these were quenched on the addition of methane. This observation is different than that of Herbelin and Cohen who saw increased $NF(b^1\Sigma^+)$ and $NF(a^1\Delta)$ emissions when methane was injected downstream of an RF discharge through NF_3. Also, they did not report observation of CN emissions.

A detailed flow analysis was not conducted. However, qualitatively, a very definite dependence of CN emissions on methane flow rate was observed. With a flow of NF_3 of approximately 14 cc/min and a total flow of 4600 cc/min (i.e., a 0.3% mix of NF_3 in He); the CN emission was optimized at a flow of approximately 6 cc/min of methane. There was a very sharp maximum in intensity with methane flow at the above flowrate. It should also be

mentioned that these intensity observations were made at a fixed distance from the injector. Visually, the flame changed from relatively diffuse to very sharp (tight flame conditions) with changing flows. Observation of CN emissions was reproducible over a wide range of flow and pressure conditions. The carrier in which the methane was introduced was unimportant. Pure methane, methane in nitrogen and methane in helium all yielded CN emissions.

Because a large amount of CN emission was produced, it was impossible to distinguish that emission which may have been formed by energy transfer from NF from that formed by some other mechanism. Because energy transfer should yield primarily $CN(A^2\Pi, v' = 0)$, it should in principle be possible to observe anomalies in the 0-0 band of 1.1 μ. However, this is very difficult in practice because of the limited detector sensitivity at 1.1 μ and also because no single detector had reasonable response to both the $\Delta v = 0$ and $\Delta v \geq 1$ bands. These detector limitations combined with the relatively small signals at 1.1 μ made results of these experiments inconclusive.

Several other substances were substituted for methane. Those studied were cyanogen, ethane, acetylene, methyl chloride, and Freon 22, $CHClF_2$. Observations are outlined below.

Cyanogen

No emission in the wavelength range from 2000Å to 9000Å was observed when cyanogen was added to the effluent from the NF_3 discharge. However, slight quenching of both the $NF(b^1\Sigma^+)$ and $NF(a^1\Delta)$ states was observed, with very high flows of $(CN)_2$ required for complete quenching. An attempt was made to look at the 0-0 band of the $A^2\Pi$ state of CN at 1.1 μ

using the cooled PbS detector. There appeared to be some signal when the discharge through cyanogen was turned on. However, it was so close to the noise level as to be inconclusive. It is possible that there is a slow reaction between NF and cyanogen

$$NF(b^1\Sigma^+) + (CN)_2 \rightarrow CNF + CN_2 \qquad (16)$$

that would explain the observed quenching.

Ethane

Addition of ethane to the effluent from the NF_3 discharge resulted in production of CN red and blue band emissions as with methane. However, in contrast to the methane result, the $NF(b^1\Sigma^+)$ emission was enhanced with ethane addition until some critical ethane flow was reached at which time the signal decreased. There was a factor of 4 difference in $NF(b^1\Sigma^+)$ emission intensities when methane and ethane were present. Addition of D_2 upstream of the ethane nozzle also caused some enhancement of the CN intensity at low flows of D_2. This is again in contrast with the methane result.

Acetylene

Addition of acetylene to the effluent from the NF_3 discharge also resulted in CN red and blue band emissions. These emissions were approximately a factor of 4 less bright than those observed upon addition of methane or ethane. As with methane and ethane the CN emission intensity was optimum at a relatively low acetylene flows. The $NF(b^1\Sigma^+)$ emission was quenched with increasing acetylene flow as is shown in Table 1. Addition of D_2 upstream of the acetylene decreased CN emission intensity

TABLE 1

VARIATION OF NF ($b^1\Sigma^+$) EMISSION INTENSITY WITH ACETYLENE FLOW

Acetylene Flow (cc/min)	Intensity
0	8.05
5.6	7.42
8.6	7.01
15.0	6.45
20.6	6.10
31.6	5.59
35.8	5.35
51.4	5.02

even though nitrogen first positive emission increased. This was similar to the result obtained with methane.

Methyl Chloride

Addition of methyl chloride to the discharge effluent resulted in CN red and blue band emissions that were approximately a factor of 2 higher than with methane. Slight quenching of the NF($b^1\Sigma^+$) state was observed.

Methylene Chloride, Chloroform and Freon 22

These substances were added as a check to determine whether active nitrogen is the species responsible for the CN emission. Broida[13] and other workers have reported brightest chemiluminescent emissions in active nitrogen with chlorinated hydrocarbons. In these experiments little or no CN emission was produced when halogenated hydrocarbons (with the exception of methyl chloride) were added to the effluent from the NF_3 discharge. In the best case, that of methylene chloride, the CN emissions were more than a factor of 10 less intense than with methane. This indicates that the normal active nitrogen mechanism is not occurring under these conditions.

Conclusions

The experiments conducted above were not conclusive in showing that energy transfer from NF($a^1\Delta$) to CN($A^2\Pi$) was occurring. The major difficulties were: (1) the production of CN($X^2\Sigma$) ground state in sufficient concentrations that definitive results could be obtained and (2) the problem of detecting the 1.1 μ emission emitted by the 0-0 band of the CN(A - X) transition. However, the experiments did demonstrate the feasibility of CN excited state production from the interaction of the effluent from an NF_3 discharge with various hydrocarbons. Since similar products appear to

be formed in the NF_3 combustion system, it seems likely that these modes of CN production should apply equally well to that system. Thus, excited state CN production has been demonstrated.

It is interesting to speculate on a possible mechanism responsible for the experimental observations. It is first interesting to consider the following mechanism proposed for active nitrogen reactions with methane[14].

$$N_2(A^3\Sigma^+) + CH_4 \rightarrow CH_3 + N_2(X^1\Sigma^+) + H \quad (17)$$

$$N + CH_3 \rightarrow HCN + 2X \quad (18)$$

$$N + CH_3 \rightarrow HCN + H_2 \quad (19)$$

$$H + CH_3 \rightarrow H_2 + CH_2 \quad (20)$$

$$N + CH_2 \rightarrow CN + 2H \quad (21)$$

$$\rightarrow CN^* + H_2 \quad (22)$$

$$\rightarrow HCN + H \quad (23)$$

$$H + CH_2 \rightarrow CH + H_2 \quad (24)$$

$$N + CH \rightarrow CN^* + H \quad (25)$$

$$H + CH \rightarrow C + H_2 \quad (26)$$

In the above mechanism, reaction (22) and (25) are postulated as the steps which produce the $A^2\Pi$ and $B^2\Sigma$ states observed in emission. With methane, steps (20) and (24) are endothermic, whereas if halogens are substituted for the hydrogens, the reactions are exothermic. This is used to explain why halogenated halocarbons produce more CN emission than saturated hydrocarbons in active nitrogen. If the discharged NF_3 is considered, the species present are NF_3, NF_2, $NF(X^3\Sigma)$, $NF(a^1\Delta)$, $NF(b^1\Sigma^+)$,

F, and possibly some N and $N_2(A^3\Sigma)$. Note that CH_n radicals can now be formed by fluorine atom reactions such as:

$$F + CH_4 \rightarrow HF + CH_3 \quad (27)$$

$$F + CH_3 \rightarrow HF + CH_2 \quad (28$$

$$F + CH_2 \rightarrow HF + CH \quad (29)$$

$$F + CH \rightarrow HF + C \quad (30)$$

These reactions are not exothermic when H is replaced by halogens. Thus, methane and methly chloride (which has only one chlorine) should lead to numerous radicals which could react by reactions (22) and (25). In addition to F atom reactions, it is also necessary to consider NF radical reactions of the type:

$$NF + CH_3 \rightarrow CH_3F + N \quad (31)$$

$$NF + CH_2 \rightarrow HF + HCN \quad (32)$$

$$\rightarrow HF + CH + H \quad (33)$$

$$\rightarrow CH_2F + N \quad (34)$$

$$NF + CH \rightarrow CN + HF \quad (35)$$

which are energetically feasible. Reaction (35) has an exothermicity of 163 kcal/mole which is sufficient to produce both the $B^2\Sigma$ and $A^2\Pi$ states of CN. However, most of these reactions are 4-center reactions which could be kinetically slow. If reactions (31) and (34) proceed at a reasonable rate, they could provide an additional source of nitrogen atoms.

Finally, reactions of NF with CN other than energy transfer should be considered. The two reactions are:

$$NF + CN \rightarrow CN_2 + F \quad (36)$$

$$NF + CN \rightarrow CNF + N \quad (37)$$

Reaction (36) is near the thermoneutral. Since the thermodynamics of NF and CN_2 are not well known, the energy of this reaction cannot be easily characterized. Reaction (37) is approximately 40 kcal/mole exothermic and could cause serious competition with the energy transfer. However, because N atoms are formed, it could lead to CN formation by reaction (25).

Other reactions may also be possible in this system which are not included here. The mechanism is of interest and is discussed in detail because the species mentioned are likely to be present in any NF_3 combustion system. The mechanism shows that CN excited state production can occur in this system by methods other than energy transfer. Thus, the system appears to present a good chemical method of CN excited state production, regardless of whether the energy transfer mechanism is valid.

$NF(b^1\Sigma^+)$ Transfer to Cl_2 or ClF

The flowtube sketched in Figure 5 was used for these studies. The $b^1\Sigma^+$ state of NF was generated by passing a mixture of NF_3 in helium through the microwave discharge. Chlorine or chlorine fluoride was added through the first mixing nozzle downstream of thr discharge. For each experiment, the spectrum was first scanned from 2000 - 8000Å with the NF_3 - He mixture in the discharge and no gases added downstream. It was then scanned with the NF_3 - He mixture in the discharge with either chlorine or chlorine fluoride downstream.

With chlorine added, a small emission peak dependent on both the

NF_3 and Cl_2 flows was observed centered at 6650Å. However, this spectral feature was very weak and could not be intensified enough to enable it to be characterized. Quenching of the $NF(b^1\Sigma^+)$ emission by chlorine was studied. For these studies the NF_3 in He flow was held constant and the spectrometer was set to observe the 5288Å peak of the $NF(b^1\Sigma^+)$ emission at a fixed distance of 8 cm from the mixer. A semilog plot of I/I_o versus chlorine concentration was linear as shown in Figure 6. I is the $NF(b^1\Sigma^+)$ emission intensity at a given chlorine flow whereas I_o is the $NF(b^1\Sigma^+)$ intensity with no chlorine flow. Analysis of the slope of this plot gives a quenching rate of 1.5×10^{-11} cm^3 $molecule^{-1}$ sec^{-1}. The experiment did not conclusively prove that this quenching was due to energy transfer. With the excess energy in the $b^1\Sigma^+$ state of NF, a reaction with chlorine to form ClF and NCl could be exothermic. However, such a four-center reaction would not be expected to be as fast as the measured rate constant.

The addition of chlorine fluoride to the effluent of the discharge produced visible quenching of the $NF(b^1\Sigma^+)$ emission. Qualitative spectral studies showed the quenching rate was of the same order as that observed with chlorine. Spectral scans showed no emission that was attributable to the addition of chlorine fluoride.

It should be noted that chlorine fluoride behaves very much like fluorine and requires passivation of all apparatus through which it flows. Passage through flowtubes resulted in popping in the vacuum line. Problems were also encountered upon completion of the experiment after all chlorine fluoride had been pumped from the lines. Opening the vacuum system resulted in a chlorine odor that permeated the room and could be detected for several days afterwards, even though careful steps were taken to seal

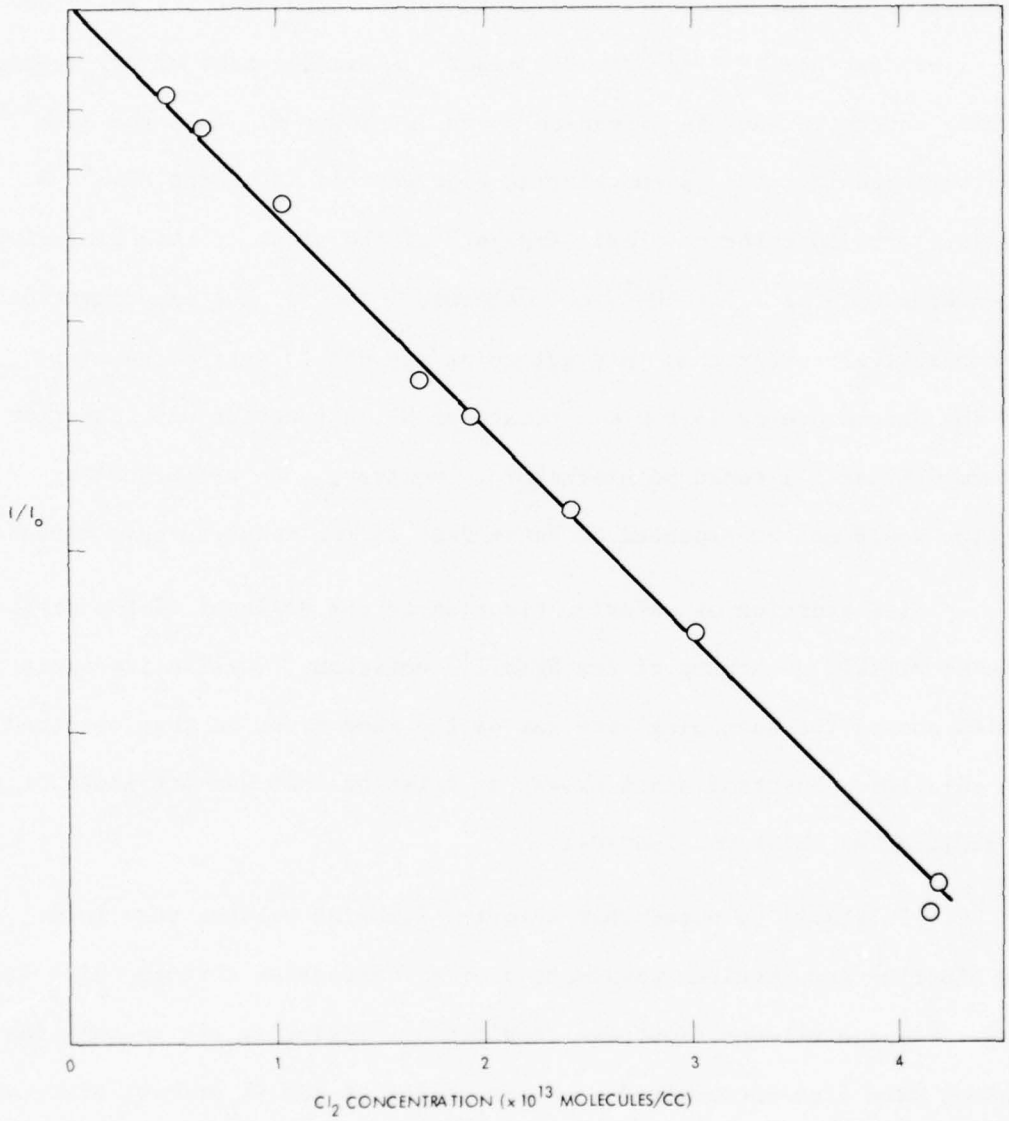

Figure 6. Semilog plot of I/I_o versus chlorine concentration

all vacuum lines carefully and to remove all possible sources of leaks. This was an unexpected hazard in the handling of ClF.

2.2.3.2 $H + NF_2$ Experiments

The main production mechanism of $NF(a^1\Delta)$ in $NF_3 - H_2$ systems is the reaction of hydrogen atoms with NF_2 radicals. Thus, an experiment where these two reactants are mixed directly should provide a relatively pure source of $NF(a^1\Delta)$ and should avoid complicating species which are produced in a discharge.

Experimental

The apparatus used for this study is shown in Figure 7. Hydrogen atoms are produced by a microwave discharge through hydrogen. A platinum wire probe can be inserted into the flow to measure the hydrogen atom concentration by the method of Tollefson and LeRoy.[15] The probe is removed before addition of N_2F_4 to avoid a reaction on the surface of the wire which changes the characteristics of the probe. The NF_2 radicals needed for the study are generated by heating tetrafluorohydrazine, N_2F_4, which has a $F_2N - NF_2$ bond strength of 20 kcal/mole.[16] Studies[17] have reported that a temperature of 150°C will cause almost total dissociation of N_2F_4 into NF_2 radicals. The tube through which N_2F_4 enters is heated by a set of cylindrical heaters. Heating tape is wrapped around the flow tube up to the hydrogen nozzle to insure dissociation of N_2F_4 up to the mixing region. Temperature is controlled using variacs and is measured at several points along the tube with thermocouples. The hydrogen atom and NF_2 streams are mixed using a concentric tube arrangement as sketched. A secondary injector downstream allows addition of possible energy transfer

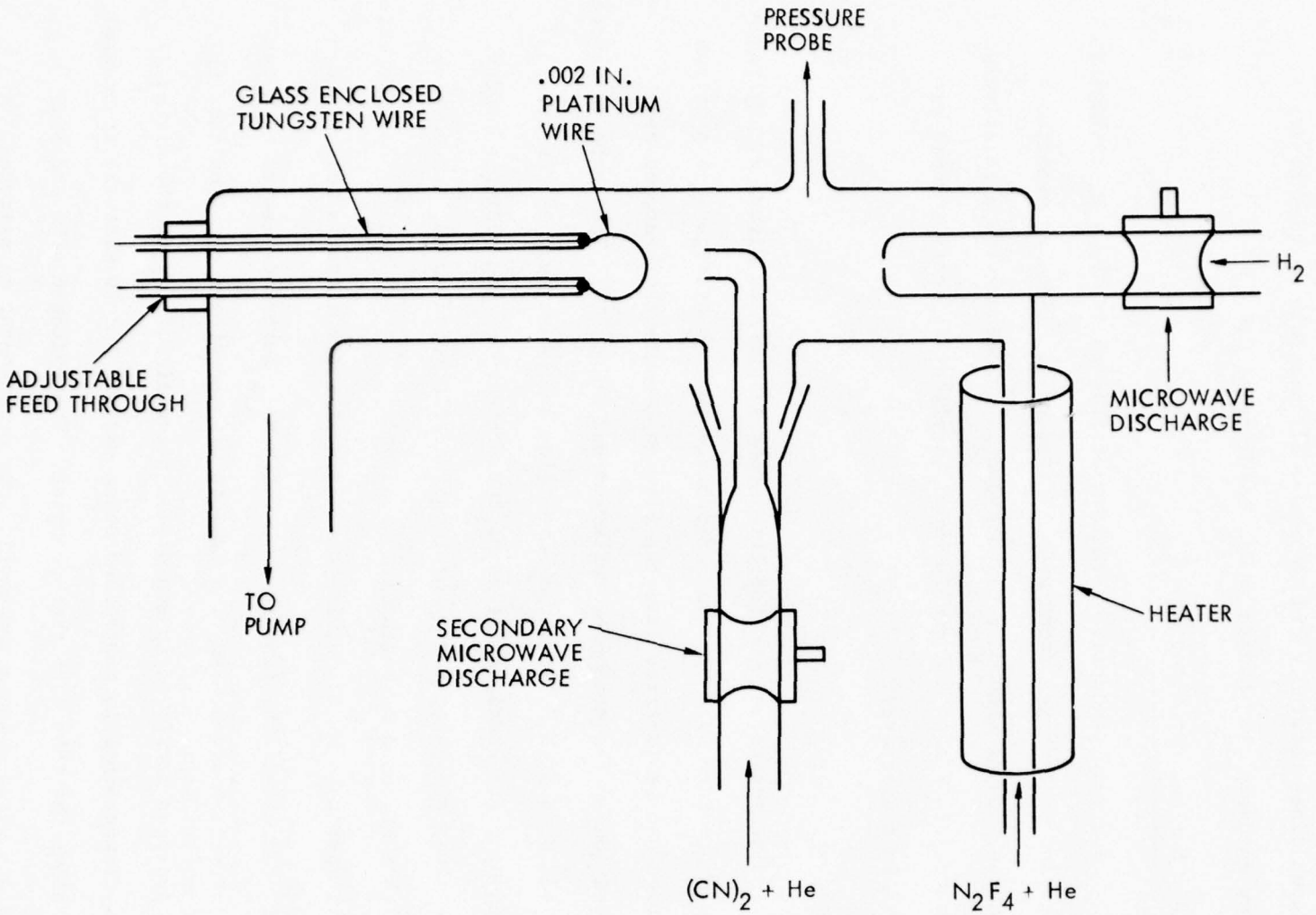

Figure 7. Schematic drawing of flow apparatus used for H + NF_2 experiments.

acceptors. Emission is observed with the McPherson spectrometer mounted on a milling table to allow intensity versus distance measurements.

Availability of N_2F_4 proved to be a major problem in conducting this experiment. The only manufacturer who produces N_2F_4 at present is Hercules, Inc. in Magna, Utah. The problem in obtaining N_2F_4 from them was lack of a permit to ship more than very small samples. This situation has since changed and a purchase order for a 1/4 lb bottle has been sent. However, during the duration of the contract, only a 3 gram and later a 10 gram sample could be obtained. There was also a time interval between obtaining the first and second samples. Both as a safety measure and to conserve N_2F_4 a 5% mixture of N_2F_4 in helium was prepared for use in these experiments.

Hydrogen and the 5% mix of N_2F_4 in helium were added through Matheson 600 flowtubes. There was some concern in using these flowtubes with N_2F_4 because of its strong oxidizing nature. In practice, however, no problems were encountered with the exception of some etching of the inside of the flowtube. This made periodic recalibration of the flowtube necessary. A calibrated orifice would be preferable to the flowtube for use with pure N_2F_4. In later experiments, it was found that a lower flow of hydrogen than could be conveniently measured with the 600 flowmeter was needed. For these experiments a calibrated oil manometer flowmeter was used to measure hydrogen flow.

A series of tests were conducted to optimize hydrogen atom production and to perfect the hydrogen atom measurement technique. These tests illustrated the necessity of coating the tubing near the discharge region

with orthophosphoric acid to enhance hydrogen atom production. This coating is thought to work by preventing hydrogen atom recombination on the walls.[18] The measurement technique worked very well with no modifications to the method of Tollefson and LeRoy. Thus, these experiments will not be described here. Under a typical run condition with several torr of hydrogen in the discharge region, 1% of the hydrogen was measured to be dissociated into atoms at the detector. Addition of helium through the side tube did not affect the measurement. The orthophosphoric acid coating tended to degrade with time, hydrogen atom concentration being optimum when the tube was first coated and then decreasing slowly with time. Thus, the coating had to be renewed periodically. Judgement of when to renew the coating was made on the basis of emission intensities observed in the $H + NF_2$ experiment.

Results

Initial experiments concentrated on production of $NF(a^1\Delta)$. For these experiments, H_2 was flowed through the discharge region and the 5% mixture of N_2F_4 in helium flowed through the tube heated to 120°C. In the first experiments, no visible emission was seen in the mixing region. However, spectral analysis showed the presence of $NF(a^1\Delta)$ emission at 8742Å. Clyne and White had reported the presence of nitrogen first positive emission and green $NF(b^1\Sigma^+)$ emission in a similar experiment. Thus, it was somewhat surprising that $NF(b^1\Sigma^+ - X^3\Sigma)$ and nitrogen first positive emissions were not observed in the mixing region. When the flowtube was carefully observed in the dark, a yellow-orange glow due to nitrogen first positive emission was seen in the heated tube through which the N_2F_4 entered the flowtube. This indicated backstreaming of the hydrogen into

this region. By decreasing the hydrogen flow, the colored emissions moved into the interaction region where spectral analysis showed they were $NF(b^1\Sigma^+ - X^3\Sigma)$ and nitrogen first positive emissions. The intensity of the $NF(a^1\Delta - X^2\Sigma)$ emission was also higher than observed previously. These spectral observations are consistent with those of Clyne and White.[19] All emissions increased with N_2F_4 flow over the range of flows available with the 600 flowmeter. Total pressures in the flowtube in these experiments ranged from 0.5 to 1 torr.

By choosing proper flow conditions, the $NF(a^1\Delta)$ emission could be made dominant over the nitrogen first positive emission. Under some conditions, only $NF(a^1\Delta)$ and $NF(b^1\Sigma^+)$ emissions were observed. Under these conditions: hydrogen flow = 23.1 cc/min; tetrafluorohydrazene in helium flow = 33.4 cc/min; pressure = 1 torr; a study of $NF(a^1\Delta - X^3\Sigma)$ emission intensity versus distance was conducted. A semilog plot of intensity versus distance was linear as shown in Figure 8. The slope of the plot is 0.15 cm^{-1} which with the velocity in the tube of 60 cm/sec gives a slope of 9 sec^{-1}. Because of the limited amount of N_2F_4 available, a detailed study of intensity versus distance at various N_2F_4 concentrations could not be conducted. This type of study with extrapolation to zero pressure of N_2F_4 would be necessary to obtain a realistic estimate of the $NF(a^1\Delta)$ lifetime.

$NF(a^1\Delta)$ Transfer to $CN(A^2\Pi)$

Two methods were used in an attempt to introduce ground state CN radicals in this system. The first was a microwave discharge through either a cyanogen-helium mixture or a methane-nitrogen-helium mixture. The other

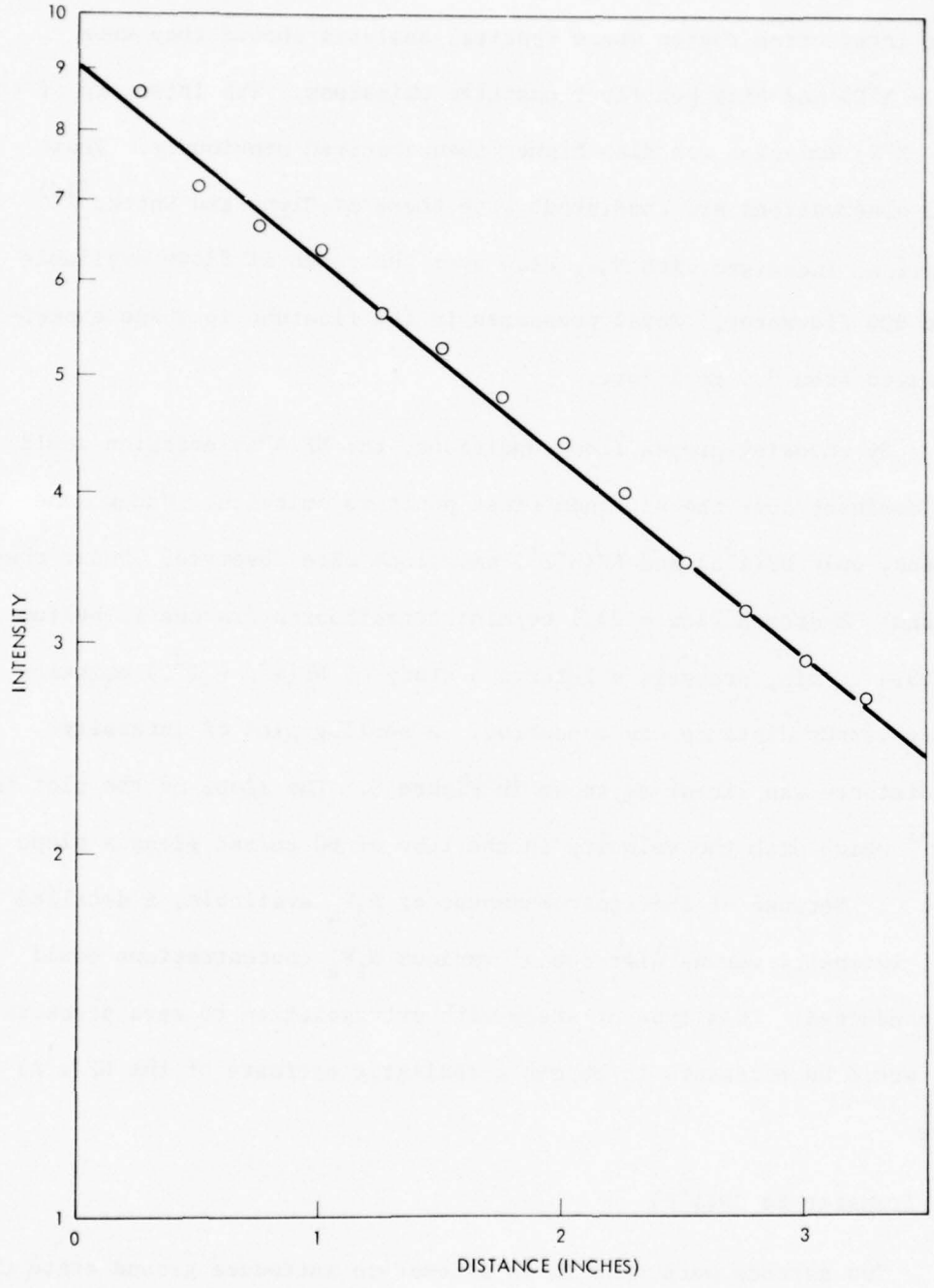

Figure 8. Semilog plot intensity of NF($a^1\Delta$) emission versus distance.

was by passing cyanogen over a platinum filament heated to a white glow. To determine whether the discharge had an effect, the $NF(a^1\Delta)$ emission was first monitored to determine if any quenching occurred. The emission intensity of the $NF(a^1\Delta)$ line remained constant whether or not the discharge was on. With the methane-nitrogen-helium mixture the $CN(A^2\Pi)$ and $CN(B^2\Sigma)$ emissions were seen as with the discharge experiments. Because of the ineffectiveness of the discharge, an experiment was designed to determine if CN radicals were indeed being produced in any reasonable concentrations. This experiment is described in the next section.

Detection of CN Radicals

An absorption experiment was designed to detect whether CN radicals were entering the flowtube. The experimental apparatus is shown schematically in Figure 9. The cyanogen or methane-nitrogen-cyanogen mix was passed either through a microwave discharge or over a heated wire. They then entered the cylindrical absorption cell either through 8 mm tubing or through a nozzle as used in the experiments. The absorption cell was 85 mm in diameter and 120 mm long. In experiments where there was emission, this emission tended to appear uniform in the cell indicating approximately constant concentrations. The vessel had two symmetrical pumping outlets and the residence time of radicals in the cell was approximately 0.1 sec. A microwave discharge through a slowly flowing mixture of 30 parts argon, 1 part nitrogen and 5 parts methane at 1 mm pressure provided the source of $CN(B^2\Sigma - X^2\Sigma)$ violet band emission. The radiation was passed through a White's cell[20] set to pass the radiation four times through the reaction vessel to give an effective path of 48 cm. An EMI 6256S photomultiplier at the exit of a spectrometer was used to monitor

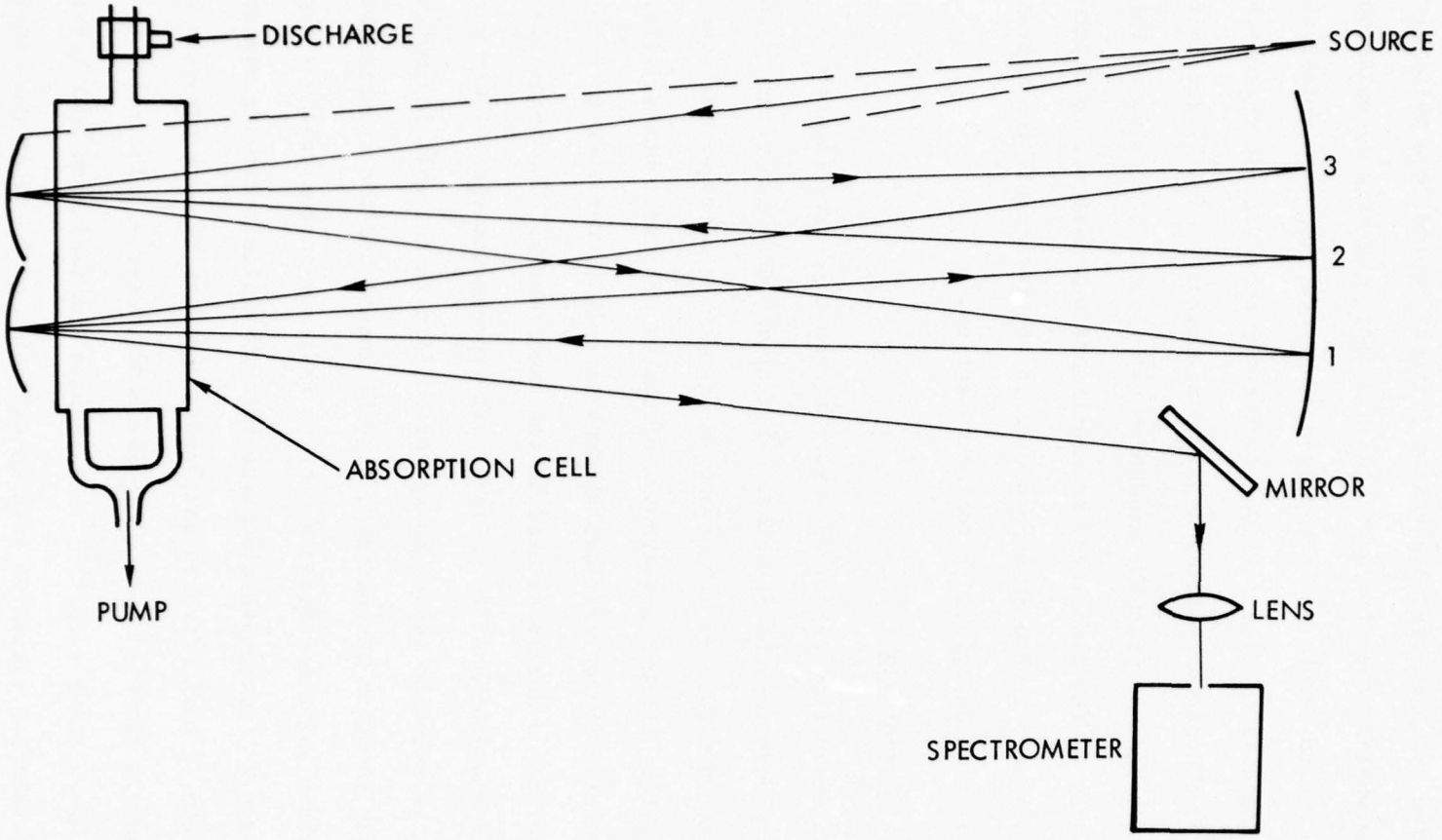

Figure 9. Experimental arrangement for CN absorption measurement

the radiation. Phase sensitive detection was used to correct for emissions from the absorption cell.

Only very small (<1%) absorptions were seen even under optimum conditions where intense CN violet emission was produced in the absorption cell. This indicated CN concentrations of about 10^{10} molecules/cm^3 under the most favorable conditions. This appeared to decrease even more upon passage through a nozzle.

These experiments aid in explaining why as much difficulty was encountered in studying $NF(b^1\Sigma^+)$ to CN energy transfer. With such low concentrations of CN being produced, it would be surprising if quenching or emission had been seen. It appears that a chemical method of producing CN like in $F_2/H_2/(CN)_2$ flames described in the next section would be needed to generate enough CN radicals to allow a flowtube study to be conducted.

$NF(a^1\Delta)$ Transfer to Atomic Iodine

In a preliminary study of this system, molecular iodine was added to the $H + NF_2$ stream through the secondary nozzle. This resulted in quenching of the nitrogen first positive and $NF(a^1\Delta)$ emissions. However, an unexplained five-fold increase in $NF(b^1\Sigma^+)$ emission intensity was observed. Some emission was observed at 1.315 μ where the $I(^2P_{1/2})$ state emits. The dependence of this emission on iodine flow indicates iodine rather than HF overtone emission. Limitations in N_2F_4 supply and time did not permit more detailed studies.

2.2.4 Transfer Experiments in Laser Device

As a test to determine whether emission could be observed, cyanogen was added to the cavity of the combustion driven laser after flows had been adjusted to optimize NF emission intensities. Flows are

NF_3 = 2 x 10^{-3} moles/sec, H_2 = 4.2 x 10^{-3} moles/sec, F_2 = 2 x 10^{-3} moles/sec, D_2 = 1 x 10^{-3} moles/sec and $(CN)_2$ = 1 x 10^{-3} moles/sec. Upon addition of cyanogen the color of emission in the cavity changed from yellow to white. Spectral scans showed the presence of both CN red and violet band emissions. Vibrational levels up to v' = 9 were observed in the CN red band emission. Substitution of methane or ethylene for cyanogen resulted in even brighter emission. A scan with a calibrated spectrometer and integration of the resulting emission spectrum showed the presence of greater than 1 x 10^{14} molecules/cm^3 of the $A^2\Pi$ state of CN. The spectral distinction indicated that the CN emission was probably produced by a mechanism other than energy transfer. It can be postulated that active nitrogen reactions are responsible for the emission. A possible mechanism is the same as presented for the flowtube observations in Section 2.2.3.1. These experiments were significant in that they proved that CN red band emissions could be produced in high intensities in a purely chemical system. Implications for further research are that active nitrogen reactions could possibly be studied in a purely chemical system that would allow direct assessment of chemical laser potential.

2.3 $CN(A^2\Pi)$ Studies in Flames

The experiments which will be described in this section are a side result of the NF excited species studies described in Section 2.2. As described in that section, NF_3 and H_2 were burned in the precombustor of a chemical laser device with H_2 or D_2 being added through the cavity injector. When hydrocarbons or cyanogen were added through the cavity injector with the hydrogen, a white emission appeared. Spectral analysis showed this emission to be due to the $B^2\Sigma - X^2\Sigma$ and $A^2\Pi - X^2\Sigma$ bands of

CN. The study had been aimed at studying the $NF(a^1\Delta)$ to $CN(A^2\Pi)$ transfer mechanism as described in Section 2.2. Thus, when CN emission was observed on addition of cyanogen, it was felt that a mechanism of the type

$$F + (CN)_2 \rightarrow FCN + CN \tag{38}$$

$$NF(a^1\Delta) + CN \rightarrow CN(A^2\Pi) + NF(X^1\Sigma) \tag{39}$$

may have been contributing to the emission. Consequently, the spectrometer was set to observe the 0 - 0 band of the $CN(A^2\Pi - X^2\Sigma)$ transition at 1.1 μ since the $v' = 0$ should be prodomenantly populated by the transfer mechanism. Flows were then adjusted to optimize the emission in this band. Suprisingly, the emission became optimum when the NF_3 flow was stopped and only Fluorine flowed through the precombustor and hydrogen and cyanogen in the cavity. Under these conditions the visible emission was red in color and blindingly intense. A scan of the spectrum showed emission only from the $A^2\Pi - X^2\Sigma$ transition of CN. The combined observation of only one electronic transition and high emission intensities indicated the presence of high number densities of the $A^2\Pi$ state of CN. At the very least, this observation showed that chemical production of CN radicals for use in the transfer scheme would be no problem. However, the high chemiluminescent emission intensities indicated that the system could be interesting itself as a potential chemical laser system. To investigate this possibility, several experimental diagnostic measurements of the laser cavity were made to determine excited state number densities, temperature, ground state populations and gain. The experimental measurements and results are described below.

2.3.1 Experimental Techniques and Analysis

Chemiluminscence Measurements

Chemiluminescent emission spectroscopy is a straightforward method for measuring kinetic temperatures and concentrations of excited state species. Details of the experiment are diagrammed in Figure 10. The spectrometer is a 0.3 m McPherson. This was used in conjunction with different gratings and detectors depending on the wavelength region of interest. For studies of the $\Delta v = 0$ and $\Delta v = -1$ bands of the $A^2\Pi - X^2\Sigma$ system of CN, a 600 line/mm grating blazed at 1.6 μ was used in the spectrometer. The detector for this region was cooled lead sulfide, PbS. For studies of the $\Delta v \geq 1$ bands of the $A^2\Pi - X^2\Sigma$ system of CN, a 1200 line/mm grating balzed at 7500Å was used in the spectrometer. The detector was a Hammamatsu S-1 response, side-on photomultiplier. Some studies of the $B^2\Sigma - X^2\Sigma$ emission of CN used a 1200 line/mm grating blazed at 3000Å. The detector for this spectral region was an EMI 6256S photomultiplier. Measurement of absolute intensities in units of watts/cm^2 ster is obtained by calibration against an Eppley standard filament lamp.

Temperatures were determined both from HF/DF and CN($A^2\Pi \rightarrow X^2\Sigma$) chemiluminescence measurements. For the HF/DF measurements, the following analysis is used. This analysis assumes an optically thin medium. Line intensities for transitions between levels $v'j' \rightarrow v''j''$ are given by

$$I_{line}(v',j' \rightarrow v'',j'') \quad (\text{watt cm}^{-2}\ \text{ster}^{-1}) \qquad [2]$$

$$= \frac{16\pi^3 \cdot 10^{-7}}{3} \cdot c \cdot \nu^{-4} \cdot |\langle v'j' \mid M(r) \mid v''j'' \rangle|^2 \cdot m \cdot \frac{\int N_{v'j'}\, dy}{2j' + 1}$$

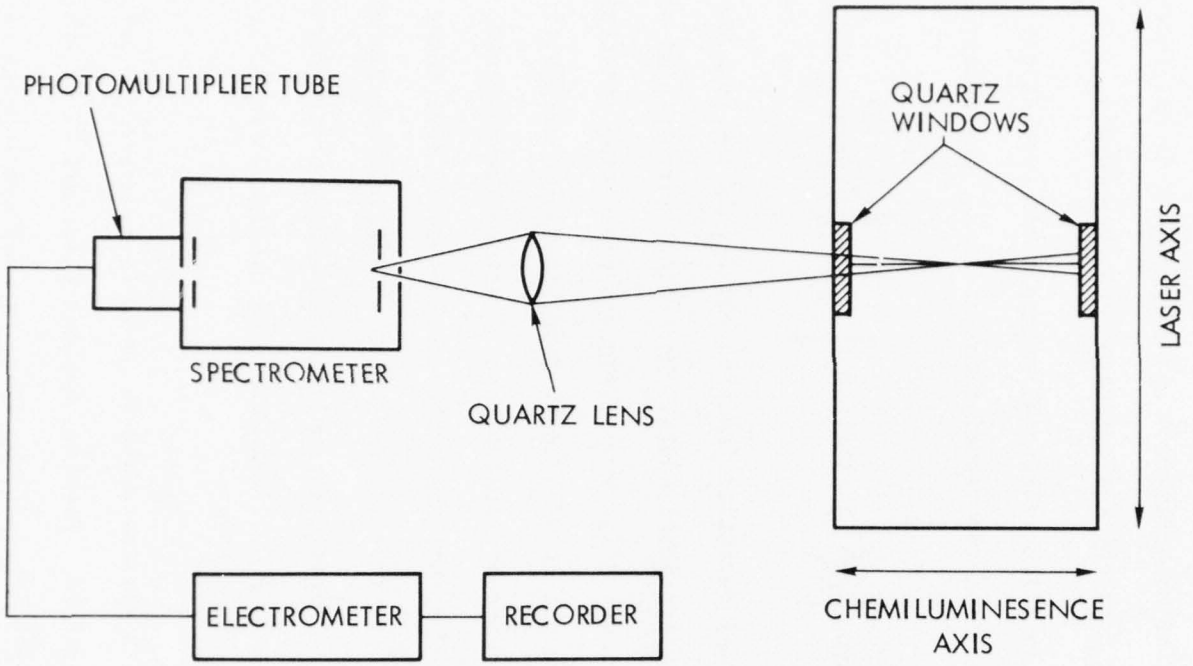

Figure 10. Experimental layout for chemilumenescence measurements. For experiments in the infrared spectral region, a PbS detector was substituted for the photomultiplier and a chopper and lock-in amplifier allowed phase sensitive detection.

The squared expression above is the dipole moment matrix element and m is equal to (j' + 1) or j' for the P and R branches, respectively. The state number density integral $\int N_{v'j'}, dy$, normalized by the rotation degeneracy term 2j' + 1, has units of molecules/cm^2 and corresponds to the integration along a line of sight defined by the optics of the experiments.

For a medium in which rotational energy level populations are in Boltzmann equilibrium at a rotational temperature T_r, one obtains

$$\frac{\int N_{v'j'}\, dy}{2j' + 1} = \exp\left[\frac{-hc}{kT_r}\, j'(j'+1)\, B_{v'}\right] \frac{\sum_{j'} \int N_{v'j'}\, dy}{Q_{rot}(T_r)} \qquad [3]$$

where Q_r is the rotational partition function and $B_{v'}$ is the rotational constant for the upper vibrational state. On a semilogarthic plot of $(2j' + 1)^{-1} \int N_{v'j'}\, dy$ vs $j'(j' + 1)$, points representing spectral lines originating from a given vibrational upper level follow a straight line whose slope is inversely proportional to the rotational temperature. Boltzmann distribution of rotational sublevels has alwasy been found to exist in chemical lasers investigated thus far, and the rotational energy indicated is equal to the kinetic (translational) energy of the medium. Vibrational populations $\sum_j \int N_{v'j'}\, dy$, are also obtainable from the chemiluminescence data.

In principle, a similar analysis could be conducted to obtain the CN rotational temperature. However, because there are 12 branches in each band of the $A^2\Pi - X^2\Sigma^+$ transition, there is much overlapping of rotational lines which makes isolation of enough pure rotational lines for a temperature determination difficult. Thus, CN rotational temperatures

were approximated by comparing chemiluminescence data with synthetic spectra. The construction of these synthetic spectra is discussed in Appendix B. This measurement is not as precise as the HF/DF determination. Thus, this comparison was performed mainly to check that the HF/DF and CN rotational temperatures were equal. This was found to be the case in all cases tested. Thus, in general, the temperature from HF/DF was used. However, some qualification should be made about the HF/DF measurement. It has been found that a change of slope can occur in the semilog plot of $(2j' + 1)^{-1} \int N_{v'j'} dy$ versus $j'(j' + 1)$ at high j values. Higher j values than normally used were required for the measurement in these experiments because of the high temperatures involved. It has not been ascertained whether the slope effect observed in HF experiments still occurs at these higher temperatures.

Absorption/Gain Measurements

It was very desirable to know how much of the $X^2\Sigma$ state of CN is being produced in the flame experiments and also to determine if gain is present. Two different experimental configurations were used for these measurements.

In the first set of experiments, absorption of the (0,0) band of the CN violet system ($B^2\Sigma^+ \leftrightarrow X^2\Sigma^+$) was used to measure concentrations of ground state CN radicals. The experimental arrangement to achieve this is shown in Figure 11. The CN violet radiation used for the measurement was emitted from a microwave discharge through a slowly flowing 30:1:5 mixture of argon:nitrogen:methane at 1 torr pressure.[21] The discharge region was viewed side on through a 1 cm length rather than end-on to

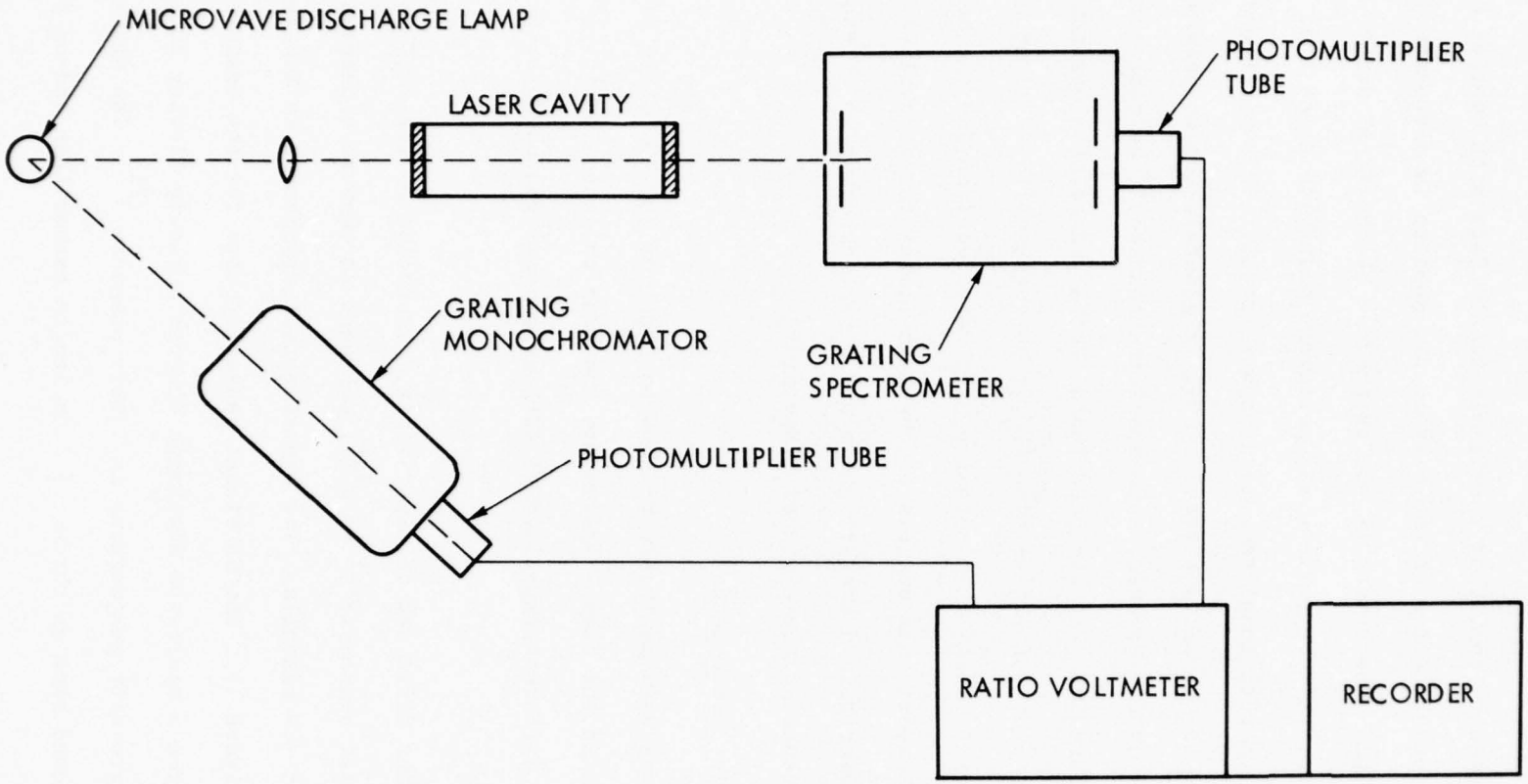

Figure 11. Absorption experiment to monitor CN($X^2\Sigma$ - $B^2\Sigma$) intensity.

minimize problems due to self-reversal. The lamp signal was monitored with the McPherson spectrometer. Changes in lamp signal with an without gas flowing in the laser cavity was used to measure absorption. A correction was made for CN violet emission from the cavity. An active length of 30 cm was used in these experiments.

For analysis of the data, the overall extinction coefficient calculated by Boden and Thrush[21] of $\sim 1 \times 10^{9}$ cm^{3} $mole^{-1}$ cm^{-1} was used. This gives only an estimate of the ground state. However, relative measurements under different experimental conditions are valid.

The second experimental arrangement is sketched in Figure 12 and a photograph is shown in Figure 13. This experiment is designed to give a direct measure of the absorption or gain in the $CN(A^{2}\Pi - X^{2}\Sigma^{+})$ red system. The source in this experiment is a cyanogen-deuterium-fluorine flame run under conditions where emission from the 0 - 1 and 0 - 2 bands of the CN red system was optimum and also where emission was most stable. The spectrometer was set so as to isolate individual rotational lines of the CN red system. A description of how the spectral lines were identified is presented in Appendixes A and B. The reference signal is chopped before passing through the active medium. Phase sensitive detection of this signal is then used to eliminate interference from the chemiluminescence signal from the active medium. The amount of absorption that can be detected by this technique is limited by the stability of the reference. It was possible to stabilize this so there were at most 2% fluctuations from the mean signal. This did not present a problem in the measurements since strong effects were observed.

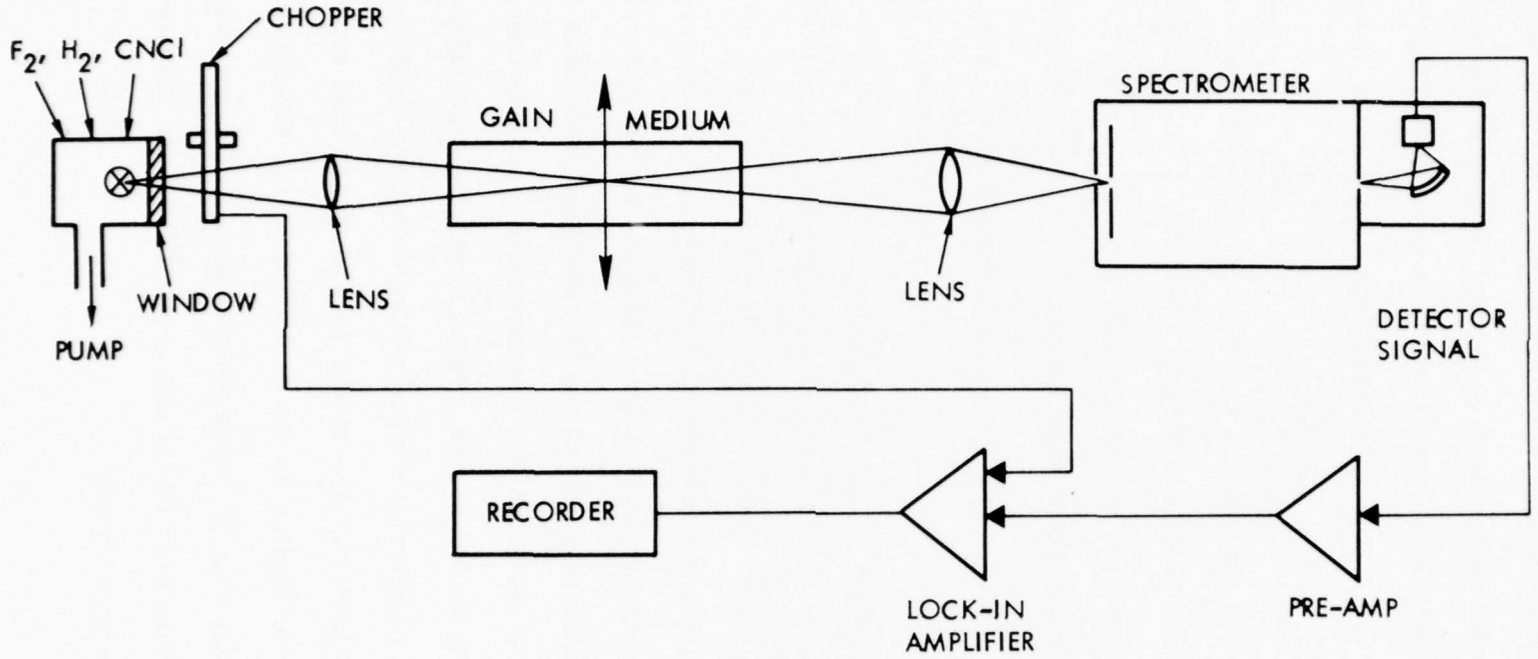

Figure 12. Schematic diagram for absorption/gain measurements.

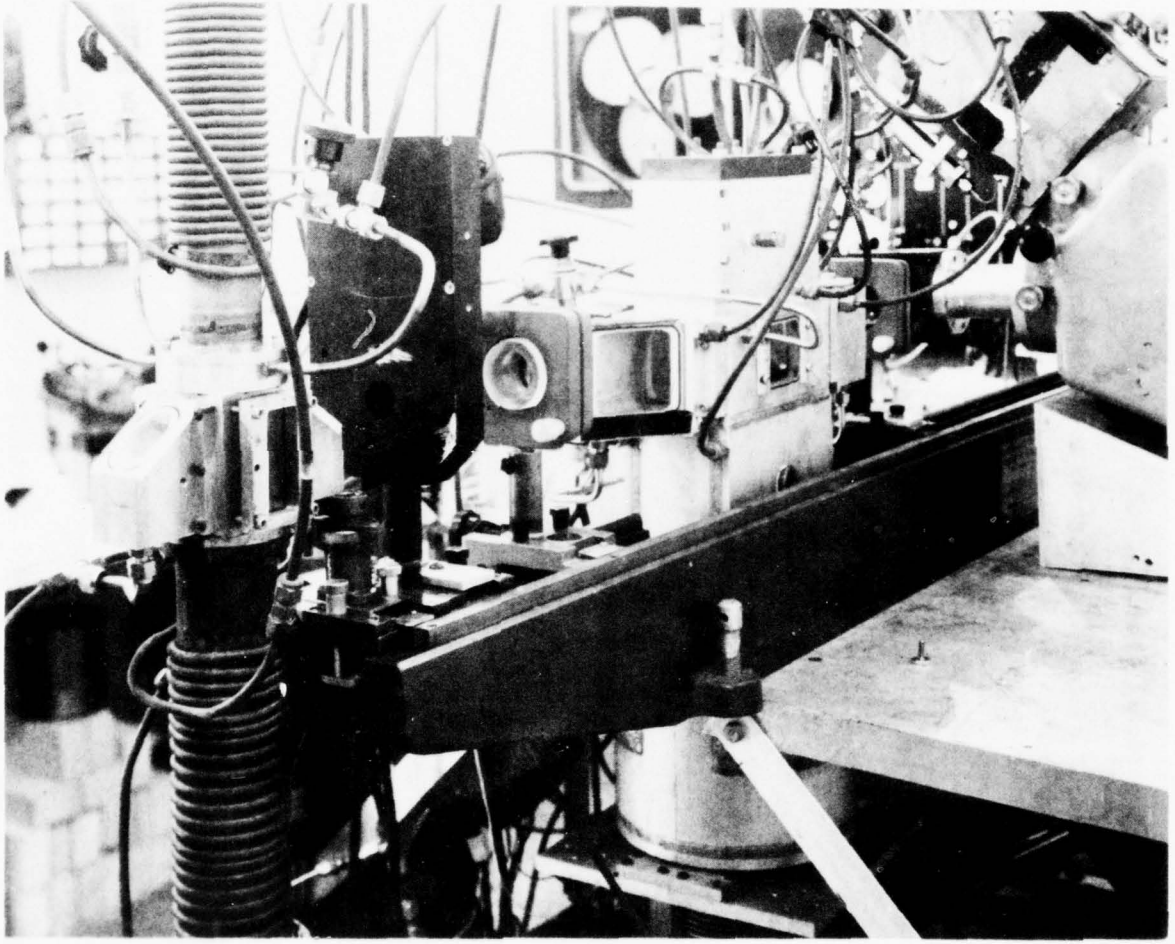

Figure 13. Photograph of absorption/gain experiment.

The analysis of an absorption experiment becomes greatly simplified if the probing source is a continuum and the absorbing lines of the medium being probed are optically thin; since in this case the amount of absorption or "effective width" of the absorbing line is linearly related to the lower level number density integral along the line of sight. In practice, it is difficult to establish ground state molecular concentration using a continuum source because of the conflicting requirements that all molecular lines within the chosen spectral bandpass be optically thin (or have a well-established curve of growth) and that the amount of absorption be measureably large (at least 1%). To increase the measurement sensitivity, one therefore wishes to reduce the spectral bandpass until it is of the same order as the width of the absorbing line, or to use a narrow line source centered at the appropriate wavelength as the probing source. Since the Doppler widths of the absorbing lines were generally 0.05 to 0.10 cm^{-1} for the CN red system (at 2000°K) and the limiting resolution of grating spectrometers of convenient size is about 1 cm^{-1}, highest measurement sensitivity is obtained by using a CN red line emitter as the probing source. Measurement sensitivity is thereby greatly improved and the spectrometer slit widths can then be opened to a degree sufficient to separate individual spectral lines. Therefore, this method was chosen to determine the CN (X) ground state concentration. Mitchell and Zemansky[22] give the formula for absorption by a given isolated rotational line as

$$A_K = \frac{k_{o,K}\,\ell}{(1+\alpha^2)^{1/2}} \qquad [4]$$

The above expression assumes both small absorption and Doppler broadening in both the source and absorption medium. In the above, ℓ is the path

length and α is the ratio of Doppler widths in the source and in the absorbing CN and equals the square root of the ratio of corresponding translational temperatures. $k_{o,K}$ is the absorption coefficient for the line and is equal to[18]

$$k_{o,K} = \left(\frac{\ln 2}{\pi}\right)^{1/2} \frac{N\lambda^2}{4\pi\tau\Delta\nu_a} \frac{q_{v',v''}}{Q_{v''}} \frac{S_K}{Q_R} \exp\left(-\frac{K(K+1)}{Q_R}\right) \quad [5]$$

Where N is the total lower state number density, $q_{v',v''}$ is the Franck-condon factor for the vibrational transition, S_K is the rotational line strength, Q_R and Q_V are rotational and vibrational partition functions at the medium temperature, τ is the lifetime of the electronic transition and ν_a is the Doppler width of the absorbing lines. Numerical evaluation of Equation [5] for K = 15 of the Q_{11} branch CN(A - X) system gives

$$k_{o,15} = 1 \times 10^{-15} \cdot N \quad [6]$$

Equations [4] and [6] can be combined to allow computation of the number density from the measured absorption.

To compute a CN ground state concentration from Equations [4] - [6] several requirements need to be fulfilled. First, of course, is an accurate measurement of absorption, A_K, for a particular spectral line. Considerable effort was spent identifying individual lines of the CN red band $\Delta V = -1$ and $\Delta V = -2$ sequences at 1.4 and 2.0 microns in the CN burner light source. Rotational lines in the Q_{11} branch of the particular vibrational band which were separated from the nearest line by at least 0.5 cm^{-1} were used as the probing lines. A discussion of the lines used is presented in Appendix C. A second requirement is that both the source and absorbing

medium be truly Doppler-broadened, and that the corresponding width ratio α be known.

Considerations of Doppler width and pressure broadening coefficients lead to the conclusion that Doppler half-widths should exceed the collision broadening half-width by about one order of magnitude at T = 2000 K° and pressures of 10 to 100 torr.

The Doppler width (full width at half-maximum) is given by

$$\frac{\Delta W_D}{W_O} = \frac{2\sqrt{R\ln 2}}{c} \sqrt{\frac{T}{M}} \approx 6.10^{-6} \qquad [7]$$

while collision width is given by the classical Lorentz expression

$$\Delta W_L = \frac{2}{\pi c} \sigma_L^2 N \sqrt{2\pi RT\left(\frac{1}{M_1} + \frac{1}{M_2}\right)} \qquad [8]$$

where M_1 and M_2 are molecular weights of CN and its principal collision partner, N the total number density, and σ_L^2 is an "optical" collision cross section which generally is about 5.10^{-15} cm^2. Typical values for ΔW_D are 5.10^{-2} cm^{-1} at 1.4μ (V' - V" = -1) and 9.10^{-2} cm^{-1} at 6900 Å (V' - V" = 3). The value of ΔW_L is therefore about $1.7.10^{-3}$ cm^{-1} at 10 torr and $8.5.10^{-3}$ cm^{-1} at 50 torr. The assumption of Doppler broadening is therefore justified at the burner and absorber pressures and low optical depths encountered in the absorption experiment. However, it is still important to establish that the burner emission lines are not self-reversed due to a cool absorbing layer near the window.

To obtain increased confidence in the validity of the Doppler broadening assumption, an attempt was made to spectrally resolve the true width of an isolated spectral line, using a scanning Fabray-Perot interferometer. Available interferometer plates necessitated that the

measurement be made using visible lines in the wavelength region 6000 - 7000 Å. A spectrum of the burner in this region is shown in Figure 14. At these wavelengths, the finesse F (ratio of free spectral range to spectral resolution) was only about 7. The available interferometer plates had peak reflectivity (98%) and finesse ($\sim$ 30) in the region 4500 - 5500 Å. A plate spacing of t = 2.5 cm was initially chosen to provide a free spectral range of

$$F_W = \frac{1}{2t} = 0.2 \text{ cm}^{-1} \qquad [9]$$

and a spectral resolution of $\left(\frac{F_W}{F}\right) \approx .03 \text{ cm}^{-1}$, somewhat less than the expected Doppler width. When this was done using a 4, 0 spectral line at 6293 Å, no fringe pattern was observed. (The 6293 Å line had been isolated by a grating spectrometer with $\sim$ 2 cm^{-1} resolution placed in front of the Fabray-Perot). At that point it appeared that a pure spectral line had not been chosen and that there was more than one component to the chosen "line". The "washing out" of the fringe pattern when the interferometer plates were scanned at high resolution was attributed to the presence of these two components. To confirm this interpretation, the interferometer plate separation was reduced to 2 mm, resulting in a free spectral range of 2.5 cm^{-1} and a spectral resolution of about 0.5 cm^{-1}. This was insufficient to resolve Doppler profiles but sufficient to resolve narrowly spaced lines. A resulting interferogram obtained with this plate spacing is shown in Figure 15. The separation of the two components in this case is indicated to be about 0.8 cm^{-1}. The unequal heights of the two components tends to confirm that two separate spectral lines were present.

For the reasons stated above, the interferometric measurements

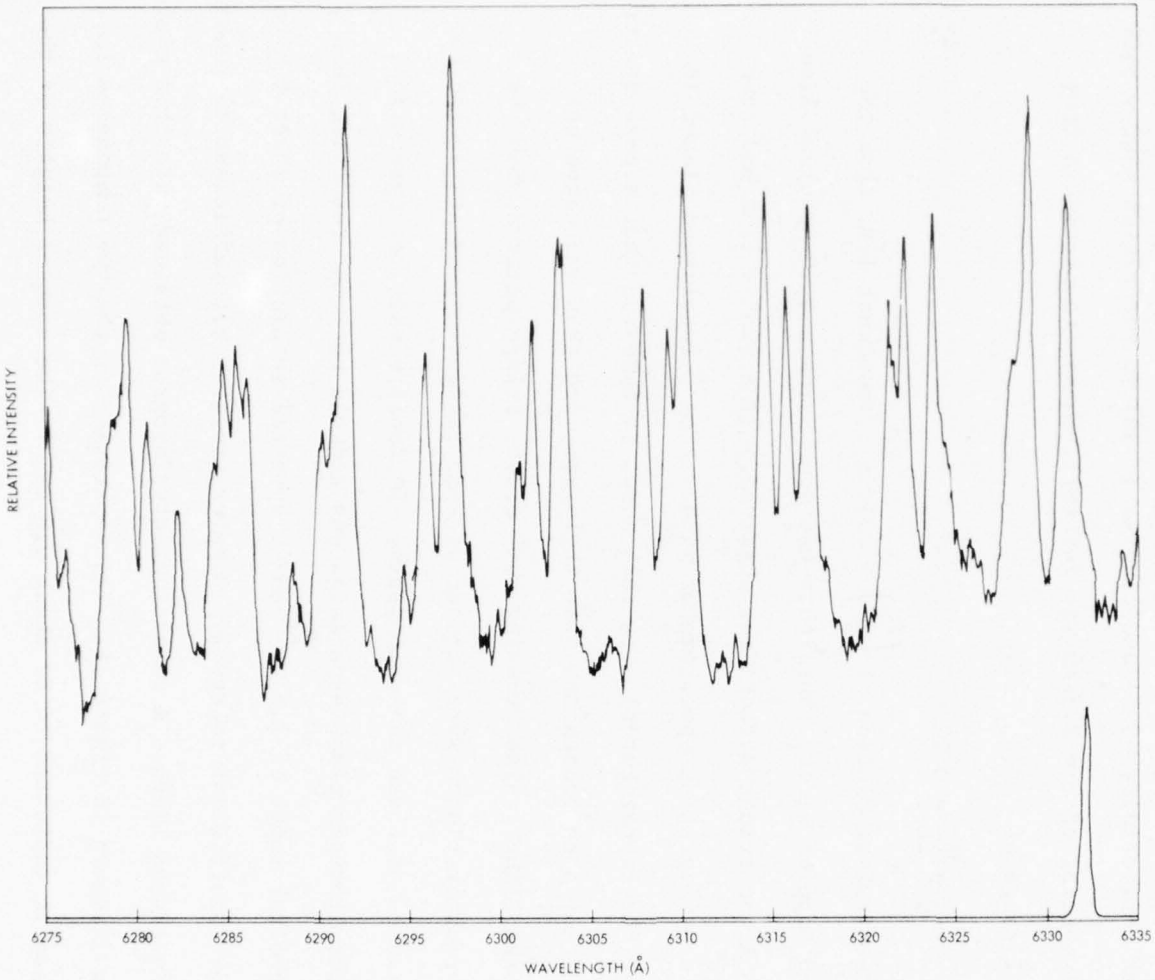

Figure 14. Spectrum of CN burner in 6000 - 7000 Å spectral region.

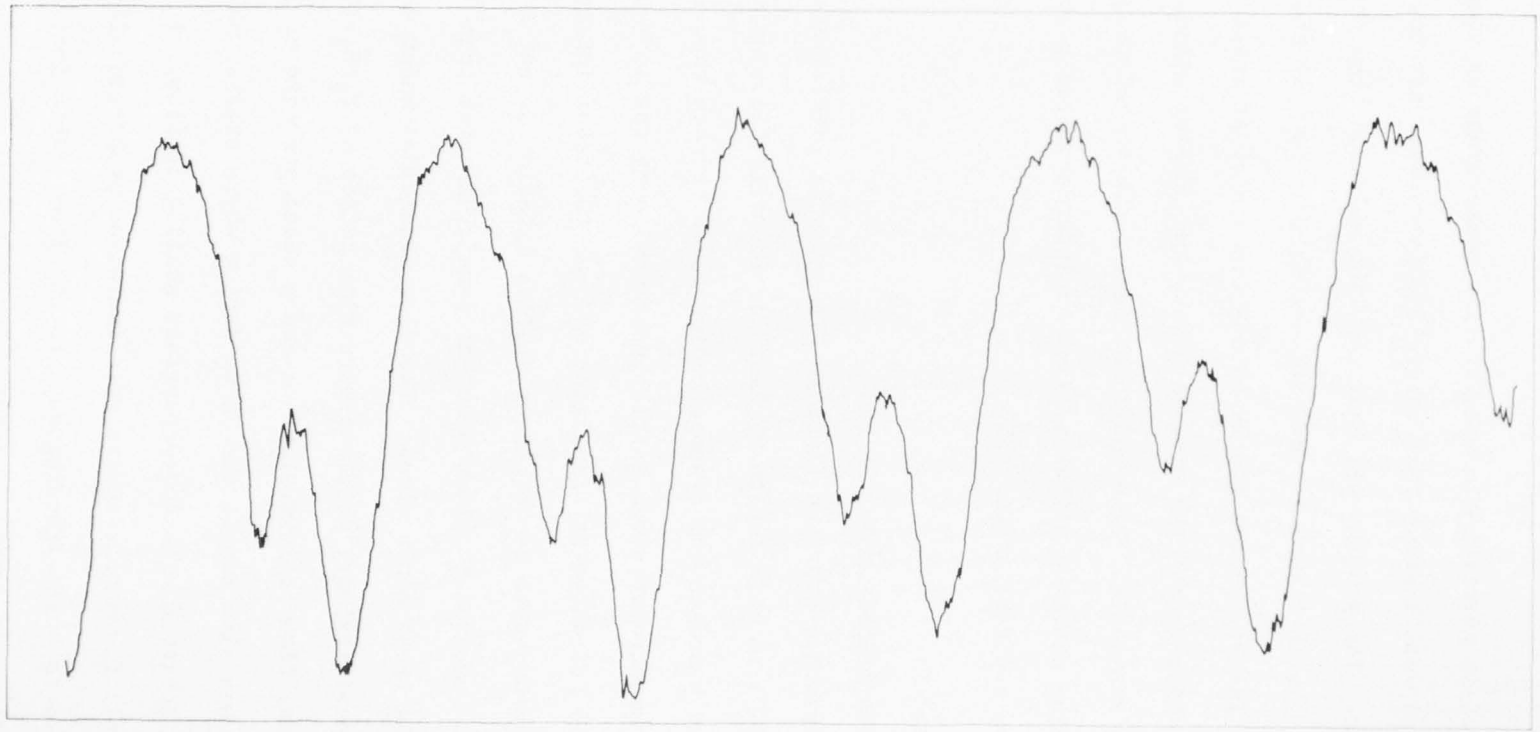

Figure 15. Interferogram obtained at 6293 Å with a free spectral range of 2.5 cm^{-1} and a spectral resolution of 0.5 cm^{-1}.

were unsuccessful in permitting a quantitative measurement of source Doppler width and verification that harmful self-reversal are not present in the CN burner. The problem was that the line selected from the high resolution spectrum in Figure 14 was not spectrally pure. If the present line were used, interferometer plates with a finesse of at least 50 would be required to resolve both the spectral lines and Doppler widths. Such plates were not available. Time and funds were depleted before additional measurements using either a different line or interferometer plates with a higher finesse could be attempted.

2.3.2 Results

General Chemiluminescence Observations

a) Cyanogen-hydrogen-fluorine flames. The initial observations were made in the 3 cm gain length HF laser device with fluorine in the precombustor and hydrogen and cyanogen being added through the cavity injector. The spectrometer was initially scanned over the $\Delta v = 0$ bands using the cooled PbS detector. Integration over the total intensity in these bands combined with use of the radiative lifetime of the $A^2\Pi$ state of CN of 7 μsec combined to yield a number density greater than 10^{15} molecules/cm^3 in these bands alone. The flow conditions under which these number densities were obtained were flow ratios of F_2:H_2:$(CN)_2$ of 9:4:1, a total flow of 10 mmoles/sec and a total pressure of 30 torr. The experiment was also run in the 30 cm device where similar number densities were achieved with an appropriate scaling of flow. It was found that if all flows of reagents were increased proportionally the intensity tended to scale proportionate to the flow. This indicates that the experiment is easily scalable.

b) Cyanogen-deuterium-fluorine flames. Substitution of deuterium for hydrogen was attempted to aid in clarifying the mechanism by which the CN emission was being produced. If an excited state of a hydrogen compound were responsible for the excited state production, substitution of deuterium should result in lower emission intensities. It was found that identical flows of deuterium produced identical CN ($A^2\Pi$) state emissions. In other experiments, D_2 was sometimes substituted for H_2 to eliminate HF 1st overtone emissions.

c) Cyanogen chloride-hydrogen/deuterium-fluorine flames. It was found that cyanogen chloride could be substituted for cyanogen. However, a somewhat higher flow of CNCl in proportion to hydrogen and fluorine was required to produce optimum emission intensities. With cyanogen chloride, optimum intensity was obtained at much lower pressures than with cyanogen. Figure 16 shows a plot of emission intensity versus total cavity pressure. Pressure was varied by reducing the pumping speed through use of a valve. This plot showed a dramatic increase in intensity at $\sim$ 6 torr total pressure, reaching a maximum at 8 torr and then dropping again at 10 torr. Under conditions where less cyanogen chloride was used, an increase in intensity with pressure up to 50 torr was observed. Thus, the ratio of reactant flows has a pronounced effect on how intensity varies with total pressure.

Under certain conditions the cyanogen-fluorine flame could be maintained with no hydrogen. However, under these conditions, emission intensities dropped dramatically. These flows were also critical as evidenced by the fact that the emission could be turned on and off by turning the hydrogen on and off. The cyanogen-hydrogen flame was almost

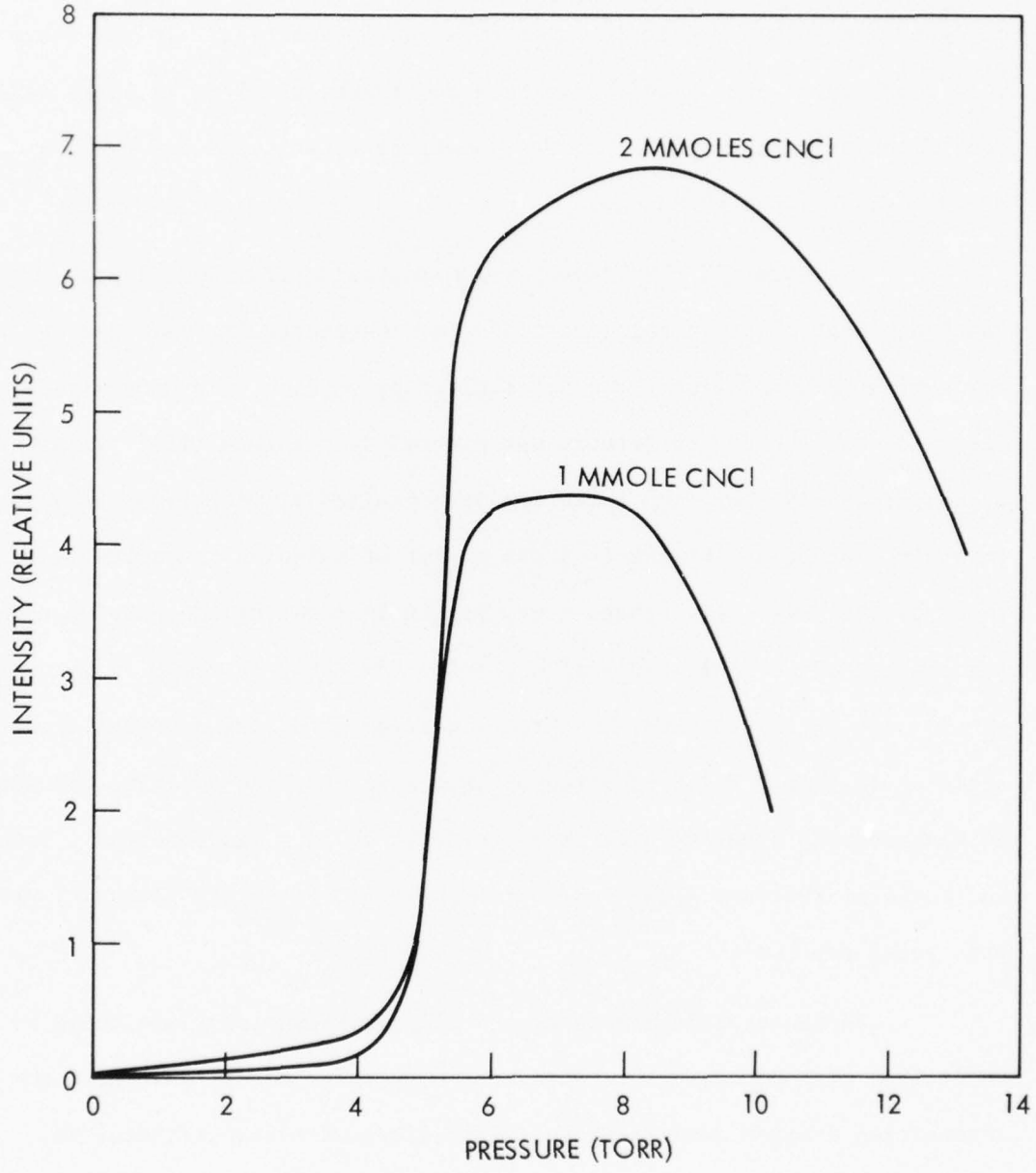

Figure 16. Plot of CN emission intensity versus cavity pressure.

impossible to maintain under the flow conditions used without some fluorine.

d) Hydrogen cyanide-hydrogen/deuterium-fluorine flames. One experiment was run in which hydrogen cyanide was substituted for cyanogen. The hydrogen cyanide used was synthesized by dropping sulfuric acid on sodium cyanide. Consequently, only a small quantity of HCN was available for experimentation. A commercial supplier for HCN has recently been found and additional HCN ordered. However, the gas wasn't obtained in time to allow further data to be obtained for this program. The fluorine-deuterium-hydrogen cyanide flame visually resembled the flames obtained with fluorine, deuterium and cyanogen or cyanogen chloride. That is, the same blinding red chemiluminescence was observed. No quantitative spectral measurements were made since the amount of hydrogen cyanide available did not allow sufficient run time.

e) Effect of diluent. Helium diluent was added to the flow to determine its effect on chemiluminescence intensities. When it was added with either the fluorine or with the CNCl, it caused the emission intensity in the (0-0) band to decrease. However, when it was added as a window purge the intensity initially increased with helium flow. However, an optimum diluent flow was reached after which the intensity decreased with helium flow. The initial increase may have been due to elimination of CN ground state in the window vicinity. No studies of the dependence of medium temperature on diluent flow were conducted. However, a definite temperature decrease with increased diluent flow is expected. Further experiments would be needed to determine whether the observed intensity decrease with diluent flow was due to kinetics or to strictly equilibrium thermal effects. For this study the variation of

emission intensity with temperature as well as a corresponding equilibrium analysis is needed.

Temperature Measurements

Temperatures were determined from HF/DF chemiluminescence data as described in section 2.3.1. A typical plot of vibrational state number density versus $J(J + 1)$ is shown in Figure 17 for DF chemiluminescence in a $F_2/D_2/CNCl$ flame situation. Spectra were taken under conditions where emission from the A-X band of CN was maximum. The flows were 8×10^{-3} moles/sec fluorine, 4×10^{-3} moles/sec deuterium and 2×10^{-3} moles/sec cyanogen chloride with a cavity pressure of 8.5 torr. Plots were made for both the (1-0) and (2-1) vibrational transitions. Analysis of the slopes of these plots gives rotational temperatures of 2920°K in the (1-0) band and 3070°K in the (2-1). Thus, this measurement indicates that the kinetic temperature in the medium is near 3000°K. Temperature measurements in $F_2/H_2/(CN)_2$ flames were also made. One set of data gave a temperature of 4000 ± 600°K. This data was obtained using a tape drive data acquisition system and had more scatter than normally encountered in HF chemiluminescent data. However, these temperatures are higher than any that had been measured in HF chemical lasers so a direct comparison is difficult to make. It was found that the temperature did vary with pressure. At a cavity pressure of 2 torr an HF rotational temperature of 1800°K was obtained.

It was difficult to obtain CN and HF/DF chemiluminescence data simultaneously since the two spectrometers required for this measurement were not readily available. However, qualitative estimates indicate an increase in temperature with CN(A-X) chemiluminescent intensity.

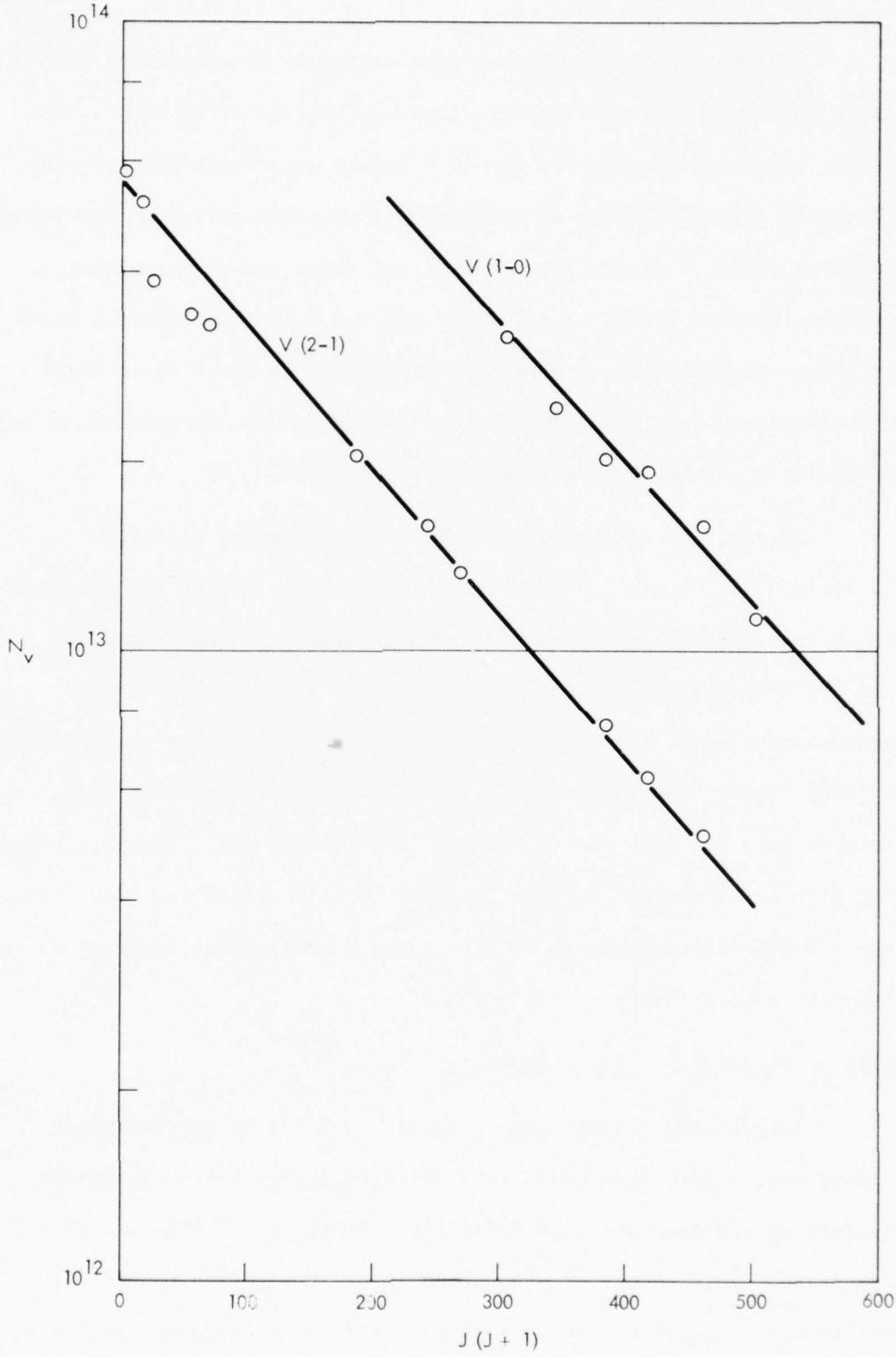

Figure 17. Plot of DF vibrational state number density versus J (J + 1).

CN rotational temperatures were estimated by comparison with computer generated synthetic spectra (see Appendix B) of CN ($A^2\Pi - X^2\Sigma$) emission. Computed spectra for the $\Delta v = 1$ band at several temperatures are shown in Figure 18 while an experimental spectrum corrected for detector response is shown in Figure 19. Best fit of these two spectra gives a temperature between 2700°K and 3000°K for the $F_2/D_2/CNCl$ flame. Other spectra run under similar experimental conditions as those where HF/DF chemiluminescence data were obtained gave temperatures which agree within error limits with the HF/DF rotational temperatures.

CN vibrational temperatures were determined by plotting $N_{v'} \propto I(v', v'')/\nu^4 \cdot g(v', v'')$ versus v' where $I(v', v'')$ is the measured emission intensity of a given vibrational transition between levels v' and v'', ν is the frequency of the transition and $g(v', v'')$ is the Franck-Condon factor. Such a plot is shown in Figure 20 for the optimized $F_2/D_2/CNCl$ flame. The anharmonicity terms were not included in this plot. Plots were made for both the $\Delta v = 3$ and $\Delta v = 4$ sequences. They are offset on the plot by a constant factor. Analysis of the slopes of these plots gave a vibrational temperature of 4180°K which is somewhat higher than the DF rotational temperature.

Absorption of $CN(B^2\Sigma^+ \rightarrow X^2\Sigma^+)$ Radiation

Very strong absorptions of $CN(B^2\Sigma^+ \rightarrow X^2\Sigma^+)$ by the medium in the laser cavity were observed. With the $F_2/D_2/(CN)_2$ system optimized to maximum CN red band emission intensity, almost 95% of the lamp signal was observed. This amount of absorption is obviously in a non-linear absorption region. Thus, the extinction coefficient discussed in 2.3.1 cannot be used to estimate number densities. However, a lower limit of

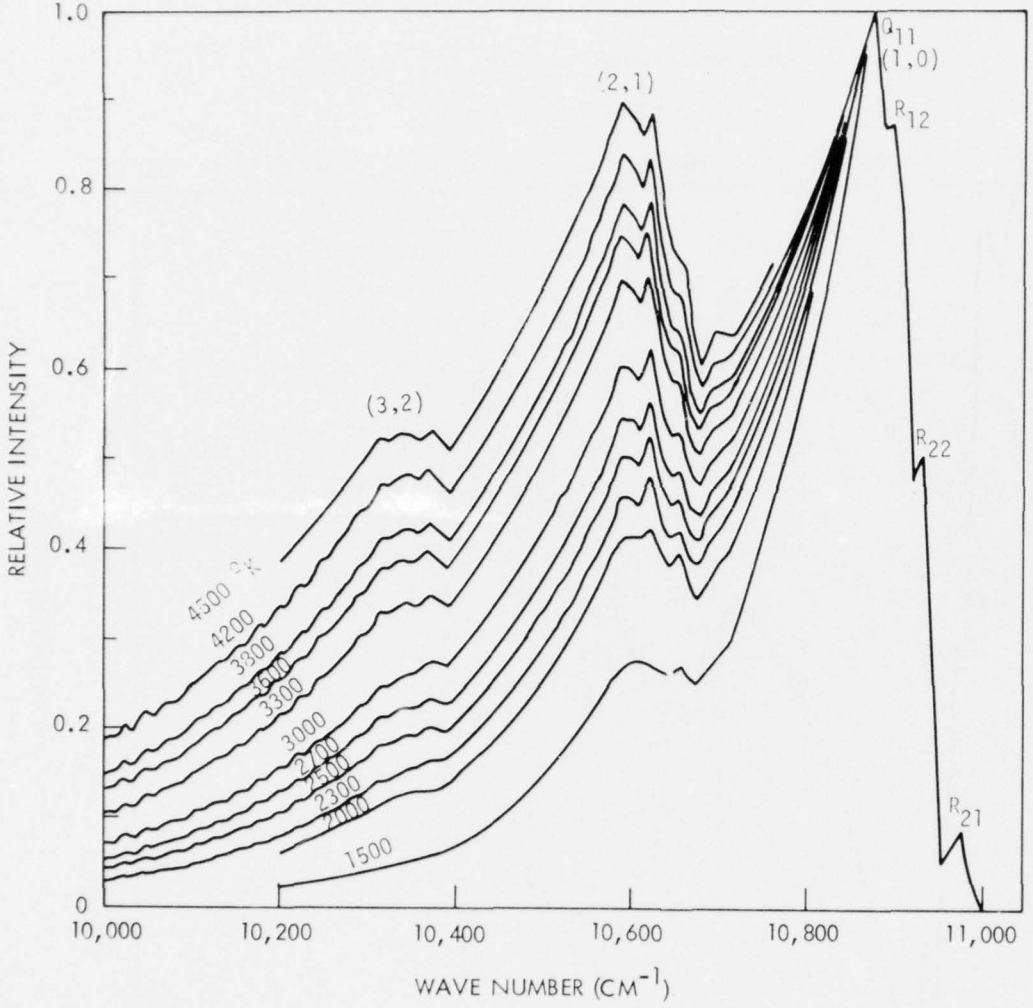

Figure 18. Synthetic Spectra for the $\Delta v = 1$ transition of CN(A-X) band emission

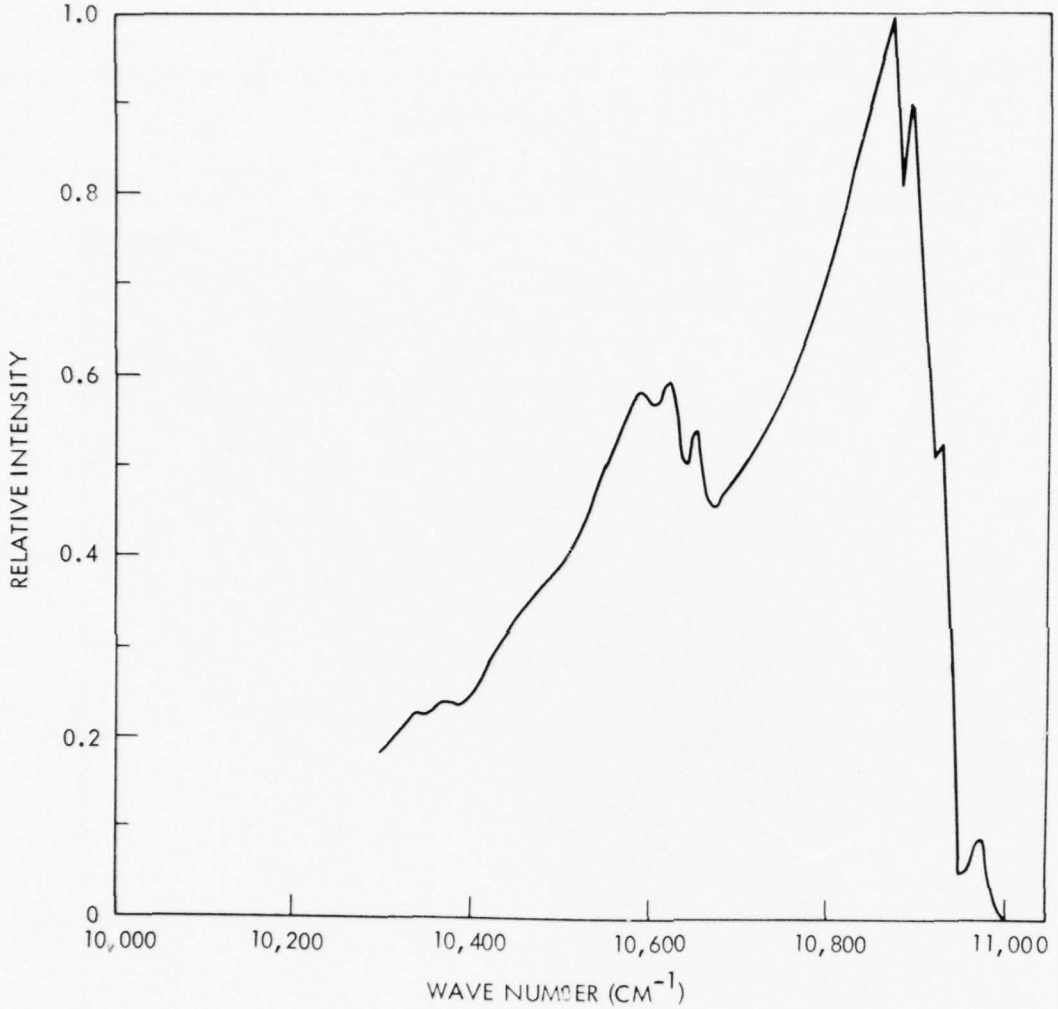

Figure 19. Experimental spectrum.

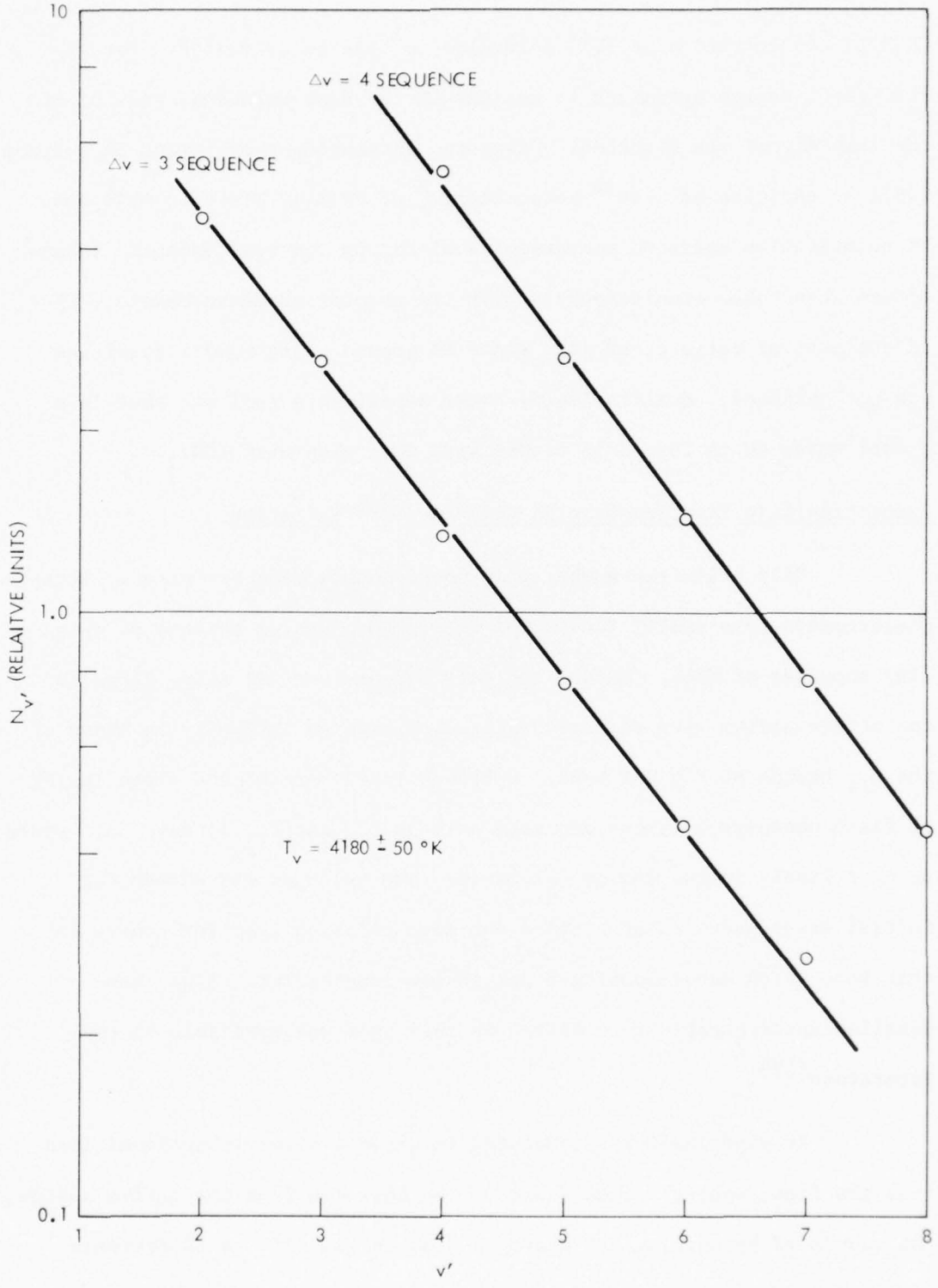

Figure 20. Determine vibrational temperature of CN.

$CN(X^2\Sigma)$ concentration of 10^{14} molecules/cm^3 can be estimated. For the $F_2/D_2/CNCl$ system optimized to maximum CN red band emission, only 5% of the lamp signal was absorbed. Using the extinction coefficient in section 2.3.1 an estimate of $\sim 10^{13}$ molecules/cm^3 of $CN(X^2\Sigma)$ state is obtained. No quantitative emission measurements of the CN red band emission intensities were taken simultaneously with the absorption measurements. Thus, an estimate of ratio of excited state to ground state number densities was not obtained. Qualitatively, these experiments indicate that less ground state CN is formed in flames with CNCl than with $(CN)_2$.

Absorption/Gain Experiments with $CN(A^2\Pi - X^2\Sigma)$ Radiation

Only a limited number gain measurements were performed. Those measurements were restricted to the $F_2/D_2/(CN)_2$ system because of dwindling supplies of CNCl. Before the gain measurement was made, flows to the active medium were adjusted to produce maximum intensity in lines of the Q_{11} branch of the 0-1 band. Q branch lines were chosen since lasing in flash photolysis lasers occurred only on Q_{11} and P_{11} lines. Gain would be most likely in the 0-2 or 0-1 bands. The 0-1 band was chosen for initial experiments because there was more emission from the source in this band which made choosing a particular line easier. Also, more detailed spectroscopic information on this band was available in the literature[19].

An experiment was conducted in which a given vibrational line from the flame source was monitored. The emission from the active medium was modulated by turning the hydrogen flow on and off. A 5% decrease in the flame signal was observed when the hydrogen was on and the medium emitting over when the hydrogen was off, i.e. absorption rather than gain

was observed. This shows the presence of more ground state than excited state for the particular transition monitored. Several other rotational lines were monitored with equivalent absorptions being observed. Several different flow conditions were tried. Under some conditions a smaller amount of absorption was observed. However, emission intensities had also decreased. A similar effect was observed on addition of helium diluent to the cavity. Decreases in absorption corresponded to decreases in emission intensity. The experimental arrangement did not permit simultaneous acquisition of quantitative emission and absorption data. Consequently, absolute densities of upper and lower state densities could not be determined. These measurements would allow absolute determination of upper and lower state number densities and allow determination of the ratio of these densities. This would indicate by how large a factor the lower state number densities would have to be decreased for the upper state number densities increased to reach a condition of positive gain.

2.3.3 Discussion

The intense chemiluminescence observed in the $F_2/H_2(D_2)/R\text{-}CN$ (R = CN, Cl or H) experiments described previously was totally unexpected on the basis of kinetic and thermodynamic analysis. To illustrate this, it is profitable to write down a series of possible reactions to determine if they could be responsible for the observed emission. Some possible reactions are:

$$F + H_2 \rightarrow HF(v) + H \quad (40)$$

$$H + F_2 \rightarrow HF(v) + F \quad (41)$$

$$F + RCN \rightarrow RF + CN \quad (42)$$

$$F + RCN \rightarrow FCN + R \quad (43)$$

$$H + RCN \rightarrow HR + CN \quad (44)$$

$$H + RCN \rightarrow HCN + R \quad (45)$$

$$H + FCN \rightarrow HF + CN \quad (46)$$

$$H + FCN \rightarrow HCN + F \quad (47)$$

$$F + HCN \rightarrow HF + CN \quad (48)$$

$$F + HCN \rightarrow FCN + H \quad (49)$$

$$HF(v \geq 3) + CN \rightarrow HF(v - 3) + CN^* \quad (50)$$

$$H + H + CN \rightarrow H_2 + CN^* \quad (51)$$

$$F + F + CN \rightarrow F_2 + CN^* \quad (52)$$

$$H + F + CN \rightarrow HF + CN^* \quad (53)$$

The above list does not include reactions of CN radicals. To analyze the above list it is useful to compare the dissociation energies of the various cyanogen-containing compounds. Most recent measurements[24] give the following values, all in units of kcal $mole^{-1}$: D(H - CN) = 120, D(Cl - CN) = 97, D(NC - CN) = 128, D(F - CN) $\leq$ 111 and D(C - N) = 184. Reactions (40) and (41) are inherent in all systems and may liberate the necessary energy or atoms that lead to eventual production of the CN red band emission. Reactions (46) - (49) are possible in the system for all R's. Reactions (46) and (48) are exothermic by $\sim$ 19 kcal/mole and 10 kcal/mole respectively. These reactions could produce CN radicals in their ground state but are not energetic enough to form a CN excited state. An experiment in which F-atoms were produced in the precombustor and HCN added downstream showed no CN red band emission, confirming this conclusion. Reaction (49) is not allowed by energy considerations but reaction (47) could occur, contributing to a possible chain reaction. The occurrence of reaction (50) tends to be discounted by the fact that substitution of

D_2 for H_2 still results in production of CN red band emission. Reaction (51) has been shown to be responsible for CN emission in reactions of hydrogen atoms with cyanogen chloride[25]. However, the intensity produced and spectral distributions do not match the present experimental results. Equations (52) and (53) are similar when R = H. Reactions (42) and (43) are the same as (48) and (49). The reaction to form H_2 and CN, reaction (44) is not energetically allowed. When R = CN, the situation becomes even worse since none of the reactions from (42) - (45) are energetically allowed. With R = Cl, reactions (43) and (45) are energetically allowed. They form HCN and FCN which could produce CN radicals by reactions (46) and (48).

At best, the above mechanism can explain some formation of CN radicals in their ground state but does not suffice to explain the large number densities of $A^2\Pi$ state observed experimentally. The possibility that a completely thermal mechanism was responsible for the emission occurs. Equilibrium calculations using the NEST computer code[26] were performed to determine what could occur thermally. These calculations predicted less than 3% of the R-CN would be converted to CN radicals at 3000°K. This number combined with populations predicted from Boltzmann statistics indicates that this mechanism will not explain the observed excited state number densities. A much higher temperature than determined experimentally would be needed to account for the observations.

No feasible mechanism for the CN excited state production could be deduced from the above discussion. Possibly, some non-equilibrium process which is not understood at present is responsible.

Because of the large number densities of excited state of CN

produced chemically, the system appears to be one of the most promising yet considered. The $A^2\Pi$ state of CN meets the requirements for a lasing species and the overall system meets requirements of pure chemical production and scalability. Although the initial gain measurements were not encouraging, insufficient data was obtained to completely evaluate the system. Because of the potential of this system for CW chemical laser production, it should be investigated further.

2.4 Transfer Studies Utilizing $CO(a^3\Pi)$ and $CS(a^3\Pi)$ As Energy Transfer Donors

The initial metastable species suggested for use as energy transfer donors were $CO(a^3\Pi)$ and $CS(a^3\Pi)$. These species should be formed by reactions of the type

$$C(^3P) + O_2(^3\Sigma) \rightarrow CO(a^3\Pi) + O(^3P) \quad (54)$$

$$C(^3P) + N_2O(^1\Sigma) \rightarrow CO(a^3\Pi) + N_2(X^1\Sigma) \quad (55)$$

$$C(^3P) + OCS(^1\Sigma) \rightarrow CS(a^3\Pi) + CO(X^1\Sigma) \quad (56)$$

These reactions are expected to proceed on the basis of spin correlation rules. Since the atoms involved are relatively light, spin conservation rules should be obeyed for these reactions. The $CO(a^3\Pi)$ state has a radiative lifetime of 7 msec and is 6eV above the ground state. The kinetics of the reaction of carbon atoms with oxygen have been studied and the reaction is known to proceed rapidly. However, no study of the resulting state of CO has been conducted. There is some agreement in the literature as to whether the above reaction proceeds as indicated. Johnson and Fontijn[27] proposed the above reaction to account for $CO(a^3\Pi)$ emission observed in flames. However, Ogryzlo et al [28] observed no $CO(a^3\Pi)$ emission from reaction (54) in their experiments. There are no literature reports of studies of reaction (55). Spin and energy considerations indicate that N_2 could be formed in several excited triplet states including $A^3\Sigma_u^+$, $B^3\Pi_g$, and $B^3\Sigma_u^-$ if CO is formed in its ground electronic state. The $a^3\Pi$ state of CS was shown to be formed by reaction (56) in a previous program.[29] This state has an energy 3.42 eV above the ground state. The lifetime is not well known although some measurements indicate it is of the order of 1 msec.[29]

The most promising energy transfer acceptor for the $CO(a^3\Pi)$ state is nitric oxide in its $B^2\Pi$ state. Comparison of energy levels of CO and NO shows that the $A^2\Sigma^+$ and $B^2\Pi$ states of NO are accessible for transfer from the $CO(a^3\Pi)$ state. In fact, there is experimental evidence that this transfer does occur[30] producing the $NO(A^2\Sigma^+)$ and $NO(B^2\Pi)$ states, i.e., the γ and β bands of NO in a ratio of from 1.5 to 2.0. The relative vibrational populations resulting from this transfer for NO(A,v' = 0,1,2) were 1.0:0.2,0.1 and for NO(B,v' = 0,1) were 1.0:0.2. Thus, the v' = 0 level is selectively populated by the transfer. The overall quenching rate of the CO Cameron band emission by NO was found to be very rapid with a rate constant of 2×10^{-10} cm^3 $molecule^{-1}$ sec^{-1}. There is some evidence that only 15% of this quenching goes into the NO A and B states although the method by which this was estimated was open to error. Hence, a range of rates for the transfer should be considered. The $B^2\Pi$ state is the most interesting state for consideration as a laser candidate. Its radiative lifetime of 3 μsec[31] puts it barely in the range of possibility as a chemical laser candidate. It also has the advantage that the most probable emission is from the v' = 0 level to the v'' = 6 level, creating a favorable population inversion for lasing. The V-RT rate for NO (v = 1) self-relaxation in the ground electronic state is 7.7×10^{-14} cm^3 $molecule^{-1}$ sec^{-1} whereas the v-v rate is 3.85×10^{-12} cm^2 $molecule^{-1}$ sec^{-1} [32]. No rates have been measured for the relaxation of the v = 6 rates. However, V-RT rates generally increase with increasing v'. Hence, the relaxation of the lower lasing level may be slow in comparison with the radiative lifetime in NO. This means that the lower state may not be depleted as rapidly as it is filled. This would reduce the lasing zone but would not

prevent lasing. The above initial considerations indicate that the $CO(a^3\Pi)$ - $NO(B^2\Pi)$ may be a viable lasing system.

The kinetics of the CO-NO transfer system can be considered to determine theoretical feasibility. The important reactions to be considered are listed below.

$$C + O_2 \rightarrow CO(a^3\Pi) + O \quad (57)$$

$$C + O_2 \rightarrow CO(X'\Sigma) + O \quad (58)$$

$$CO(a^3\Pi) + O_2 \rightarrow CO_2 + O \quad (59)$$

$$CO(a^3\Pi) + M \rightarrow CO + M \quad (60)$$

$$CO(a^3\Pi) + NO \rightarrow CO + NO(A^2\Pi) \quad (61)$$

$$CO(a^3\Pi) + NO \rightarrow CO + NO(B^2\Pi) \quad (62)$$

$$CO(a^3\Pi) + NO \rightarrow \text{other products} \quad (63)$$

$$NO(A^2\Pi) \rightarrow NO + h\nu \quad (64)$$

$$NO(B^2\Pi) \rightarrow NO + h\nu \quad (65)$$

The sum of rates of reactions (57) and (58) has been measured to be 3×10^{-11} cm^3 $molecule^{-1}$ sec^{-1} (33). For a first order calculation, it will be assumed that this is the rate of reaction (57). The rate of reaction (59) has been measured to be 1.4×10^{-10} cm^3 $molecule^{-1}$ sec^{-1} (34) whereas the rate of reaction (60) for M = Ar is 4×10^{-16} cm^3 $molecule^{-1}$ sec^{-1}. (34) The sum of rates (61), (62) and (63) has been measured to be 2×10^{-10} cm^3 $molecule^{-1}$ sec^{-1}. For a first order calcualtion, values of $k_{61} = 1.3 \times 10^{-10}$ cm^3 $molecule^{-1}$ sec^{-1} and $k_{62} = 6.7 \times 10^{-11}$ cm^3 $molecule^{-1}$ sec^{-1} are used. The rates of k_{64} and k_{65} correspond to the inverse of the radiative lifetime and are 5×10^6 sec^{-1} and 3.3×10^5 sec^{-1} respectively.

The rate equations corresponding to the above set of reactions were solved numerically using a Runge-Kutta integration scheme. Initial concentrations of C, O_2 and NO of 1×10^{16}, 1×10^{16} and 2×10^{16} molecules/cm^3 were used. The results of the calculation are plotted in Figure 21. This plot shows that a number density of $NO(B^2\Pi)$ of 7×10^{14} molecules/cc can be obtained at these initial concentrations.

The number densities in the upper and lower states can be related to the optical gain α by the following gain equation:

$$\alpha = \left(\frac{\ln 2}{\pi}\right)^{1/2} \frac{g' A}{4\pi} \frac{\lambda^2}{\Delta\nu} \left(\frac{N'_{v', J'}}{g'} - \frac{N''_{v'', J''}}{g''}\right) \qquad [10]$$

where g' and g'' are the degeneracies of the levels, A is the Einstein coefficient for spontaneous emission at the wavelength λ with an effective line width of $\Delta\nu$, and v and J are the vibrational and rotational quantum numbers.

A single prime designates the excited electronic state and a double prime the lower electronic state. The above expression can be approximately evaluated for the v' = 0 to v'' = 6 transition in the NO(B-X) system at 2892.6Å. To do this, a Doppler line-width is assumed, all vibration in the upper state is assumed to be in the v' = 0 state and a Boltzmann distribution of rotational levels is assumed. This evaluation gives:

$$\alpha \backsimeq 1.5 \times 10^{-17} \left(N_{v'} - 1/2 N_{v''}\right) \text{ cm}^{-1} \qquad [11]$$

The above expression indicates that for a 10^{-3} cm^{-1} gain, the quantity

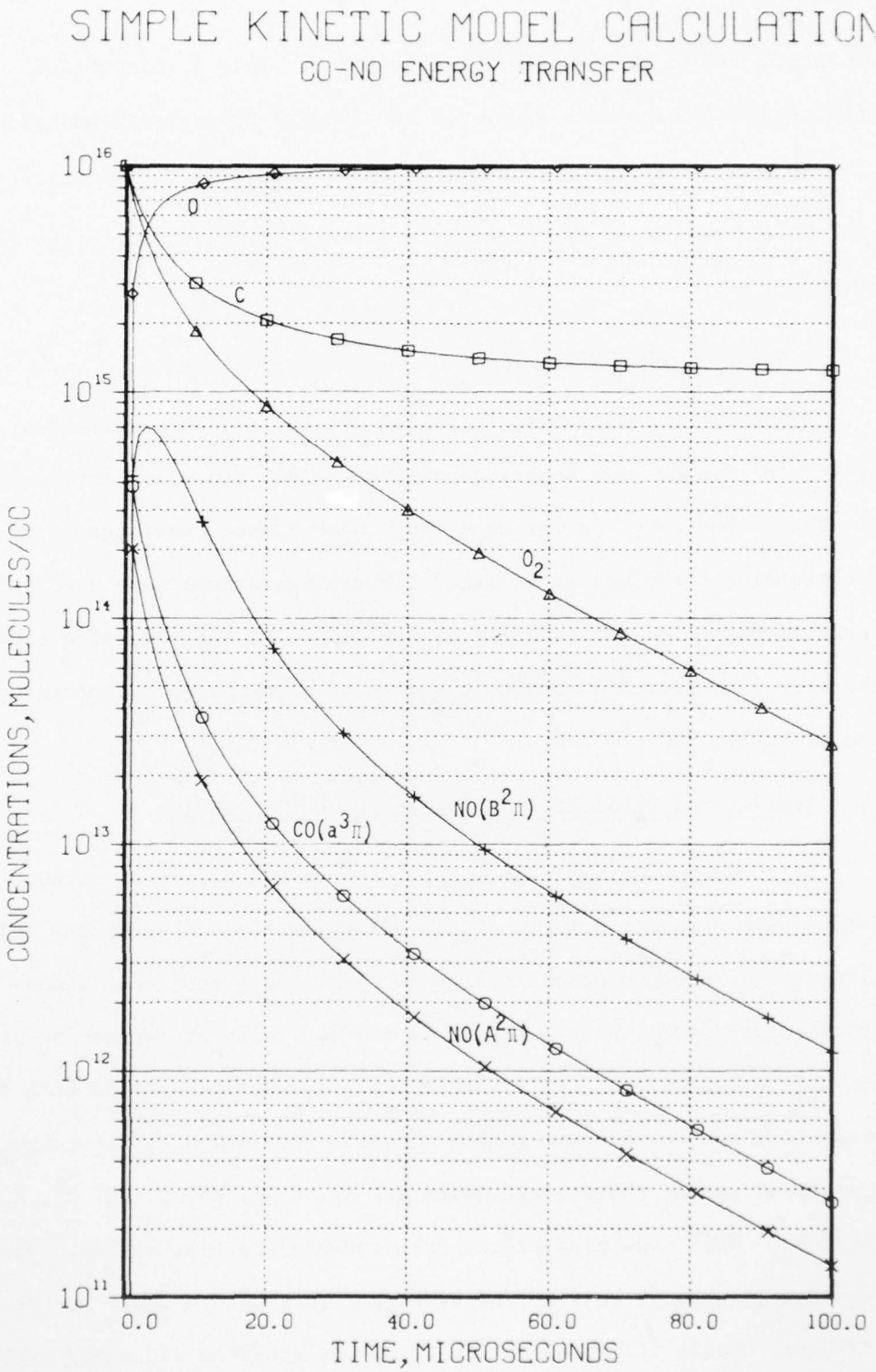

Figure 21. Plot of concentrations of important species versus time for $CO(a^3\Pi)$ to NO energy transfer.

in parenthesis should be 6.9×10^{13} molecules/cc. This is higher than the number density calculated above for the initial concentrations assumed.

Thus this system could be feasible if sufficient carbon can be produced. A discussion of experiments to do this is presented in the following section.

2.4.1 Atomic Carbon Production

A necessary requirement for using $CO(a^3\Pi)$ as donor molecules is the ability to produce high number densities ($\sim 10^{15}$ atoms/cc) of atomic carbon. The method proposed for achieving these number densities is heating carbon containing compounds in an arc. Two configurations were used for these experiments. The first used a powder feeder to feed graphite powder into the arc. The second involved injecting a gaseous carbon containing compound directly into the arc.

2.4.1.1 Theoretical Prediction of Carbon Production in Arc

Prior to performing experimental arc tests, potential carbon atom donors were screened using the NEST (N-Element-System) computer code. The calculations were performed assuming a total pressure of one atmosphere in the arc-plenum and a molar mixture of 0.9 diluent (either N_2 or Ar) with 0.1 carbon donor. All possible products were considered with the code predicting concentrations of each product. For example, using C_2N_2, and Ar as input gases, the product gases are Ar, C_2N_2, CN, C, C_2, C_3, C_4, C_5, N, and N_2. NEST code predictions for condensed carbon, allene, tetrafluoroethylene, carbonyl sulfide and cyanogen are shown in Table II for argon diluent. Table III shows calculations for ethylene and acetylene with both Ar and N_2 diluents. Note in this table that 2×10^{-8} mole/cm^3

Table 2

NEST Calculation (Equilibrium Plenum)

p_o = 1.0 atm Mole fraction Ar = 0.90 Mole fraction carbon donor = 0.10

Carbon Donor	Arc Power / Total Flowrate (kW/gm-sec)	T_o (°K)	Atomic Carbon Concentration (Particles/cm^3)
Condensed Carbon	4	3975	4.4×10^{16}
Allene (C_3H_4)	2	2480	5.0×10^{12}
	4	3352	5.2×10^{15}
	6	3815	3.6×10^{16}
Tetrafluoroethylene (C_2F_4)	2	2732	1.1×10^{14}
	4	3093	1.3×10^{15}
	6	3972	4.9×10^{16}
Carbonyl Sulfide (COS)	2	3090	3.4×10^{10}
	4	5606	1.5×10^{16}
	6	6753	6.1×10^{16}
Cyanogen (C_2N_2)	2	2948	6.1×10^{14}
	4	4288	1.1×10^{17}
	6	5472	2.0×10^{17}

TABLE 3. NEST CALCULATION (EQUILIBRIUM PLENUM)

INPUT SPECIES	90% Ar + 10% C_2H_4		90% Ar + 10% C_2H_2		90% N_2 + 10% C_2H_4		90% N_2 + 10% C_2H_2	
CHAMBER PRESSURE = 1 ATM								
Arc Power into Gas kW/g/sec	4	6	4	6	4	6	4	6
Gas Temperature °K	3370	4050	3870	4540	2800	3220	3140	3580
MOLAR CONCENTRATIONS (MOL/CM^3)								
Ar	$3 \cdot 10^{-6}$	$2 \cdot 10^{-6}$	$3 \cdot 10^{-6}$	$2 \cdot 10^{-6}$	--	--	--	--
N_2	--	--	--	--	$3 \cdot 10^{-6}$	$3 \cdot 10^{-6}$	$3 \cdot 10^{-6}$	$3 \cdot 10^{-6}$
H	$4 \cdot 10^{-7}$	$7 \cdot 10^{-7}$	$4 \cdot 10^{-8}$	$4 \cdot 10^{-7}$	$1 \cdot 10^{-7}$	$3 \cdot 10^{-7}$	$2 \cdot 10^{-7}$	$3 \cdot 10^{-7}$
H_2	$2 \cdot 10^{-7}$	$5 \cdot 10^{-8}$	$3 \cdot 10^{-8}$	$5 \cdot 10^{-9}$	$6 \cdot 10^{-7}$	$3 \cdot 10^{-8}$	$1 \cdot 10^{-7}$	$4 \cdot 10^{-8}$
C_2H	$2 \cdot 10^{-7}$	$1 \cdot 10^{-7}$	$1 \cdot 10^{-7}$	$3 \cdot 10^{-9}$	$2 \cdot 10^{-8}$	$1 \cdot 10^{-7}$	$6 \cdot 10^{-8}$	$1 \cdot 10^{-7}$
C_2H_2	$4 \cdot 10^{-8}$	$3 \cdot 10^{-9}$	$2 \cdot 10^{-8}$	$< 10^{-9}$	$2 \cdot 10^{-8}$	$3 \cdot 10^{-8}$	$2 \cdot 10^{-8}$	$6 \cdot 10^{-9}$
HCN	--	--	--	--	$2 \cdot 10^{-7}$	$3 \cdot 10^{-7}$	$2 \cdot 10^{-7}$	$1 \cdot 10^{-7}$
CN	--	--	--	--	$1 \cdot 10^{-9}$	$1 \cdot 10^{-8}$	$1 \cdot 10^{-8}$	$5 \cdot 10^{-8}$
C_2N_2	--	--	--	--	$1 \cdot 10^{-9}$	$5 \cdot 10^{-9}$	$5 \cdot 10^{-9}$	$9 \cdot 10^{-9}$
C	$4 \cdot 10^{-9}$	$7 \cdot 10^{-8}$	$5 \cdot 10^{-8}$	$2 \cdot 10^{-7}$	$< 10^{-9}$	$2 \cdot 10^{-9}$	$< 10^{-9}$	$1 \cdot 10^{-8}$
C_2	$4 \cdot 10^{-9}$	$3 \cdot 10^{-8}$	$3 \cdot 10^{-8}$	$6 \cdot 10^{-7}$	$< 10^{-9}$	$1 \cdot 10^{-9}$	$< 10^{-9}$	$1 \cdot 10^{-8}$
C_3	$1 \cdot 10^{-8}$	$2 \cdot 10^{-8}$	$5 \cdot 10^{-8}$	$1 \cdot 10^{-8}$	$< 10^{-9}$	$5 \cdot 10^{-9}$	$2 \cdot 10^{-9}$	$3 \cdot 10^{-8}$

corresponds to 10^{16} carbon atoms/cm^3 for comparison with Table II. For both tables, expansion through a supersonic nozzle will decrease concentrations by a factor of approximately 30. Study of the tables indicates that condensed carbon is perhaps the most desirable carbon donor both because of high number densities produced and because it is "clean", yielding a smaller number and quantity of product gases. Carbonyl sulfide and cyanogen both produced high concentrations of carbon atoms but also produced side products that are quenchers of metastable species. Acetylene and ethylene were both good donors with acetylene being somewhat better. Also, the CH_n side products should not interfere with metastable formation and quenching. The calculations also showed that nitrogen diluent is undesirable because of formation of nitrogen compounds at the expense of atomic carbon. These calculations indicate that number densities of carbon produced in experiments with nitrogen can be expected to be more than an order of magnitude lower than those with argon. In some experiments reported in the next section, nitrogen was used with a resulting decrease in concentrations.

2.2.1.2 Description of the Arc Experiments

An arc-driven HF laser facility which was slightly modified for this program was used for experiments. Figure 22a shows the basic experimental configuration and Figure 22b shows an expanded view of the mixing region.

Two different arc jet configurations were used in these experiments. The first was the BA1007 configuration of the Thermal Dynamics Corporation F-80 arc jet head. Both nitrogen and argon diluents were tested with this configuration. With nitrogen, an equilibrium injector-

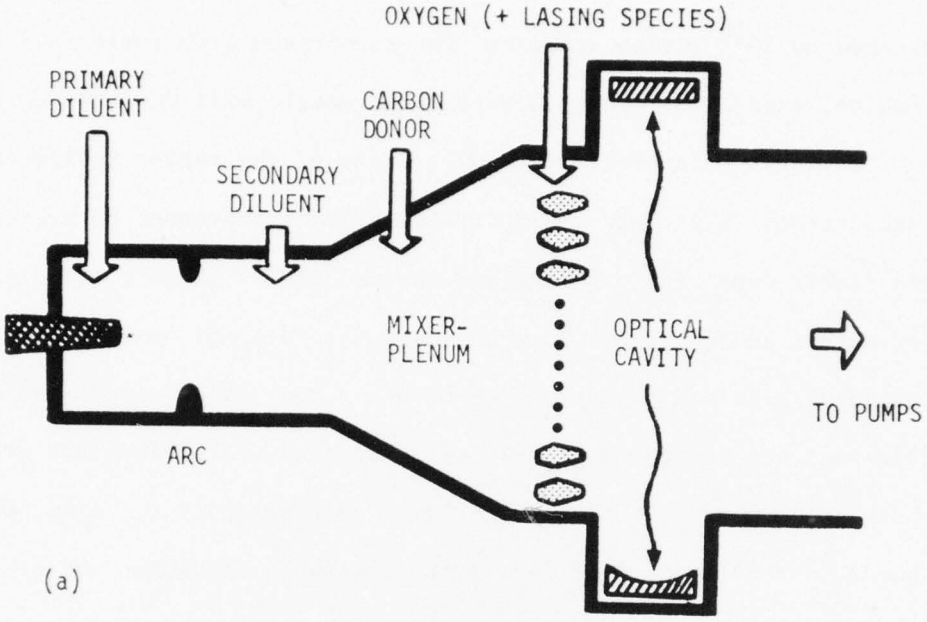

(a)

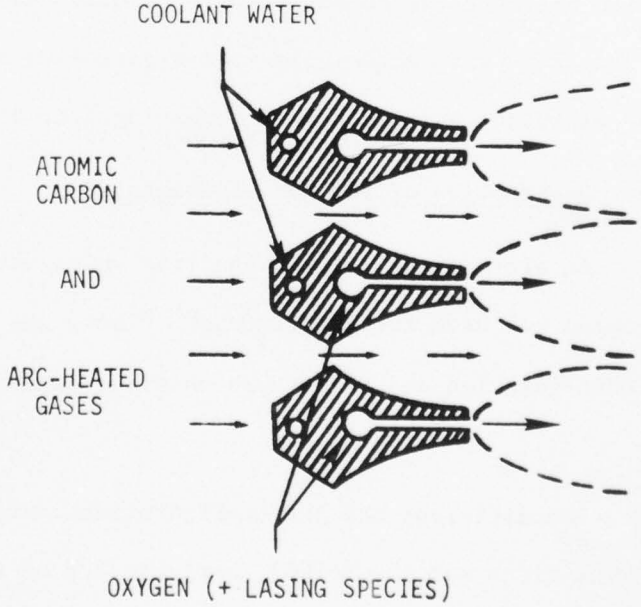

(b)

Figure 22. a) Basic arc configuration.

b) Expanded view of the mining region.

throat stagnation temperature of 3800°K was achieved. With argon, the maximum temperature achieved was 2000°K. Modifications in design of cooling passages could increase this. The CA-1218 configuration of the F-80 arc head was also tested. Similar temperatures to those with the BA1007 configuration were achieved.

For some tests an Aerospace Corporation Mesa III arc jet head was used. This arc had the advantage that the particulate could be injected with the diluent directly into the arc jet head. An equilibrium injector-throat stagnation temperature of 2300°K was achieved with this arc using argon diluent.

A commercial powder-feeder (Thermal Dynamic model #PI-2001) was used for testing graphite powder as a carbon atom source. Other carbon donors were gaseous and could be directly injected into the arc plenum.

Four nozzle arrays were used for mixing the appropriate oxidizer with the arc effluent. There were:

- a 1" x 7" CL-II (15:1 expansion ratio, 36 mixing zones)
- a 1/2" x 7" CL-II (15:1 expansion ratio, 36 mixing zones)
- a 1/2" x 7" HCl-I (7:1 expansion ratio, 72 mixing zones)
- a showerhead nozzle (axisymmetric sonic orifices, 36 mixing zones
- a 1/2" x 7" slot injector (12:1 expansion ratio, 72 mixing holes)

Several of these nozzle arrays are shown in Figure 23.

2.4.1.3 Carbon Atom Diagnostics

The primary technique for monitoring carbon atoms was atomic

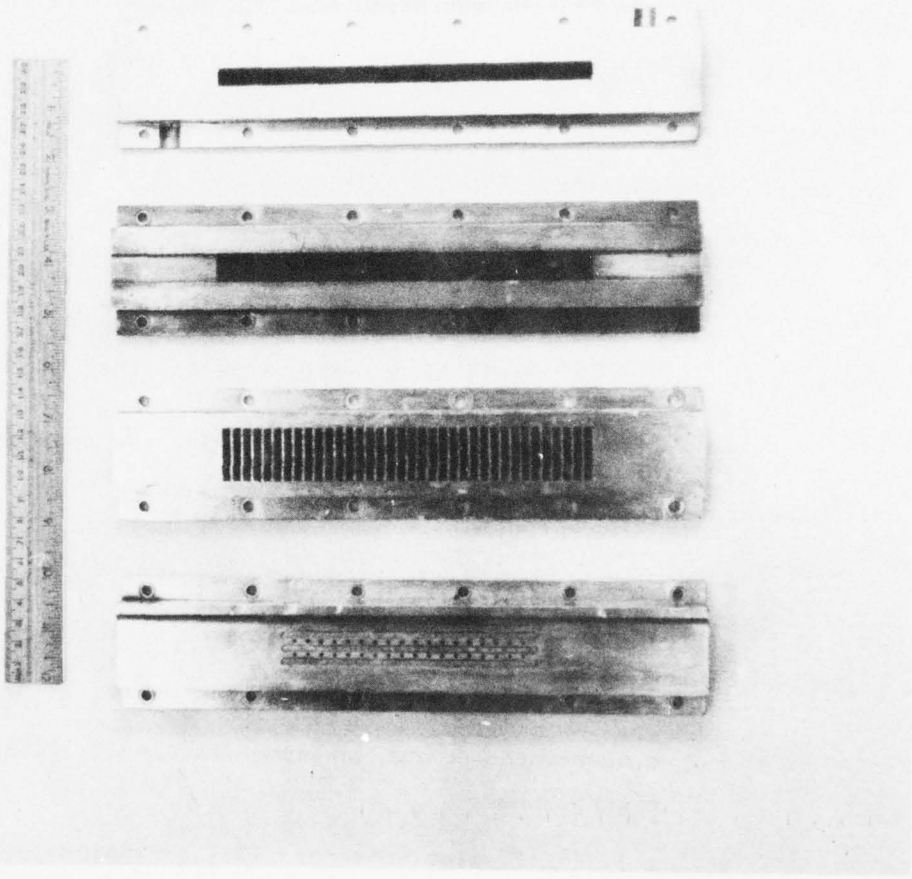

Figure 23. Photograph of several available nozzle arrays. From top:
1) 1/2" x 7" slot injector
2) 1/2" x 7" HCl-I
3) 1" x 7" Cl-II
4) Showerhead

resonance absorption. An atomic carbon lamp was used as the source for these studies with the attenuation of the carbon line at 1656Å being monitored. A 0.3m McPherson spectrometer with a 2400 line/mm grating blazed at 1500Å was used to monitor the carbon lamp emission. The interior of the spectrometer was evacuated to less than .01 torr pressure to avoid air absorption of the carbon line. Ultraviolet grade sapphire windows and optics were used throughout to transmit the 1656Å wavelength. A photograph of the resonance lamp setup is shown in Figure 24 and a photograph of the spectrometer setup is shown in Figure 25. In Figure 25, the arc is located to the right whereas the cavity is located to the left. The lamp could be aligned in positions 3 cm and 20 cm downstream from the injector nozzle.

For some experiments, enough carbon was produced to completely absorb the resonance lamp emission. Under these circumstances, a titration with O_2 or COS was used. Either emission of $CO(a^3\Pi)$ or $CS(a^3\Pi)$ or change in absorption of the carbon resonance line was used as the detection technique. These experiments will be discussed later.

2.4.1.4 Powdered Graphite as Carbon Atom Donor

Puratek G-1059, 325 mesh, 99.9% pure graphite was added to the arc effluent through a powder feeder for these tests. Initial tests were performed using a nitrogen diluent with the F-80 arc. When the graphite was turned on, intense white luminescence was observed in the flow. Careful observation indicated that a high flux of white hot particles was responsible for the observed luminescence. Observation of the injector and mixer after the test revealed a black deposit. The deposit was observed

AD-A031 010 TRW SYSTEMS GROUP REDONDO BEACH CALIF F/G 20/5
ADVANCED LASER CONCEPTS.(U)
JUL 76 J A BETTS, J F FRIICHTENICHT F29601-73-A-0036
UNCLASSIFIED AFWL-TR-75-289 NL

2 of 2
ADA031010




END
DATE FILMED
11 -76

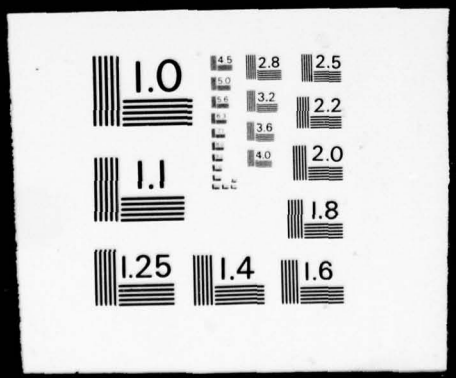

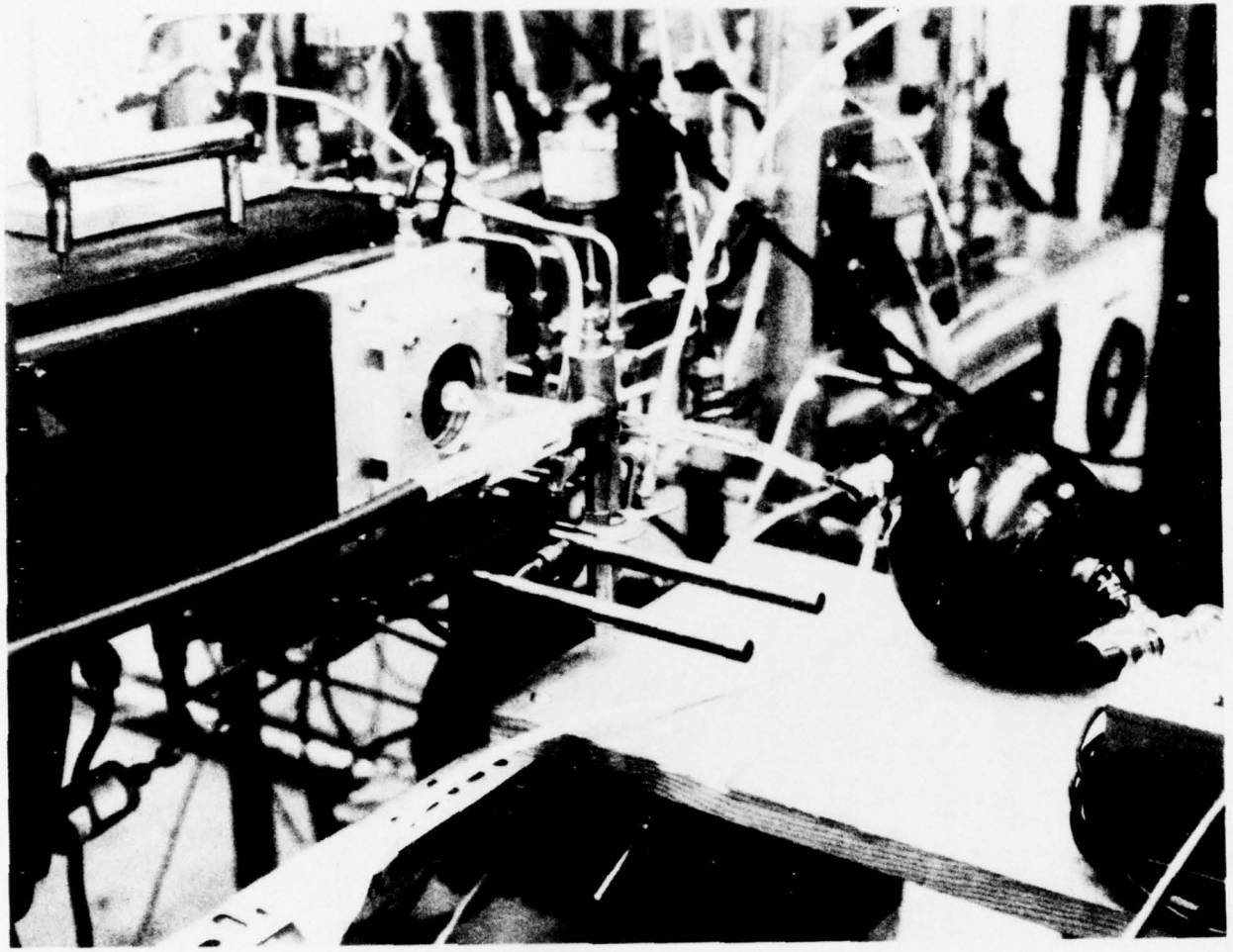

Figure 24. Photograph of carbon resonance lamp.

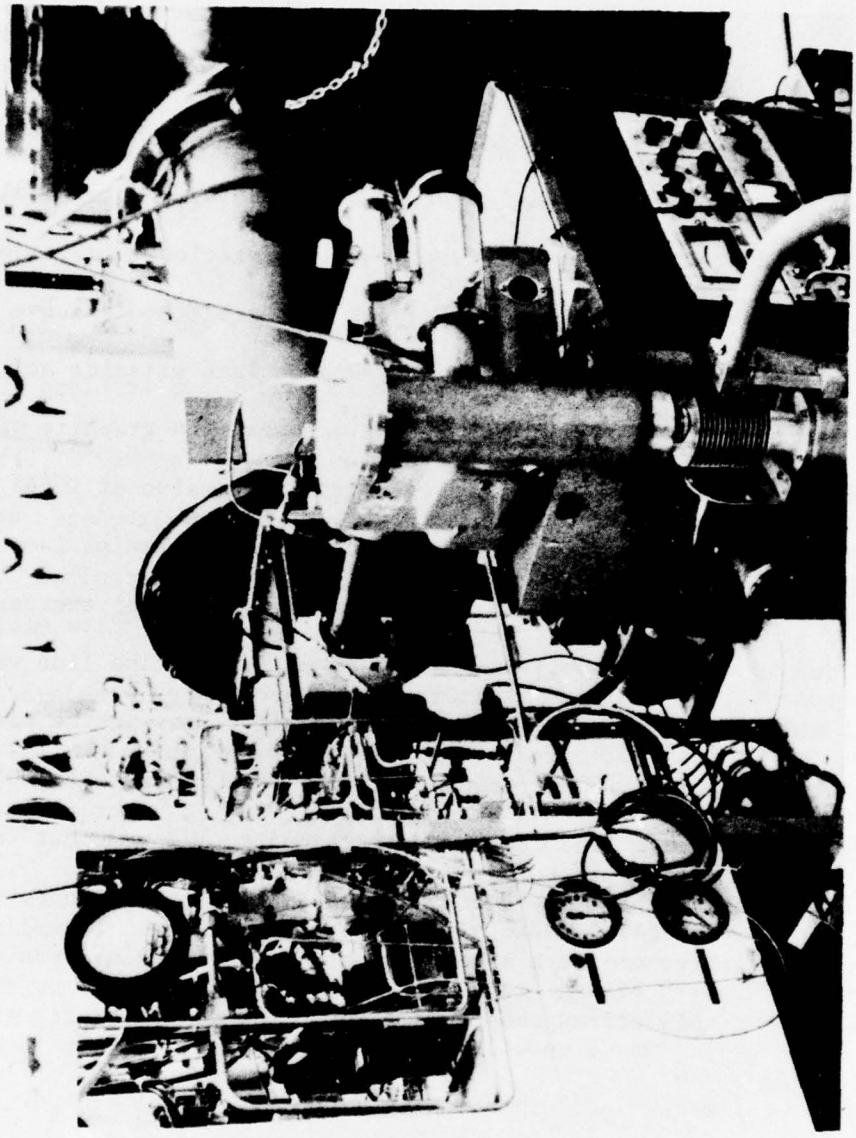

Figure 25. Photograph of spectrometer setup.

under a 50 power microscope. The particles in the deposit were more rounded than in the original graphite sample,indicating partial melting.

The next tests were run using the Mesa arc with argon diluent. Again, a large flux of white particles was observed when graphite powder was injected. Emission spectra were recorded which showed the emission was due to blackbody radiation from the hot carbon particles. Addition of oxygen to the carbon stream changed the peak of the blackbody curve indicating a temperature drop. The carbon resonance lamp emission at 1656Å was then monitored. Absorption was observed when the graphite was injected. However, increasing arc power resulted in emission at 1656Å in the arc, making the carbon lamp diagnostic useless. A bromine lamp with a line at 1633Å was monitored to verify that absorption of the carbon line was due to carbon atoms. No absorption of the bromine line was observed. It should be noted that there were impurity lines in the carbon lamp which overlap with the 1656Å-resonance line. This means that 100% absorption of the resonance line does not correspond to $I/I_o = 0$ but rather to $I/I_o = 0.45$. Measurements were made which optimized carbon absorption. A point was reached where complete absorption of the carbon line occurred. It is estimated that this corresponds to a carbon atom concentration greater than 10^{13} atoms/cm^3.

Because of the intense visible emission from particulate matter, it was felt that study of chemiluminescent reactions in the near ultraviolet and visible spectral ranges would be impossible. Because of this, it was decided that a gaseous carbon donor would be preferable for spectroscopic studies. Thus, the powder feeder was abandoned at this point in favor of a gaseous carbon donor.

2.4.1.5 Gaseous Carbon Donors

Ethylene was chosen as the first gaseous carbon donor for study. It was selected because of its high vapor pressure, availability and the NEST code predictions. The first tests were conducted using the Mesa III arc with an argon diluent. Addition of ethylene caused complete absorption of the carbon resonance line. Also the arc effluent appeared blue upon addition of ethylene. A scan of the spectrum showed a weak continum beginning at 2750Å and extending to longer wavelengths. Swan band lines of C_2 could be recognized as sitting on top of the continuum.

Several tests were conducted using different nozzles. Initial tests were performed with the showerhead nozzle. With this nozzle the color coming from the arc was not uniform,and the intensity decreased rapidly with distance from the nozzle. The CL-II and HCL-I nozzles were next tested. More intense and uniform luminescence was observed with these nozzles. However, carbon deposited in the slits between the injector ports causing a rapid decrease in the amount of carbon entering the cavity with time. Spectroscopic measurements showed emission intensities decreased by more than a factor of 2 in one minute, making reproducibility difficult to obtain. The nozzles could be cleaned by running oxygen through the arc for several minutes between runs. This allowed several sets of data to be taken before it was necessary to dismantle the system for cleaning.

Because the conventional nozzles clogged with carbon so rapidly, a nozzle designed to avoid this problem was built on TRW IR&D funds. This nozzle contained a single slot with the hole injectors along the slot to allow addition of oxidizer. The nozzle is pictured in Figure 26. It has

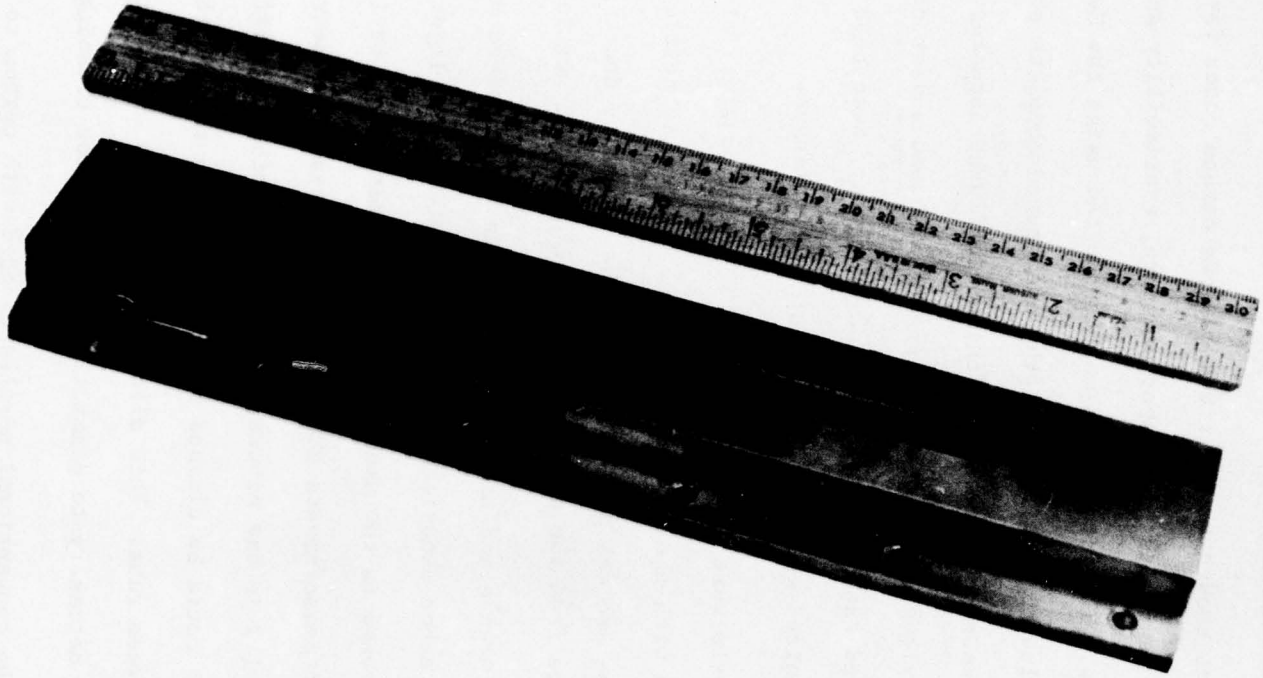

Figure 26. Improved nozzle design.

a 12:1 expansion ratio with 72 injector holes. When this nozzle was used a new problem arose. The nozzle is water-cooled to prevent it from melting in the hot arc effluent. However, because of the facility design, a cooled surface area of 1" x 7" of the nozzle was exposed to the flow from the arc. The slot area open to the flow was only 2% of the total nozzle area. Thus, a large part of the flow from the arc contacted a cold surface and deposited much of its carbon on the surface. Only a small fraction of the flow passed through the nozzle without first hitting a cold surface meaning only a small fraction of the carbon produced in the arc entered the cavity. Emissions observed with this nozzle were much less intense than those observed with either the CL-II or HCL-I nozzles.

Emission spectra were observed under several conditions. With only argon in the arc, the gas stream appeared purple and numerous atomic argon lines were observable. Upon addition of ethylene, the argon lines were suppressed and a continuum beginning at 2750Å was observed. When oxygen was added through the mixing nozzle CO Cameron bands were observed between 2000 and 2500Å. However, the blue color still persisted. Carbonyl sulfide was then added through the mixer. $CS(A^1\Pi)$ and $CS(a^3\Pi)$ emissions were observed under these circumstances. No quantitative measurements were made because of the rapid clogging of the nozzle with carbon. Acetylene and methane were also used as carbon atom donors. Theoretical calculations indicated that acetylene should be superior to ethylene. However, experimental tests using $CS(a^3\Pi)$ emission intensity from the C + OCS reaction as an indicator (see next section for discussion of this technique) showed no significant improvement in carbon atom production over that observed with acetylene. Experiments with methane showed slightly lower carbon atom

production than with ethylene. However, this decrease was at most a factor of 2. Carbon depositing on the nozzle was a problem with both these carbon donors. The fact that there was little change in experimental observations on changing carbon donors indicated that the limiting factor in the experiment is carbon deposition from the arc effluent before it reaches the cavity.

2.4.2 Observations of $CS(a^3\Pi)$ and $CO(a^3\Pi)$ Emissions

Quantitative spectral studies were performed with nitrogen in the arc and ethylene as the carbon donor. The HCl-I mixing nozzle was used. No clogging of the nozzle occurred with nitrogen because of lower carbon production. Hence, measurements reported here are lower limits to what should be obtainable using argon diluent.

Studies were made of the variation of $CS(a^3\Pi)$ emission intensity as a function of carbonyl sulfide flowrate at several ethylene flowrates and at a fixed distance of 3 cm from the mixing nozzle. The resulting plots are shown in Figure 27. Note that except at the lowest ethylene flowrates the plots peak at the same COS concentrations.

The experiment was next set up to look at emission from the carbon resonance line. The observation point was set up as far down stream as possible ($\sim$ 10 inches) to allow maximum contact time between reactants. The intensity of the lamp emission at 1656Å was monitored as a function of COS flowrates for a fixed ethylene flowrate of 0.015 g/sec. A plot of lamp intensity versus COS concentration is shown in Figure 28. This plot is not as exact as the preceding ones because fewer data points were taken. The reason for the observed increase in intensity with in-

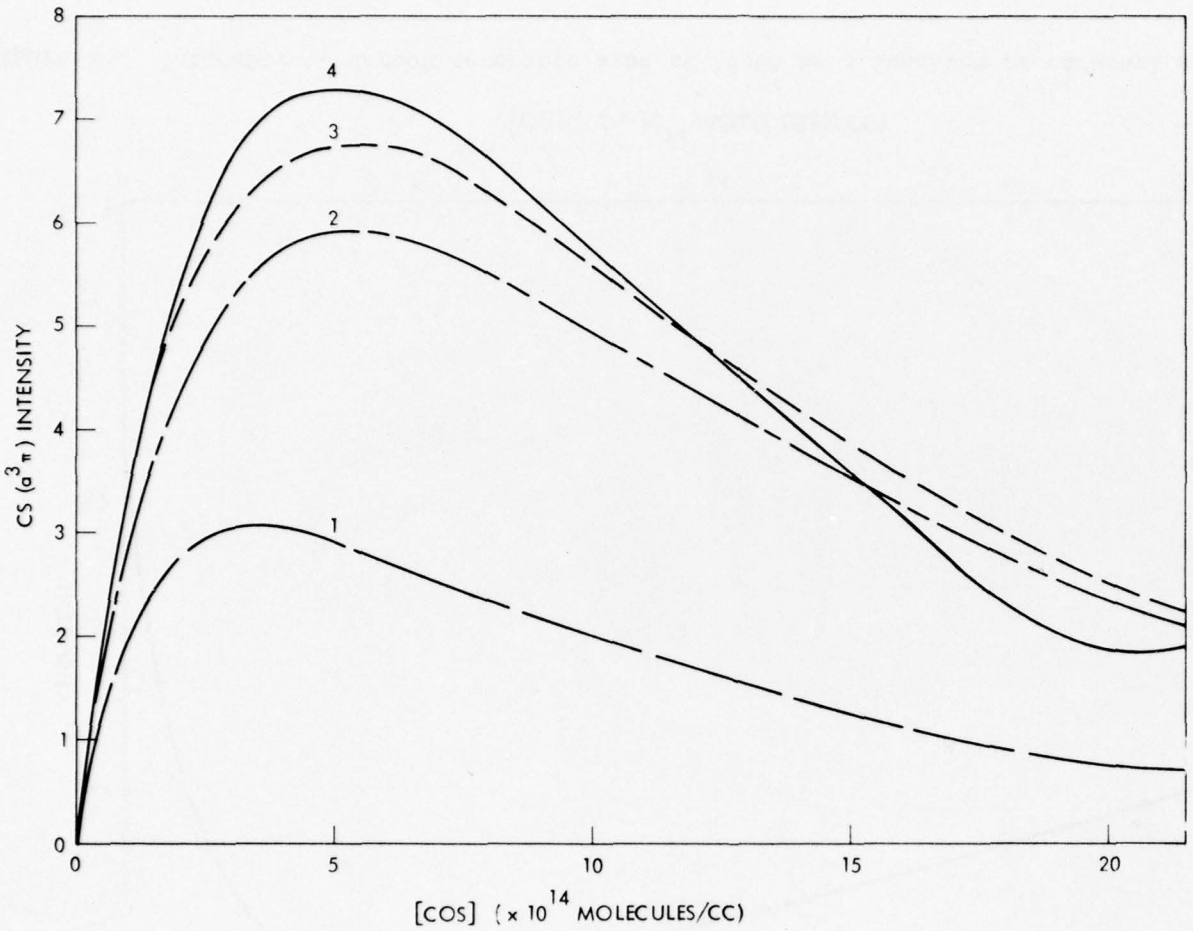

Figure 27. Plot of CS($a^3\Pi$) Emission Intensity as a Function of Carbonyl Sulfide Concentration for 4 Ethylene Flow Rates: 1-0.01 g/sec; 2-0.02 g/sec; 3-0.03 g/sec; 4-0.04 g/sec.

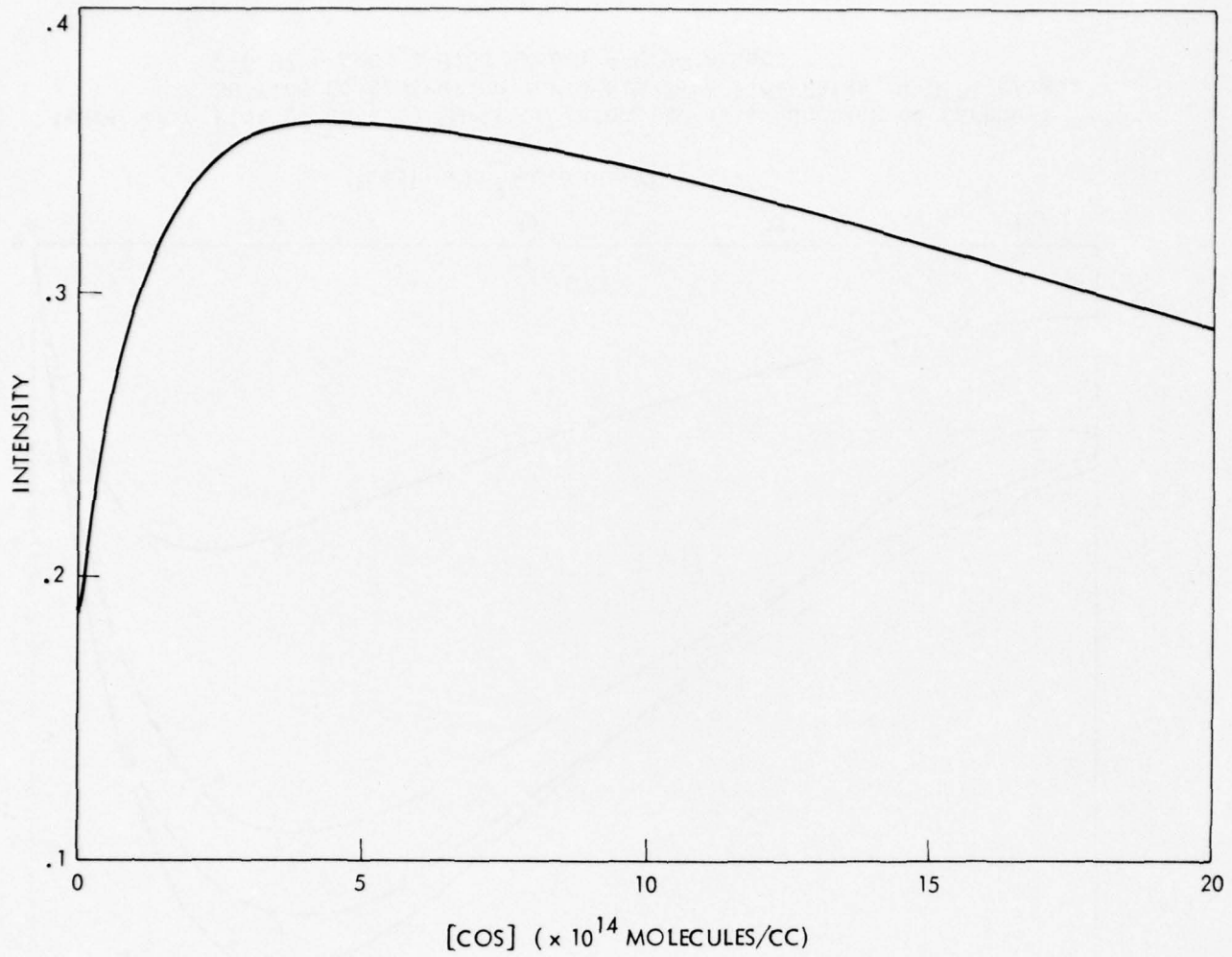

Figure 28. Intensity of carbon resonance line at 1656Å as a function of carbonyl sulfide concentration

creasing COS flowrate is that the COS is reacting with carbon atoms, resulting in less resonance absorption. The decrease at high flowrates is due to absorption of the carbon line by COS. It can be noted that the maximum in this plot is near the maximum observed in Figure 27 showing agreement in techniques. It should also be pointed out that the maxima in plots in both Figures 27 and 28 correspond to a molar flow of carbonyl sulfide five to ten times greater than that of ethylene. Even taking into account that there are two atoms of carbon per mole of ethylene, the flowrate of COS is still two to five times greater than the flowrate of carbon. This may be accounted for by a consideration of kinetics and the flow velocity. For an example, assume the rate constant for reaction between carbon and carbonyl sulfide to be 1×10^{-10} cm^3 $molecule^{-3}$ sec^{-1}. Also assume a contact distance of 3 cm and a flow velocity of 10^5 cm/sec. The carbon concentration is assumed to be 1×10^{14} molecules/cc while that for carbonyl sulfide is 5×10^{14} molecules/cc. Under these conditions it can be shown that only 75% of the carbon would have reacted at a distance 3 cm from the mixer. Thus the peak of the plot does not necessarily correspond to equal flows of carbon and carbonyl sulfide.

The spectrometer and photomultiplier combination was calibrated at the 0-0 band of the $CS(a^3\Pi)$ emission. This was to determine approximately how much excited state was produced. At flowrates of 1.4×10^{-3} moles/sec ethylene and 4×10^{-3} moles/sec carbonyl sulfide the line of sight emission intenisty was 1.9×10^{17} photons/sec/cm^2 integrated over the 0-0 band. The lifetime of the $CS(a^3\Pi)$ state is not well known. Estimates range from 10^{-4} to 10^{-2} second. Thus, depending on the lifetime, concentrations could be between 2×10^{13} to 2×10^{15} molecules/cc.

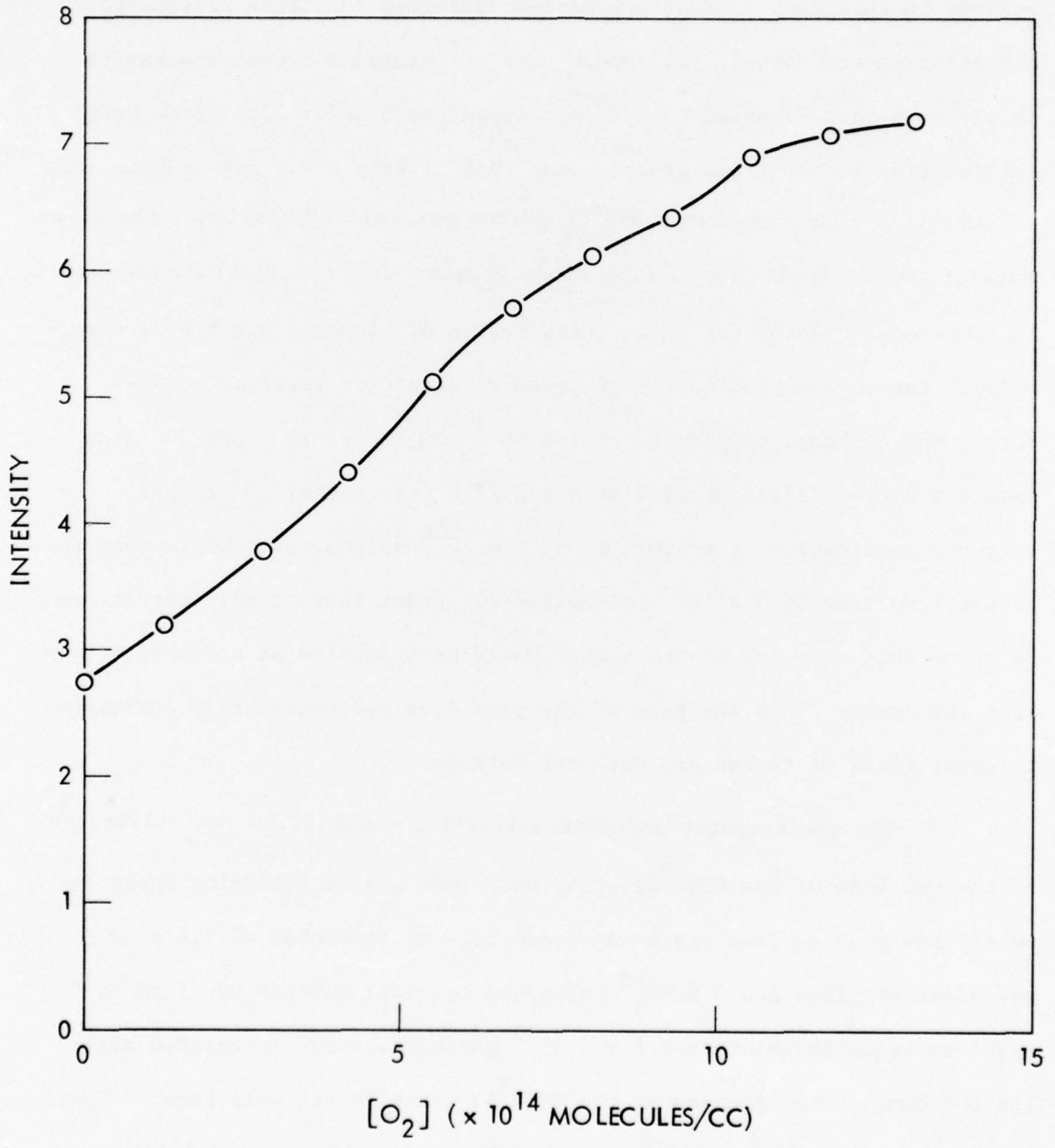

Figure 29. Plot of Carbon Lamp 1656Å Emission as a Function of Oxygen Concentration.

Further tests were performed with the F-80, BA-1007 arc jet with argon as a diluent. This eliminates interference from CN species. With argon and the same HCL I nozzle, the nozzle clogged with carbon in 1 minute run time. No carbon deposition was observed with nitrogen diluent. This indicates that more carbon is produced with argon diluent as predicted by the NEST calculations. However, quantitative data as in Figures 27, 28 and 29 were impossible to obtain in this configuration because of rapid intensity changes due to less flow getting through the obstructed nozzle. However, the initial $CS(a^3\Pi)$ emission intensity was higher than in tests with nitrogen. A nozzle designed to avoid clogging would be needed to truly optimize this system.

Further tests were made adding O_2 to the ethylene and nitrogen flow. The carbon resonance lamp intensity was monitored as a function of O_2 flow. A representative plot is shown in Figure 29 . The intensity seemed to continue to increase up to the maximum flows used. It was found that some emission at 1656Å, probably due to the $CO(A^2\Pi)$ band, occurred at high oxygen flow rates. Even correcting for this emission, the plots did not show as sharp a maximum for the titration as that with COS presented in Figure 28 .

An attempt was made to calibrate the spectrometer at the $CO(a^3\Pi)$ emission wavelengths. However, the calibration of the standard lamp which was available extended to only 2500Å and hence had to be extrapolated to shorter wavelengths. Flowrates of 7×10^{-4} mole /sec ethylene and 7×10^{-3} mole /sec oxygen were used with no attempt being made to optimize the $CO(a^3\Pi)$ emission intensity. An estimated photon density of between 3×10^{14} and 1×10^{15} photon cm^{-3} sec^{-1} was observed. Since the CO life-

time is 7 msec, this corresponds to a number density of from 2 to 7 x 10^{12} molecules/cc. Again it should be emphasized that these measurements were made at far from ideal conditions.

2.4.3 Conclusions on Carbon Atom Production

The tests described above indicated that carbon atom number densities of the order of from 10^{13} to 10^{14} atoms/cc could be produced. This was disappointingly low based on theoretical calculations of the number densities which should be produced in the arc. The deposition of carbon in the apparatus indicates that this is the limiting factor in the arc experiments rather than the actual carbon atom production. Thus, a superior mixing scheme in which surface contact of the arc affluent with the mixer is minimized is required. This requirement of thorough mixing in a supersonic flow with minimum surface contact presents a serious design problem. Therefore, unless an adequate mixing scheme can be devised that minimizes carbon deposition, the use of the otherwise interesting carbon atom reactions will be limited by the number of carbon atoms that can be made to survive the journey to the reaction zone.

2.4.4 Transfer Experiments Involving $CO(a^3\Pi)$

The work statement for the first phase of the program restricted experimental study of acceptor species to iodine chloride and chlorine. As mentioned in the introduction to this section, transfer from $CO(a^3\Pi)$ to NO has already been characterized. One study was performed in which NO was added with O_2 to the effluent of the arc. The expected NO emissions were observed. This test was used to verify that $CO(a^3\Pi)$ was present.

An investigation of excited state products resulting from the

interaction of $CO(a^3\Pi)$ with ICl and Cl_2 was performed using a low pressure discharge flow tube described in Section 2.2 and shown in Figure 4 . The method of production of $CO(a^3\Pi)$ is by the interaction of metastable argon atoms produced in the discharge with carbon dioxide. Either ICl or Cl_2 are mixed into the flow through the secondary nozzle downstream of the pinwheel. Emission was scanned from 2000Å to 1μ using a 0.3m McPherson spectrometer. For the shorter wavelengths, a 1200 line grating blazed at 7500Å was used. For the spectral region from 2000Å to ~5500Å, an EMI 6256S photomultiplier was used to monitor emission. For longer wavelengths, an Hamamatsu type R200, GA2338, photomultiplier tube with an S1 spectral response was used to monitor the emission. The complete spectrum was first scanned with only argon and CO_2 flows. Then either ICl or Cl_2 was added and the spectrum again scanned. In neither case was any emission in the spectral region scanned observed. This indicates that excited state products which emit in the spectral region from 2000Å to 1μ are not produced as a result of this interaction. No observation were made at wavelengths longer than 1μ leaving open the possibilities of production of $I(^2P_{1/2})$ from interaction with ICl.

The quenching of $CO(a^3\Pi)$ emission by chlorine was studied to determine if any interaction between the two species had occurred. For these experiments, the CO_2 and Ar flows were held constant. The spectrometer was set to look 14 cm downstream of the chlorine injection nozzle. The $CO(a^3\Pi)$ line at 2060Å was monitored with changing flowrate of chlorine. Then the ratio of the intensity with chlorine to that with no chlorine was plotted versus chlorine concentration on a seimilog plot shown in Figure 30. Such a plot is linear with a slope equal to 3.53×10^{-13} cm^{-3}

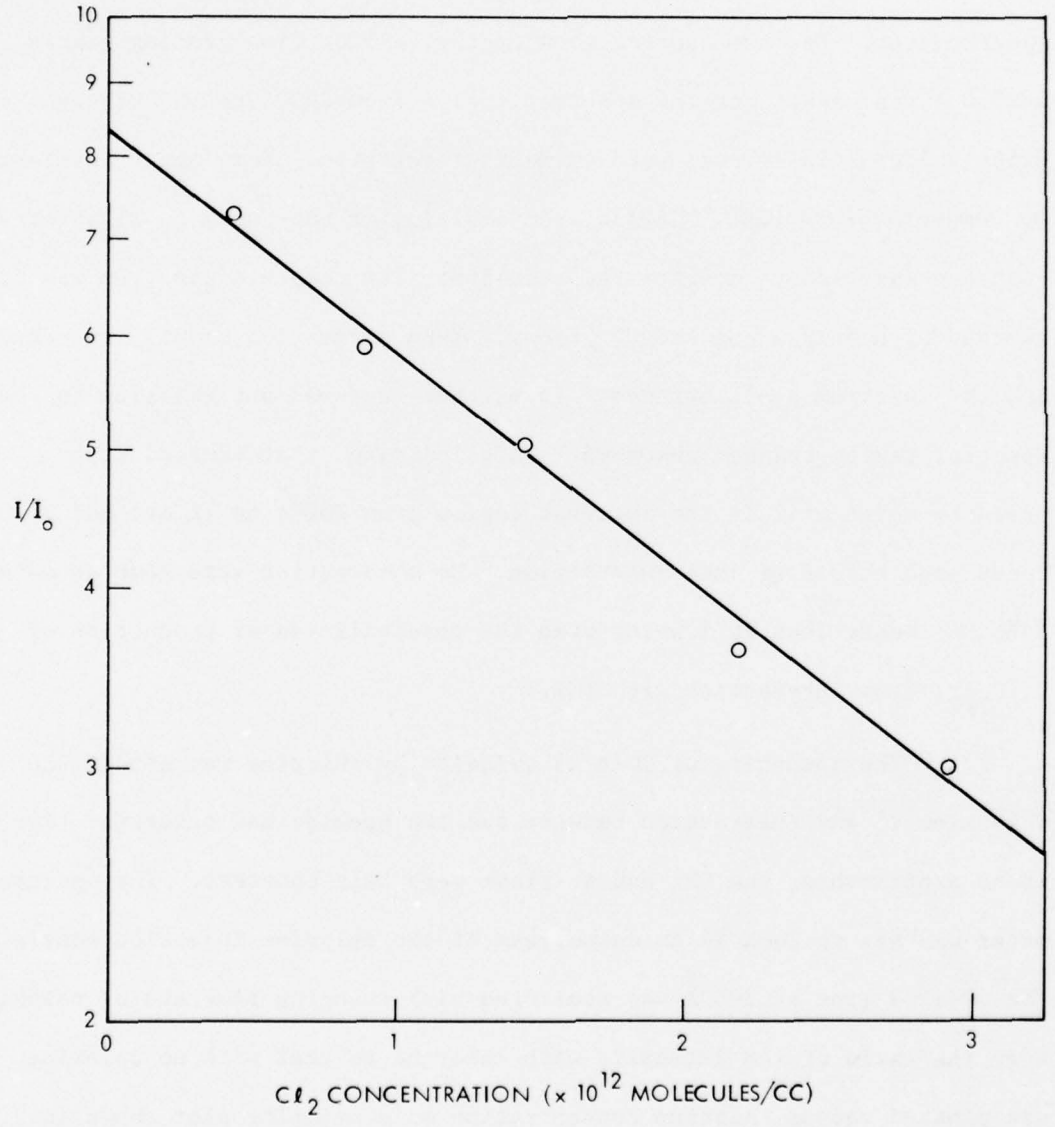

Figure 30. Plot of intensity of CO* emission versus chlorine concentration

molecule^{-1}. From the flow distance of 14 cm and the velocity of 2.3 x 10^3 cm/sec, a rate constant of 2.85 x 10^{-11} cm^3 molecule^{-1} sec^{-1} was calculated. This is a reasonably fast rate, indicating some interaction between CO($a^3\Pi$) and Cl_2. Similar results are expected from ICl, based on observed decrease of the CO($a^3\Pi$) signal upon adding this species to the flow.

The above results indicate that the $A^3\Pi$ states of ICl and Cl_2 are not formed from the interaction of CO($a^3\Pi$) with ICl or Cl_2. However, they do indicate that some interaction, most likely dissociation of the halogens, is occurring. The experiments did not preclude the possibility of electronically excited halogen atoms which would radiate in the infrared spectral region being formed.

2.5 General Conclusions for Task I

The major technical achievement in this task was the demonstration that large number densities of the $A^2\Pi$ state of CN could be produced in a combustion system. This state of CN has molecular properties required for a chemical laser species so the systems studied have the potential for lasing directly. The advantage of these systems is that they involve strictly chemical production so no external energy sources are needed to promote excited state production. They also have the potential for scalability to larger systems as increased flows of reactants lead to production of higher number densities.

There is much potential for further study. In the NF_3 - H_2 combustion system, experiments indicate that atomic nitrogen may be produced. This presents the potential for studying a wide range of reactions including those producing the $A^2\Pi$ state of CN. The preliminary experiments

also indicated that the transfer scheme from $NF(a^1\Delta)$ produced in this experiment to atomic iodine may be efficient, and this deserved further study. Definitive conclusions on the laser potential of $F_2/H_2(D_2)$/R-CN combustion systems were not reached, and this system deserves further study because of the high number density of excited state produced.

The only systems studied which have limitations are those that involve carbon atoms. The problems of producing high number densities of carbon and efficiently mixing them with a second gas stream are not at all easy to solve. The feasibility of these systems depends on development of an improved technology for carbon atom handling.

3.0 TASK II. MOLECULAR BEAM STUDIES

3.1 Introduction

The principal objective of this phase of the program is to identify, by a series of experimental measurements, chemical reactions which may possess characteristics compatible with lasing in the visible region of the spectrum. The investigation is limited to reactions with sufficient exothermicity to directly populate electronic excited states of the product molecules resulting from reactions of the type

$$A + BC \rightarrow AB^* + C$$

where BC may be either diatomic or polyatomic and A represents metal atoms. The "New Gas Lasers Committee Report on Electronic Transition Chemical and Electrical Excited Lasers" [35] has identified reactions of this type, where the end product may be either a metal oxide or metal halide, as potential laser candidates. Further, it has been recommended that reactions of this type be subjected to a systematic study since relatively little information is currently available. Criteria for judging the applicability of a given reaction are established with the conclusion that experimental measurements must be an integral part of an orderly development program.

Reference 35 contained a first order screening of possible reactions involving metal atoms and eliminated certain reactions from further consideration either because of potential metal atom source problems, insufficient chemical energy release, or published data showing that the properties of some reactions were unsatisfactory. Even after this first order screening the list of potential reactions remains long. However, the number of reactions that may ultimately lead to practical lasing

systems is most likely small because of either practical or fundamental limitations. The intent of this program is to narrow at least part of the list of candidate reactions to manageable proportions by applying a series of simple, but increasingly stringent, experimental tests to a number of potentially interesting reactions. The hoped for result of these screening tests is a list of reactions with characteristics compatible with lasing applications. It is quite likely that these remaining reactions would require in-depth investigation and analysis before the decision to use them in a laser would be made.

In order to most efficiently match experimental capability with stated requirements, the investigation is limited to reactions yielding the aforementioned metal oxides and halides. The experiments are conducted in a crossed beam configuration where the metal atom beam is produced by the TRW-developed technique[36] of laser beam bombardment of thin metal foils deposited on transparent substrates. The metal vapor thus produced expands into vacuum from the irradiation site. The initially high density vapor dilutes as it expands until, at some distance from the irradiation site, the flow becomes laminar and individual atoms become collisionless. The process appears to be entirely thermal with the consequence that the expanding atom cloud contains a range of atom velocities characteristic of the temperature of the vapor cloud at the time it becomes collisionless.* A portion of the expanding vapor cloud can be collimated into a

*A detailed analysis of the velocity spectrum suggests that the observed velocity distribution derives from a Maxwellian distribution superimposed on a center-of-mass velocity component. The operative mechanism is not yet fully understood; however, this is unimportant since the velocity of atoms in the cloud is specified by their time of arrival at a remote detector.

slightly diverging atom beam and interacted with a crossed beam of target gas obtained from a room temperature nozzle source. An obvious constraint is that BC must be either gaseous or highly volatile so as to be compatible with the nozzle source. The laser bombardment technique of producing atomic beam pulses is compatible with many materials, but the most consistent results have been obtained with metal atom beams. If conditions are chosen properly, some fraction of the incident beam atoms react with the target gas molecules forming the product molecules. "Proper" conditions within this context mean that the reactions take place on a binary collision basis and that the reaction products flow from the reaction volume with only a small probability of suffering additional collisions. The trajectories of the product molecules are governed only by the conservation of energy and momentum applied to reactant pairs. Several types of measurements may be performed to determine the internal energy state of the product molecules and subsequent de-excitation characteristics.

Selected reactions are subjected to a series of tests of increasing sophistication which can be discontinued at any point upon the failure of a particular reaction to meet specified criteria. A short summary of the tests follows:

- Test for Chemiluminescence in the Visible and Near UV Wavelength Region. The absence of chemiluminescent radiation indicates that no low lying electronic bands are populated and negate the requirement for continuing the test series.
- Spectral measurement of the Chemiluminescent radiation. Initially this can be done with broad band filters. If the chemiluminescent radiation is distributed over a wide

spectral region, it can be assumed that the efficiency of converting the reaction exothermicity into possible lasing states is small and the test series can be terminated. If the radiation is concentrated in narrow bands, a requirement for higher resolution spectroscopy is identified.

- Qualitative Lifetime Measurements of Prominent Bands of the Chemiluminescent Radiation. It can be shown that the laser gain expected from a specified molecular electronic transition is inversely proportional to the radiative lifetime, τ, of the upper state and the cube of the frequency of transition, ν, i.e.

$$G \propto \frac{1}{\tau \nu^3}$$

From this relation it can be deduced that the radiative lifetime of a prospective laser candidate should be smaller than approximately 3×10^{-4} seconds. However, for pure chemical laser action, the lifetime should be greater than 10^{-6} seconds to allow sufficient time for mixing of the chemical reactants. Hence it is useful to categorize emission as either short-lived ($< 10^{-6}$ second) or long-lived ($> 10^{-6}$ second). Short-lived states would have high laser gain and may be applicable to certain fast-pulsed lasers. Long-lived states are more adaptable to pure chemical lasers.

- Quantitative Radiative Lifetime Measurements. The experimental techniques are compatible with quantitative measurements of lifetimes in the 10^{-5} to 10^{-4} second range.

- Measurement of Energy Branching Ratios. The final and most severe test of a qualifying reaction is that of determining the efficiency of producing an inverted population of excited states. Complete specification of the energy branching ratio for a particular reaction is beyond the scope of this task. It had been proposed, however, that sufficient experimental data be acquired to at least estimate this quantity. Favorable reactions would be earmarked for further study.

The truly significant feature of atomic beam measurements of this type is that the initial distribution of internal energy states is determined. It is clear that a non-equilibrium initial distribution of excited states must exist as a minimum condition if a reaction is to be useful in lasing applications. This minimum condition, however, is not sufficient, since the initial distribution may be modified rapidly by means other than spontaneous emission of photons in the pressure regimes required for practical laser systems (e.g. collisional de-excitation). It follows that additional work would be required to ultimately establish the viability of particular reactions.

Within the context of the present program, the ability to quickly and efficiently make a particular measurement depends upon the characteristics of the reaction in question. Since the intent of this task is to screen potential reactions by applying simple tests, measurements requiring a substantial effort for relatively little additional information were not undertaken. Also, it was assumed that this program was the first phase of a continuing program and emphasis was placed on obtaining preliminary data on a number of reactions rather than finishing

the sequence on specific reactions. Although the basic principles of this program had been defined prior to its inception, a significant fraction of the effort has been devoted to the refinement of techniques and apparatus to reduce data acquisition to a routine operation.

The balance of this report is organized as follows: The basic experimental apparatus is described in the following section. Section 3.3 describes the techniques and procedures used in the acquisition and analysis of the experimental data, while the experimental results are summarized in section 3.4.

3.2 Experimental Apparatus

3.2.1 Metal Atomic Beam Source

All of the experimental measurements utilize a crossed atomic-molecular beam configuration where the metal atom beam is produced by the laser volatilization of thin metal films and the target beam of molecular gas is obtained from a room temperature nozzle source. A reasonably comprehensive description of the metal atom beam source and its general characteristics are contained elsewhere.[36] The discussion here will be limited to an overview of the general technique and an updating of the previously published material.

To generate the primary metal atom beam, a thin film of the metal is irradiated with the beam from a Q-switched ruby laser. The absorption of radiant energy volatizes a small volume of the target and raises the temperature of the vapor. The subsequent expansion of the hot vapor cloud into vacuum orders the random motion into a laminar, collisionless flow. A simple collimating aperture located downstream from this point renders

the expanding cloud into a narrow pencil beam of metal atoms. The beam is in the form of a transitory burst of atoms traveling in straight line trajectories. The burst of atoms contains a broad distribution of energies. However, if the distance from the target to the point of observation is large compared to the distance over which the gas cloud remains collisional, the energy of a particular atom is specified by its arrival time (i.e., the time of transit from the target to the observation point). Thus, even though the pulse contains a wide atom energy range, all of the atoms arriving at a particular instant of time have the same energy. This consideration requires that the laser pulse duration be short compared to the atom transit time. The laser pulse length used in this work is always 100 nsec or less which more than satisfies this requirement. A short duration laser pulse is also a requirement in order to achieve the high temperature. Otherwise, conduction and other loss mechanisms lessen the efficiency of utilization of the laser energy.

The magnitude of the mean velocity and the velocity distribution of the expanding cloud depends upon a number of factors including laser energy, laser energy density, target material, target film thickness, direction of incidence of the laser beam on the target, and the direction of observation of the atomic beam. The requirements of the present program provide the motivation for maximizing the flux at the lowest possible velocity. As mentioned earlier and as discussed in detail in a forthcoming publication,[37] the velocity distribution of atoms in a given burst appears to result from the superposition of a Maxwellian distribution upon a directed center of mass motion. Reference 37 presents a model that can be used to determine the equilibrium temperature of the vapor cloud at the time it becomes collisionless. Applying this model

to typical bursts shows that the equilibrium temperature is near (or below) the vaporization temperature of the parent metal. This finding is important insofar as the final results of the present program are concerned because it has been tacitly assumed that the atoms are in the ground state and not in excited metastable states which could be the case if the equilibrium temperature were excessively high.

In practice, laser bombardment conditions can be found where the velocity distribution is consistent with the vaporization temperature of the metal film. This temperature is probably higher than would be allowed in the final application; however, the low velocity tail of the velocity distribution extends well into the region of interest.

Typical beam pulses for several metallic species are illustrated in Figure 31. Here the metal atoms were detected by means of a quadrupole mass spectrometer system described in more detail below. The signals shown in Figure 31 give the arrival time history, referenced from the laser burst, of neutral atoms at the ionizer of the mass spectrometer system. The amplitude of the signal at any instant of time is proportional to the number density ρ of atoms within the ionizer at that time. However, since the velocity of the atoms is specified by the elapsed time from laser firing, the flux J is readily determined through the relationship $J = \rho v$. The distance from the thin film target to the ionizer for the photographs of Figure 31 was 88 cm. Nominal operating conditions are 1/2 to 2 joules total laser energy, 1/2 to 2 micron thick target films, and laser beam energy densities in the 10 to 100 joules cm^{-2} range. The upper trace on each photograph is the signal from a photodiode used to monitor the laser pulse.

METAL ATOM BEAM PULSES

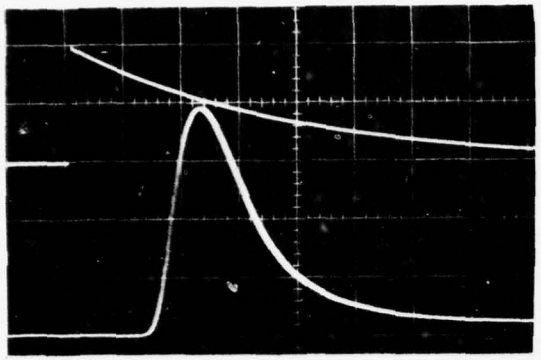

SILICON

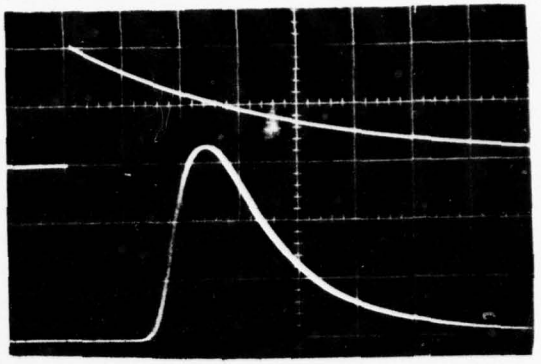

MOLYBDENUM

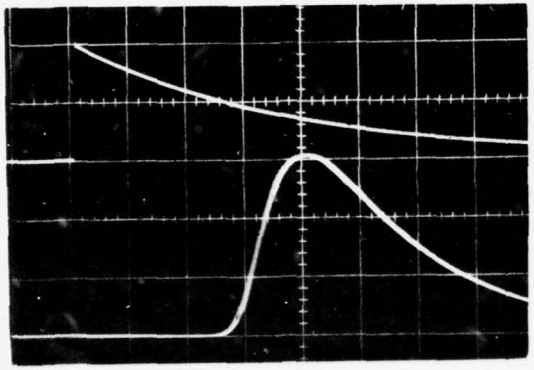

NEODYNIUM

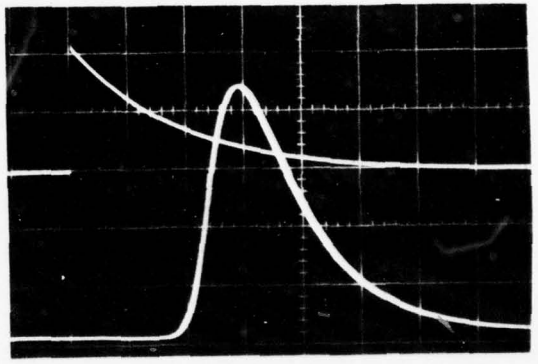

HOLMIUM

Figure 31. Metal atom beam pulses produced by the laser vaporization of thin metal films. Target to detector distance is 88 cm and the sweep speed is 100 microseconds per division.

The salient features of the pulsed atomic beam system are listed below:

- Atomic Species: The approach appears to be compatible with virtually any atomic and some molecular species with the possible exception of noble gases. Species that are stable in elemental form (e.g. metals) are most easily handled since they can be deposited in thin film form.

- Atomic Beam Intensity: Perhaps the most significant feature of the pulsed atomic beam source insofar as the present application is concerned is the high beam intensity available. Fluxes on the order of 10^{17} atoms cm^{-2} $second^{-1}$ at a distance of 60 cm from the laser target are obtained in the few electron volt energy regime. This value is six to seven orders of magnitude greater than generally obtained with "conventional" beam sources (which are often restricted to normally gaseous species). The total number of useable atoms in a pulse is on the order of 10^{13}.

- Atom Energy: Each atom pulse contains a broad spectrum of energies; however, the velocity distribution is directly measureable by the arrival time at a remote detector. There are both upper and lower limits to the achievable mean energy range. The minimum temperature must exceed the vaporization temperature of the target material which for most common metals is several thousand degrees Kelvin. The maximum temperature is limited by excessive ionization of the vapor. The requirements of the present task tend toward

the lower part of the available energy spectrum. Results indicate that high intensity beams of most of the significant elements can be obtained in the one-half electron volt energy region.

- Versatility: The ability to rapidly change from one atomic species to another is inherent in the pulsed atomic beam approach since it involves only substitution of the laser target. Different materials may have different properties with respect to the absorption of optical radiation. The laser bombardment conditions required to achieve a given energy distribution in the beam cannot necessarily be determined in advance for an arbitrary material. Usually, however, only a few test shots are required to achieve the desired parameters.

3.2.2 Target Gas Beam Source

The experiments here are primarily concerned with the evaluation of the characteristics of potential pumping reactions. In order to isolate the pumping reaction from competing reactions (e.g. collisional de-excitation) which could distort the resulting data, the use of a "thin" target gas is required. At the same time it is advantageous to localize the reaction volume as much as possible. These conditions are met by the nozzle beam source used for the target gas. To minimize system pumping requirements, the nozzle beam has been combined with a solenoid-actuated valve which limits the duration of the molecular beam pulse to a few milliseconds. The valve is opened in advance of the laser Q-switch by a time sufficient to establish steady state flow conditions. As a general

rule, the nozzle source is operated at a reservoir pressure that produces a target gas density such that the probability of reaction of a metal atom traversing the molecular beam is between 0.1 and 0.3 as determined by attenuation of the incident beam. This condition essentially maximizes the reaction rate consistent with maintaining an adequately low probability of secondary reactions within the target volume.

The nozzle orifice is a 0.25 mm diameter hole in 0.25 thick brass shim stock. The distance between the nozzle orifice and the center line of the metal atom beam is 1 cm. The solenoid-actuated valve assembly is inside of the target gas reservoir. The target gas density in the interaction region is controlled by adjusting the stagnation pressure in the reservoir. The stagnation pressure typically ranges between 5 and 50 torr.

For the stagnation pressure range and the orifice size, the nozzle beam has the characteristics of an inviscid-supersonic jet. The Mach number at the center of the interaction zone is estimated to be on the order of 10. The pressure ratio (stagnation pressure to pressure in the interaction) is in the range from 10^{-6} to 10^{-5}. Both calculations and experimental observations indicate that the effective length of the interaction region is on the order of 1 cm.

After passing through the interaction region, the gas jet from the nozzle is directed into a pumping chamber with a capacity of approximately 2000 liters sec^{-1}. The throughput of the pumps used is sufficient to return the system to a base pressure less than 10^{-6} torr in less than 0.1 sec. The gas pulse time duration and relative amplitude are monitored by a nude structure ionization gauge of the Bayard-Alpert type which is

located on the jet axis downstream from the target volume. The gauge collecting wire is placed normal to the axis,and the gauge has a buffered amplifier output to provide fast time response.

For most of the experiments under consideration here, the characteristics of the target gas beam are of secondary importance. The principal requirement is simply that the reaction probability be in the desired range. Experimentation has shown that the desired objective can be achieved by simply varying the reservoir pressure. It is quite clear, however, that fairly large density variations exist within the interaction volume of the two beams because of the expansion characteristics of the nozzle beam. Density variations within the target gas may have no significant effect on the experimental results; however, an experimental confirmation of the properties of the target gas beam was conducted using an electron beam fluorescence technique. The results obtained indicated that the characteristics of the expanding jet were as expected. Experiments were also conducted with a capillary array source which gave smaller variations in density; however, this source was not used for the experiments discussed in this report.

A complication associated with the pulsed target gas beam is that the solenoid that actuates the valve is located within the target gas reservoir and is incompatible with the use of corrosive target gases. Experiments so far have been limited to those involving target gases of NO_2 and N_2O. In anticipation of future requirements, a static gas target source using differential pumping has been tested with satisfactory results. In this case, the metal atom beam enters the target gas region through one of the differential pumping channels and the product molecules

emerge from the other.

3.2.3 Energy Selection System

In conducting certain measurements, the range of velocities inherent in the atom burst causes no problems. In fact, it is even advantageous in some cases. In other cases, however, nearly monoenergetic beam pulses may be required. The transit time of an atom from the point of origin to a point a distance x away is related to its energy by

$$E = \frac{m}{2}\left(\frac{x}{\tau}\right)^2 \qquad [12]$$

within the time interval dt a range of atom velocities dE will pass a given point as governed by the relationship

$$\frac{dE}{E} = -2\,\frac{dt}{t} \qquad [13]$$

where t is the time at which an atom with energy E reaches the point. Thus, to accomplish energy selection, we need only to block the path of the atoms except for a small time interval. This has been implemented by a simple mechanical shutter that opens for a time interval Δt at a time t subsequent to the laser burst.

The shutter consists of a slit aperture placed between the laser beam target and the reaction chamber at a distance of 50 cm from the laser target. In front of this aperture is a rotating disc with a similar slit at its periphery. The center of rotation of the disc is located such that the slits overlap once per revolution. The total "open" time of the slit is twice the slit width divided by the linear speed of the circumference of the rotating wheel. For a 1 mm slit width and a total open time of 10 microseconds, the linear velocity must be 2×10^4 cm/sec. For a 20 cm disc, this translates into a rotational

speed requirement of about 320 revolutions per second. The experimental apparatus includes such a system with a maximum rotatational speed of 400 rps driven by a variable speed synchronous motor. Synchronization of the firing of the laser beam and the opening of the shutter to deliver a beam pulse of predetermined average energy and energy range is accomplished by an electronic timing and control circuit.

The results obtained with this system are illustrated in Figure 32. In each of the three photographs the integrated pulse from the photodiode used to monitor the laser beam is displayed on the upper trace. The sweep speeds of the upper and lower traces are equal and are synchronized. Both traces are triggered by an auxilliary pulse that occurs before the laser is Q-switched. The lower trace of Figure 32a shows an aluminum beam pulse at a distance of 85 cm from the laser target with the velocity selector inoperative. Figure 32b shows the chopped beam pulse with the timing synchronized to pass a narrow band near the peak of the distribution. The two flat-topped pulses on the bottom trace identify the time of the Q-switch and the time at which the shutter opens. Figure 32c shows another transmitted beam pulse at lower velocity. Amplitude variations are within the shot-to-shot reproducibility of the beam pulse.

3.2.4 Mass Spectrometer System

A mass spectrometer system is used to detect the metal atom beam pulse. The system is normally located on the atom beam axis downstream from the interaction zone and, thus, gives a measure of the intensity of the attenuated atom beam pulse. Since most experiments are run under thin target conditions, only a small correction is needed to

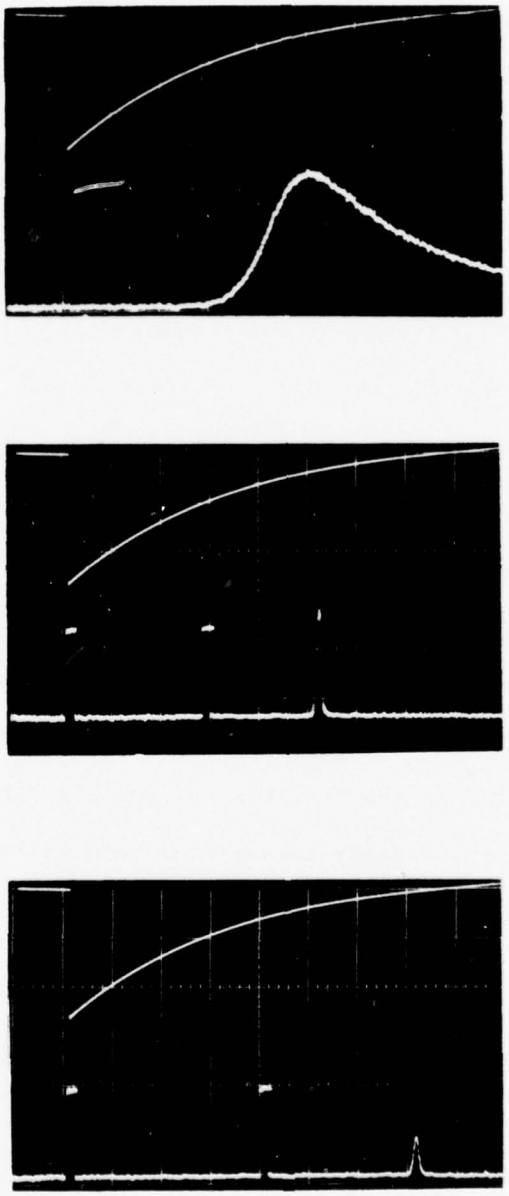

Figure 32. Oscillographs illustrating the operation of the mechanical velocity selector.

determine the beam intensity prior to reaching the target region.

The mass spectrometer system utilizes an electron impact ionizer (Extranuclear Laboratories, Inc. Type II High Efficiency Ionizer) to ionize a small fraction of the metal beam atoms. These ions are focused at the entrance of an rf quadrupole mass filter (Extranuclear Laboratories, Inc., Model 324-9). The quadrupole analyzer (QPA) transmits only ions within a given charge-to-mass ratio range. The resolution capability of the system is more than adequate to pass only a single atomic mass across the entire range of interest. Ions emerging from the quadrupole are deflected by 90° by a system of electrically biased planar grids so as to impact the first dynode of an electron multiplier tube (EMT) used to detect the ions. The EMT is an EMI venitian blind type with Be-Cu dynodes. The EMT is operated with -4 kV on the first dynode and with the anode grounded through a load resistor. Electrons produced by the impact of the high energy ions are multiplied down the dynode chain to develop a signal across the load resistor. The signal is amplified by a dc coupled operational amplifier operated in the current mode and displayed on an oscilloscope. The photographs shown previously in Figure 31 are typical of those obtained with this system.

3.2.5 Optical Detectors

Virtually all of the experiments conducted to date have used high sensitivity photomultiplier tubes (PMT's) to detect the chemiluminescent radiation. Two types of PMT's have been used routinely; RCA Type 8575 with a spectral response extending from about 2500 to 6000 Angstroms and Centronic Type 4282B with detection range from about 3000 to 6000 Angstroms. All of these tubes have been calibrated against a tungsten

standard lamp.

All of the PMT's are equipped with operational amplifiers primarily for impedance matching purposes since the signals are normally quite large. These amplifiers can be operated in either the differential (current) or integral (charge) mode depending upon the requirements of specific experiments. Some include an electronic gate to eliminate scattered light (primarily from the ruby laser) from the displayed signal.

3.2.6 Experimental System

A photograph of a typical experimental set-up is shown in Figure 33. In this view, the primary atomic beam is generated in the assembly in the foreground of the picture. The laser beam target is attached to the rod extending vertically through the air lock assembly. The air lock assembly permits rapid changing of the target without appreciably affecting the vacuum in the rest of the system. The arms extending to the left and right in the picture contain the focusing lens assembly and view ports. The laser beam is brought through a quartz window in the arm extending to the left. In an alternate configuration, a lens assembly is mounted on the end of the system in the immediate foreground of the picture. In this configuration, the laser beam is at 90° to that pictured. It has been shown that the latter configuration gives more latitude in the intensity and energy range of the atomic beam.

The ruby laser components are mounted on the I-beam at the left of the picture. Starting at the point nearest to the entrance window the components on the rail are a prism for deflecting the laser beam by 90°, a piece of plain glass (not clearly visible in the picture) set at an angle of 45° for deflecting a small fraction of the laser light into the

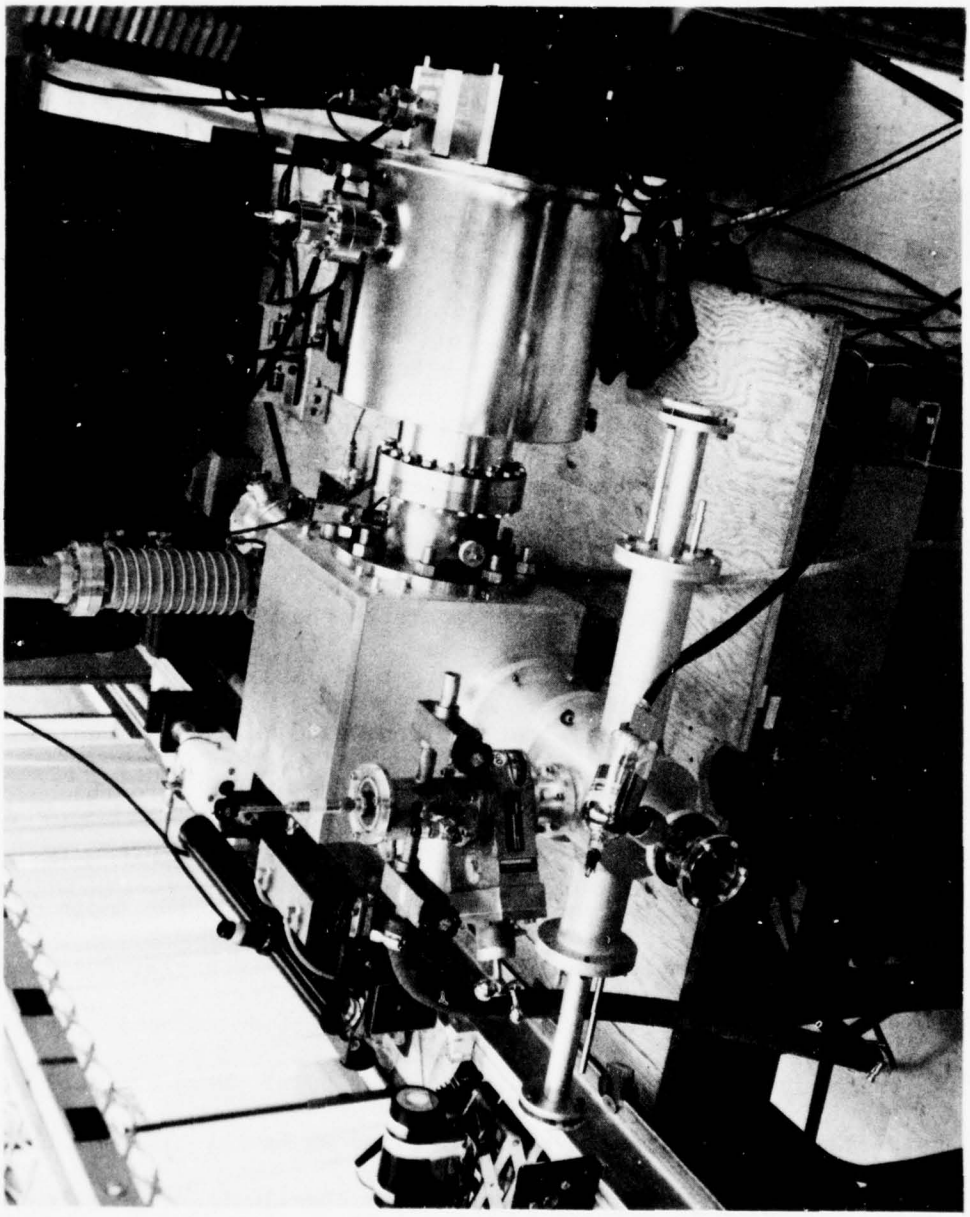

Figure 33. Photograph of the crossed atomic-molecular beam apparatus.

photodiode detector at the extreme left, an iris for collimation of the beam, the output mirror, the ruby rod housing, a polarizer, the kerr cell Q-switch, a quarter wave plate and the end reflector. Not visible in the picture is a He-Ne laser used for alignment purposes. The cylindrical black object with the eye-piece is an auto-collimator used to align the laser cavity.

The primary metal atom beam flows toward the upper right in the picture. The cubical box contains the mechanical velocity selection system and a set of electrically biased deflection plates to remove residual ions and electrons from the vapor cloud. The large cylindrical object extended from the right side of the box is a combination ion-titanium sublimation pump used to evacuate the target and velocity selection sections of the system. The sublimation pump has been replaced recently by a 4-inch oil diffusion pump to improve reliability.

A small collimating aperture separates the velocity selection region from the target gas region. The target gas assembly is hidden from view behind the velocity selector section. The nozzle is located such that the crossed beam is injected vertically downward into the throat of a baffled 6-inch oil diffusion pump. A target gas pressure monitoring system is installed on the thermal beam axis at the mouth of the diffusion pump. A pumping manifold extends from the target gas region to the velocity selector box and to the detection section. This manifold "roughs down" these two sections to the point where the sublimation pumps and ion pumps can be started. Windows in the sides of the interaction region provide visual access to the chemiluminescent radiation. In normal operation, two PMT's are used to monitor the chemiluminescence.

They lie in a horizontal plane and are hidden from view in the photograph.

Part of the product and metal atom beam detection system can be seen extending beyond the velocity selector section. This region is also isolated from the target gas region by a small aperture. The purpose of the aperture is to inhibit the flow of gas from the gas target nozzle into this region. Pumping in the region of the detector is supplied by a 100 liter sec^{-1} combination ion-titanium sublimation pump that can be seen extending vertically upward from the detector housing. The detector consists of a complete quadrupole mass spectrometer system. The detection system can be installed at different angles with respect to the incident beam axis. It is shown at the 0° position. At any angular position, the detector axis and primary beam axis intersect on the axis of the nozzle beam.

In the lifetime measurement configuration (not shown), the mass spectrometer system is replaced with a chamber containing three PMT's mounted such that they view a small segment of the beam axis. The same ion-titanium sublimation pump is used with this assembly to minimize the interaction of the atom beam with residual gas within the field of view of the PMT's.

3.3 Experimental Measurements and Procedures

3.3.1 Selection Criteria for Candidate Chemical Reactions

Within the previously defined constraints of this program a very large number of potentially interesting reactions remain. For example, nearly 50 metallic species react with N_2O with an exothermicity in excess of 1 eV. Using Suchard's compilation[31] of spectroscopic

constants for diatomic molecules as a source, it is found that nearly all of the resultant metal-oxides have energetically accessible electronic states. As a general rule, there is insufficient information available to absolutely rule out any particular reaction although there may be reasons to suspect that some of the reactions are not likely to fare well. In any case, subjecting reactions to the test sequence may require less effort and deliver more clearly definitive results than relying upon existing data. Thus, the decision was made to proceed on the basis of the availability of the metals and the ease with which thin film targets could be prepared and handled. Experiments have been conducted with Aℓ, B, Ba, Ce, Co, Cr, Fe, Ge, Ho, In, Mn, Mo, Nd, Ni, Si, Sm, Sn, and Ti interacting with N_2O and NO_2 target gases. It was expected that additional metal species and other target gases would be examined in a follow-on effort to the present program. The exothermicities for these reactions are given in Table 4. A compilation[38] of bond energies covering the literature from 1962 to 1966 was used when possible. Otherwise, the bond energies were taken from Cottrell.[39]

Descriptions of the measurement sequence and the experimental procedures used are given in the following sections.

3.3.2 Photon Yield Measurements

The basic experimental system described in the preceding section is instrumented in various configurations to accomplish specific measurements. The first step in the measurement sequence on a particular reaction is that of determining the photon yield relative to the intensity of the atom beam pulse. The instrumentation consists of the quadrupole mass spectrometer (QPA) located on the axis of the atomic beam downstream from

TABLE 4

EXOTHERMICITIES OF REACTION WITH GROUND STATE ATOMS TO FORM METAL OXIDES

Product Molecule	Bond Energy (eV)	Reaction Exothermicity (eV)	
		N_2O	NO_2
AlO	5.0	3.3	1.9
BO	8.2	6.5	5.1
BaO	5.8	4.1	2.7
CeO	8.4	6.7	5.3
CoO	3.8	2.1	0.7
FeO	4.2	2.5	1.1
GeO	7.0	5.3	3.9
HoO	6.6	4.9	3.5
InO	3.3	1.6	0.2
MnO	3.7	2.0	0.6
MoO	5.8	4.1	2.7
NdO	7.5	5.8	4.4
NiO	4.2	2.5	1.1
SiO	7.9	6.2	4.8
SmO	6.2	4.5	3.1
SnO	5.7	4.0	2.6
TiO	6.8	5.1	3.7

the interaction volume and a broad-band photomultiplier tube collimated so as to view only the interaction volume. Typical experimental results obtained in this configuration are illustrated in Figure 34. At any instant of time, the amplitude of the signal from the QPA is proportional to the number density of atoms within the ionizer volume. The integral over time, then, is proportional to the total number of atoms contained in the atom beam pulse. The integral of the PMT signal is proportional to the total number of photons emitted from the reaction volume due to the interaction of the atom beam with the target gas. The ratio of these two quantities is proportional to the photon yield. In order to determine the photon yield on an absolute basis considerably more data is required as discussed below and in the following sections.

An important factor to be considered in the interpretation of the photon yield measurements is the detection efficiency of the mass spectrometer system, since it is used to determine the number of atoms contained in the atom beam pulse. The calibration of the mass spectrometer system on an absolute basis is a difficult and time consuming task that is not done routinely. Within the context of the current program, the determination of photon yields on a relative basis is generally satisfactory. At present, pains are taken to ensure that the operating conditions of the mass spectrometer are reproduced from day-to-day. This is usually checked by producing a "standard" aluminum atom beam pulse at the beginning of any run on a different metal and the results are weighted relative to the aluminum atom pulse. Under these conditions the principal differences in the detection efficiency for the several types of metal atoms reduce to variations in the electron impact ionization

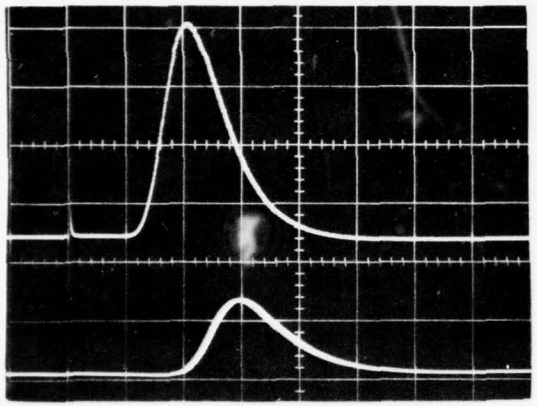

$Ho + N_2O \rightarrow HoO + N_2$

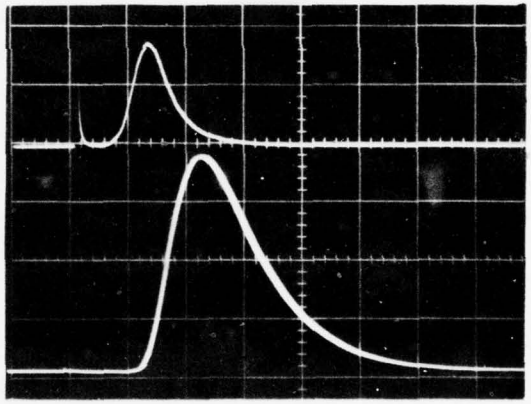

$Mo + N_2O \rightarrow MoO + N_2$

Figure 34. Examples of Chemiluminescence Measurements. The optical signal obtained with a broad-band PMT is shown on the upper trace of each photograph while the signal obtained from the quadrupole mass spectrometer is shown on the lower trace. Vertical deflection sensitivities are different for the two photographs.

cross section. Ionizing cross section data are not generally available for metal atoms, but it is assumed that differences are small. On the basis of the amount of target material evaporated during the laser bombardment, large differences in the intensity of metal atom bursts for the several types of material would not be expected. The measurements conducted with the mass spectrometer system are in agreement with this observation.

The photon yield is also proportional to the target gas density. All of the experiments were conducted at a fixed stagnation pressure in the target gas reservoir. The target gas pressure was adjusted such that the incident atom beam pulse was attenuated by about 30% in traversing the target gas as determined by measurements with the QPA.

The results of the photon yield measurements as well as the results obtained for the other measurements discussed below are presented and summarized in Section 3.4.

The approach to determine photon yields described above makes no distinction as to the efficiency of the photon yield as a function of the energy of the incident atoms. In practical chemical lasing systems, the velocity distributions of the reactants are nearly Maxwellian. It follows that the range of relative collision velocities between reactants is a function of the temperature. To predict the performance of a given chemical system, it is necessary to determine the temperature dependence of the pertinent reaction rates. In the atomic beam case, this requirement translates to the measurement of the energy dependence of the chemiluminescent reaction cross section. The photon yield from a reaction is clearly proportional to this cross section.

A technique for making these measurements has been developed under the auspices of the TRW IR&D program. Such measurements have been conducted for the $B + N_2O \rightarrow BO^* + N_2$ and $Ho + N_2 \rightarrow HoO^* + N_2$ reactions as described in Appendix D of this report. The work described in this Appendix was accomplished under IR&D funding after the funding allocated to the molecular beam task of this program was exhausted and is presented for information purposes only.

The acquisition of the basic data to determine the energy dependent cross sections of chemiexcited states utilizes the experimental configuration described above and the raw data are as illustrated in Figure 34. The PMT records the intensity of chemiluminescent radiation from the interaction volume of the crossed beams, and the QPA provides a measure of the flux of metal atoms. More precisely, the magnitude of the signal from the QPA at any instant of time is proportional to the number density of atoms within the ionizer volume. Since the time subsequent to the laser burst determines the velocity of the atoms within the ionizer volume, the flux is readily determined. Given the time dependent flux at the detector, the flux at the target gas location is also determinable. Assuming for the moment that the radiative lifetime of the excited states formed during the reaction is very short, the instantaneous magnitude of the PMT signal is proportional to the number of excited state molecules produced at that particular instant of time. The ratio of the PMT signal to the QPA signal at corresponding times is proportional to the fraction of incident atoms that produce chemiexcited product molecules which, in turn, is proportional to the reaction cross section. Measurement of this ratio as a function of time (i.e., atom

energy) yields the energy-dependent relative reaction cross section.

The results show that the chemiluminescent reaction cross section for low energy boron atoms is small compared to the gas kinetic cross section. For holmium atoms, the chemiluminescent cross section is nearly constant with energy. By inspection of the previously acquired photon yield data, it can be stated that the reactions of Ba, Ce, Fe, Ge, In, Nd, Sm, and Ti with N_2O and NO_2 target gases are similar in general characteristics to the Holmium case while the reactions of Co, Cr, Mn, Mo, Ni, Si, and Sn with N_2O and NO_2 have characteristics similar to the boron case.

3.3.3 Radiative Lifetime Measurements

The measurement of the radiative lifetime of the chemiexcited molecules is important for two reasons: (1) it effects the photon yield measurements and, (2) the lifetime must lie within specified limits (roughly 10^{-5} to 10^{-3} seconds) if the reaction is to be useful in a practical chemical laser system.

With respect to the first of these items, the product molecules remain in the field of view of the PMT for a short, but finite, time. If the radiative lifetime is very short, all of the molecules will be de-excited while in the field of view and all of the photons will be detected. If, on the other hand, the lifetime is long compared to the residence time, only a fraction of the photons will be detected. The residence time lies typically between 10^{-6} and 10^{-5} second .

The lifetime measurement technique employed here is best illustrated by considering the dynamics of the chemical reaction process.

Consider a reaction of the type A + BC → AB + C where A is an atom impinging on molecule BC and AB and C are the resultant products of the reaction. B and C may be either monatomic or polyatomic. If the reaction is exothermic, an amount of chemical energy Q is released in the reaction. The exothermicity may manifest itself by internal excitation of the product molecules, kinetic energy of the product molecules, or a combination of both. Equating the total energy of the system before and after the reaction yields.

$$E_A + E_{BC} + Q = E_{AB} + E_C + E_{int} \tag{14}$$

where the E's are the kinetic energies of the species indicated by the subscript and E_{int} is the internal energy of the product molecule AB. This assumes that A, BC, and C are all in their respective ground states. If it is further assumed that $E_{BC} << E_A$, it can be shown by straightforward analysis that

$$v_{AB} = \frac{m_A v_A}{m_A + m_{BC}} \cos\theta \tag{15}$$

$$\pm \sqrt{\frac{2m_C}{m_{AB}(m_{AB} + m_C)} \left(\frac{m_A m_{BC} v_A^2}{2(m_A + m_{BC})}\right) + Q - E_{int}\left(\frac{m_A v_A}{m_A + m_{BC}}\right)^2 \sin^2\theta}$$

where the m's are the masses of the indicated species, v_A is the velocity of the incident atom, v_{AB} is the velocity of the product molecule, and θ is the angle between the trajectories of A and AB. Equation (15) is the analytical expression for the vector sum of the velocity of the center of mass and the velocity of AB relative to the center of mass. It is valid only when the quantity under the radical is positive. If

the value of the radical is less than the first term on the right hand side for all values of θ, v_{AB} is double valued the positive term corresponding to the forward scattering of AB relative to the center of mass and the negative term to backward scattering.

If the quantities Q and v_A are known (or measured), the measurement of v_{AB} provides sufficient information to determine the value of E_{int} through the use of Equation (14). A graphical display for the $Ge + N_2O \rightarrow GeO + N_2$ reaction is shown in Figure 35. Here the velocity of the GeO molecule at $\theta = 0°$ is plotted as a function of the Ge atom velocity for several values of internal energy of the GeO molecule. For illustrative purposes, it has been assumed that the GeO molecules are in either the electronic ground state ($X^1\Sigma^+$) or the $a^3\Sigma^+$ as observed by Hager, et al [40] Again for illustrative purposes it has been assumed that vibrational levels from v = 0 to v = 5 may be populated even though Hager, et al observed emission only from the v = 0 and v = 1 levels of the $a^3\Sigma^+$ state. Spectroscopic constants for the ground state were taken from Suchard.[31] The spectroscopic constants for the $a^3\Sigma^+$ state are unknown (except for ω_o) so it has been arbitrarily assumed that they are the same as for the ground state. The vibrational broadening leads to a band of GeO molecule velocities for both electronic states. Generally, there would be fine structure within these bands; however, this is relatively unimportant in the present context.

The figure shows four bands. The upper two represent the forward scattered (relative to the center of mass) products while the lower two represent the backward scattered components. These curves show a definite correlation between the velocity of the product molecule

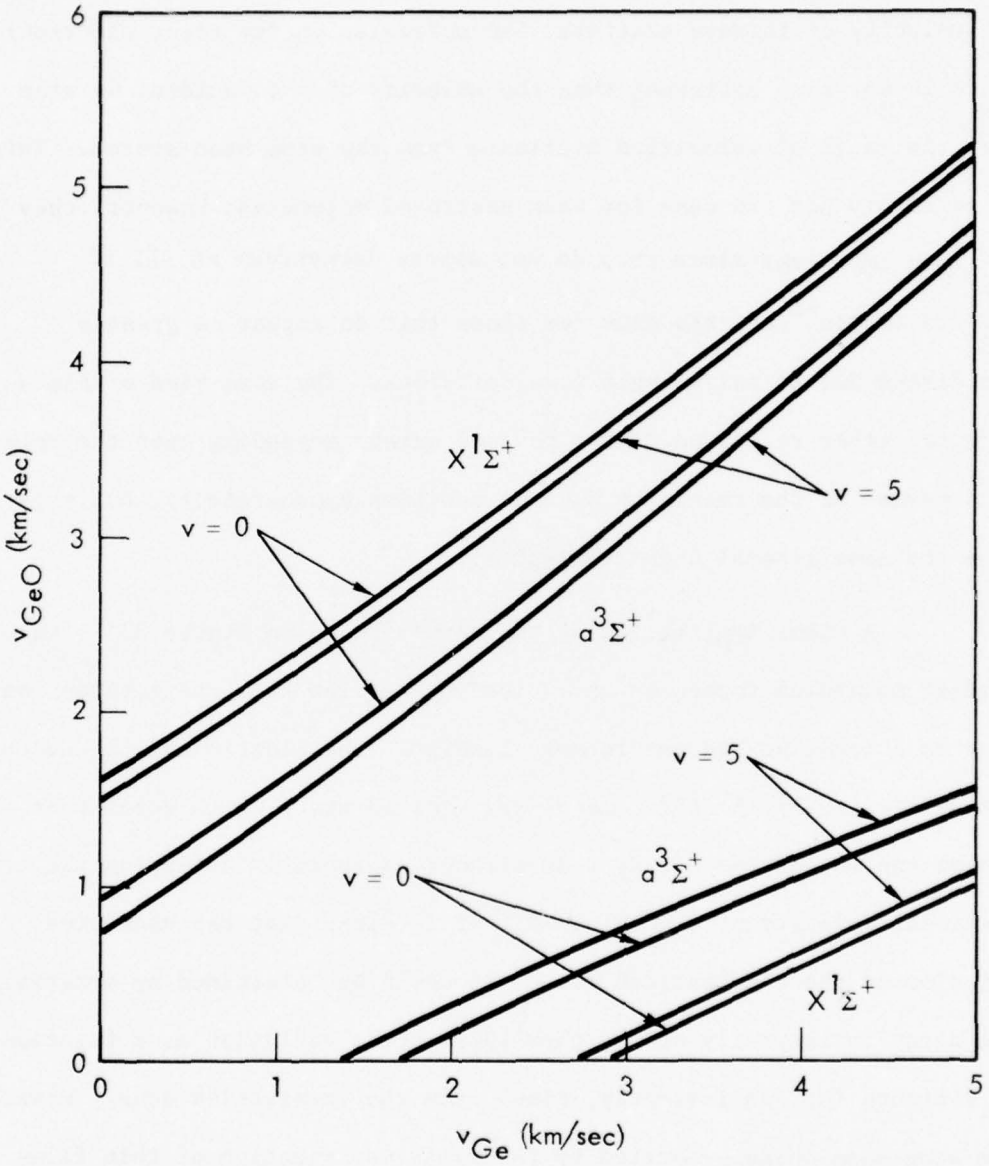

Figure 35. Curves illustrating the dependence of the velocity of GeO molecules as a function of the velocity of Ge atoms from the reaction Ge + N_2O → GeO + N_2. The effect of the internal energy of the GeO molecules is shown by the difference between the curves for $X^1\Sigma^+$ and $a^3\Sigma^+$ molecules.

and the velocity of the incident atom with the internal energy of the product molecule as a parameter. A significant point to note is that the velocity of forward scattered GeO molecules in the first electronic state is not much different than the velocity of the incident Ge atom over the range of velocities available from the atom beam source. This is certainly not the case for back scattered molecules; however, they are less important since they do not appear downstream at all if $v_{Ge} < 3$ km sec^{-1}, and the flux for those that do appear is greatly diminished due to solid angle considerations. The same kind of plots made for other reactions differ to some extent depending upon the relative masses of the reactants and the reaction exothermicity, but they have the same general characteristics.

A clear implication of the curves shown in Figure 35 is that product molecules formed in an excited state flow from the interaction zone in a cohesive and predictable fashion. The kinetics of the reaction are unaffected by the lifetime of the excited state which means that the photon can be emitted at any time without appreciably affecting the translational velocity of the molecule. It is clear that the radiative lifetime of the chemiexcited molecules could be determined by observing the decay in intensity of the chemiluminescent radiation as a function of distance (or, equivalently, time) from the interaction zone. However, the atom beam pulse generated by the laser vaporization of thin films contains a wide range of velocities which gives rise to an even larger range of product molecule velocities. In principle, the mechanical velocity selector could be used to limit the range of atom velocities permitted to reach the target gas. It follows that the range of product molecule velocities would be limited similarly. This approach would

give rise to a nearly discrete "bundle" of product molecules that would emerge from the reaction zone in accordance with the relationship illustrated in Figure 35. This approach was advocated in the original proposal. However, it introduces a degree of experimental difficulty that was deemed to be unjustified for preliminary measurements. Accordingly, the alternate approach described below was used for the initial measurements.

The radiative lifetime measurements have been accomplished by observing the decay of the radiant emission from the reaction products as they drift downstream from the reaction zone with no limitation to the velocity range of the incident beam atoms. This procedure, of course, requires the removal of the QPA. It is replaced with a linear array of three PMT's with their fields-of-view limited by collimators to small segments of this axis. The PMT's are spaced apart by 6 inches with the first one located a distance of 5.675 inches from the center of the reaction zone. The product molecules emanating from the reaction zone are collimated into a narrow cone such that all of the product molecules pass through the field of view of all three PMT's. Each PMT "sees" the photons emitted from the burst of molecules as it passes through the field of view. The flux of product molecules at a given observation point varies with time in much the same fashion as the incident atom beam. However, the width of the signal increases along the axis because of velocity spreading.

For a given reaction the PMT's are first used in a current mode. The time interval between the maxima of any pair of signals is taken as the time interval over which the measurement is made. The experiment is then repeated with the PMT's in an integrating mode. The

integrated signal amplitude is proportional to the total number of photons emitted within the field of view of the detector. The lifetime of the transition is then determined from the relationship

$$\tau = \frac{t}{\ln \frac{N_1}{N_2}} \tag{16}$$

where t is the elapsed time between the maxima of the differential signals observed at the two stations, and N_1 and N_2 are determined from the integrated signals at the respective stations.

The principal uncertainty in determining the radiative lifetime in this manner is involved with assigning a common value of t for all of the detected molecules because there are, in fact, large variations in the elapsed time between the formation of a molecule and its arrival at one of the observation stations. The assigned t is, at best, an average. On the other hand, assigning a common time interval is equivalent to assigning the same velocity to all reaction products. If this were, in fact, the case, the intensity of the chemiluminescent radiation would decay exponentially with distance along the measurement axis. With the exception of CeO, all of the reactions studied to date exhibited an exponential decrease in intensity with distance. The data obtained for some of the reactions studied are shown in Figure 36. This observation indicates that the technique is not subject to significant systematic errors. Normally, redundant measurements are performed by using pairs of measuring stations and computing the lifetime from each of the two pairs independently. The first set uses PMT's 1 and 2 separated by 6 inches and the other set uses PMT's 1 and 3 separated by 12 inches. Data between the two sets are consistent except for certain short-lived

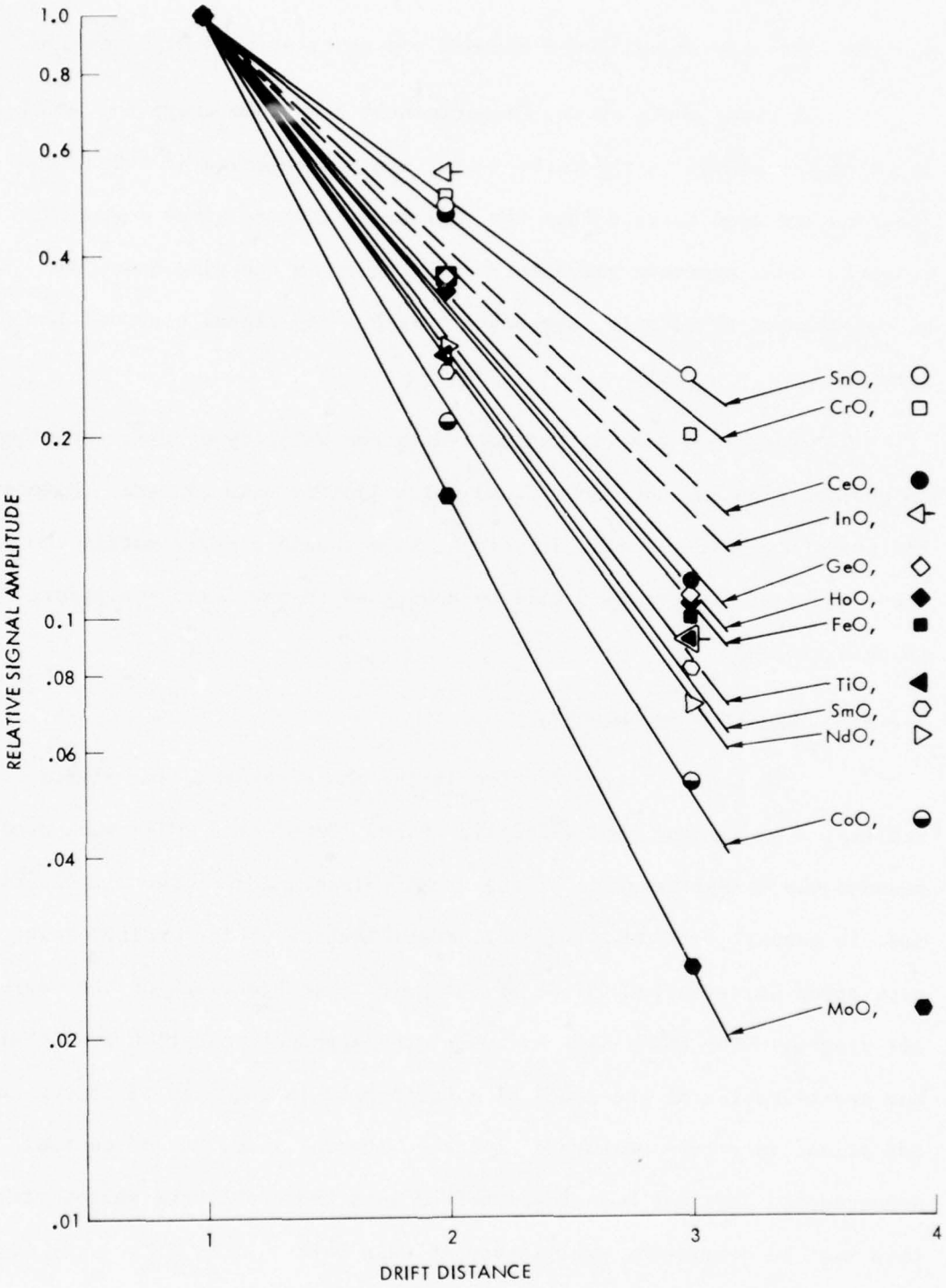

Figure 36. Graphs depicting relative signal levels from chemiexcited metal monoxide molecules as a function of distance. The measurement stations are separated by 6 inches. A straight line on a semi-log plot indicates an exponential decay of the signal strength.

species where the signal level becomes too small at the third station.

A crude check of this experimental technique where the amplitudes of the maxima in the current-mode signals observed at two of the stations are used to calculate the radiative lifetime gives comparable results. This approach gives less uncertainty in the time base, but is complicated by velocity spreading of the light signal observed downstream.

Questions have arisen regarding the validity of this technique. No obvious problems have been found which justify this concern. However, the use of an energy selected incident beam should clearly settle the issue and such measurements will be conducted in any follow-on effort to this program.

3.3.4 Spectral Measurements

The basic instrumentation in the photon yield measurements utilizes a broad-band photomultiplier tube. Broad-band PMT's were used because the characteristics of the chemiluminescent spectral distribution are, in general, unknown. In fact, specification of the excited state population distribution is one of the principal objectives of the overall program. The PMT's have a wavelength-dependent detection sensitivity and specification of the spectral distribution is required to convert the PMT signal to a true measure of relative photon yield. Such spectral measurements have not been completed as yet; therefore, the photon yield data must be considered preliminary at this point.

It was originally anticipated that spectral information on the chemiluminescent reactions would be obtained through the use of

filtered PMT's with resolution capability on the order of 100 Å. This approach requires a large number of shots and yields somewhat uncertain results because of the complicated spectral response characteristics of the individual filter-PMT combinations. An alternative approach which has been used on a preliminary basis uses a small grating monochromator in conjunction with a broad band PMT to record the chemiluminescent spectrum. This approach has the advantage that the spectral response characteristic is set primarily by the slit width and varies only slightly as a function of wavelength. It has the further advantage that the center wavelength can be set arbitrarily so that the possibility of missing prominent features that could fall between adjacent filters is reduced.

An example of a chemiluminescent spectrum obtained in this manner is given in Figure 37. The spectrum in Figure 37 derives from the $Sn + N_2O \rightarrow SnO^* + N_2$ reaction. Although the spectrum is clearly lacking in detail, its gross features are compatible with the known spectral content of chemiluminescent radiation from the SnO formation reaction. Recent experiments by Felder and Fontijn (AeroChem)[41] and Linevsky and Carabetta (G. E.)[42] have examined the spectral characteristics of chemiluminescent radiation from SnO by different techniques. Felder and Fontijn interpret their results as indicating that the A state is formed preferentially, but admit that collisional de-excitation of the upper states could distort the spectrum. The General Electric experiment, on the other hand, observed that radiation from the electronic D-state dominated the spectrum. The results obtained here, although they must be considered to be preliminary until a higher resolution spectrum is obtained, are more consistent with the General Electric result in

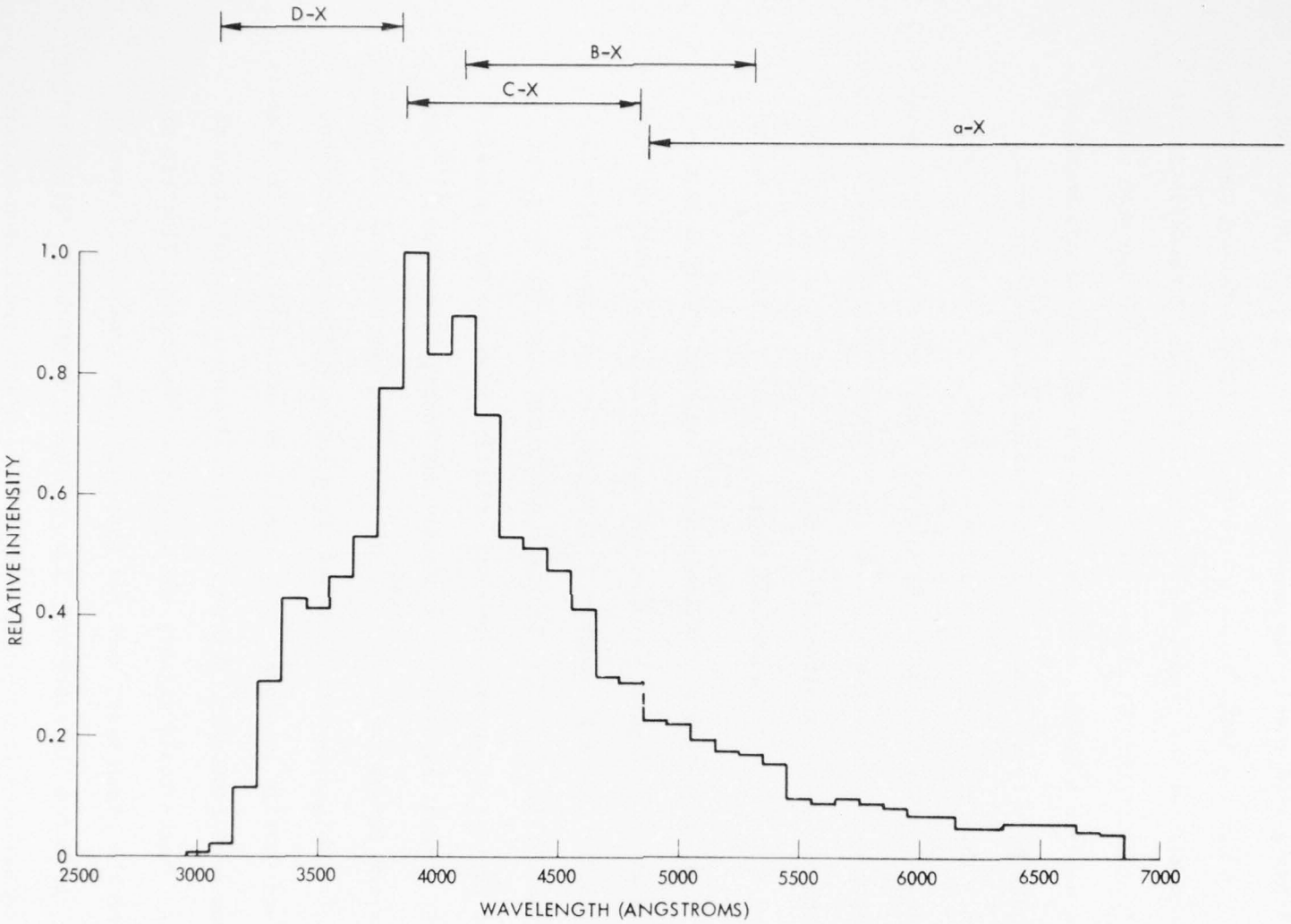

Figure 37. Chemiluminescence spectrum from the Sn + N_2O → SnO* + N_2 reaction at 100Å resolution. The transition bands shown correspond to the regions where Levinesky and Cabaretta (Ref. 21) identified spectral features.

that D and C state transitions dominate the spectrum. Within the context of determining the initial excited distribution of electronic states, the difference between our results and those of Felder and Fontijn illustrate the desirability of performing the experiments under single collision conditions.

The requirements for obtaining higher resolution spectra have been evaluated with the result that an Optical Multichannel Analyzer (OMA) manufactured by Princeton Applied Research Inc. has been ordered and will be available for future programs. The OMA utilizes an f/5 grating polychromator system to disperse light over 500 separate channels on the face of a silicon-intensifier target vidicon. Each channel may be considered as a separate detector with a quoted sensitivity of about 0.1 digital counts per incident photon (high sensitivity version). The system includes a digital readout system with background subtraction and signal averaging capabilities. Because of the pulsed nature of our experiments, a cooled detector version which permits integration over several events before readout has been ordered.

Quantitative measurements indicate that something on the order of 10^{10} photons are emitted from the interaction volume of the two beams during an event. The B + N_2O reaction was examined in a bit more detail using a f/2.5 lens set for unity magnification at a dummy slit that modeled the OMA. The polychromator within the OMA utilizes an f/2.5 optical system so that all of the photons delivered to the dummy slit would reach the OMA detector array. It was found that about 5×10^6 photons were focused through a 1 x 8 mm slit (corresponding to 400 Å resolution) and about 8×10^5 photons were focused through a 0.25 x 8 mm

slit (100 Å resolution). Taking into account transmission losses, detector sensitivity and a worse case spectral distribution (i.e., uniform distribution across the 500 channels), the measurements indicate that a minimum signal to noise ratio of 25 would be obtained at the 100 Å resolution level. Since spectra of interest will have structure, the signal-to-noise ratio for prominent spectral features will be greater which will permit higher resolution spectra to be obtained. For strong emitters, the entire spectrum can be mapped with just enough events to cover the spectrum. For less intense sources, a trade-off between resolution and integration over several events to obtain the desired signal-to-noise ratio exists, but it appears that the capability to obtain high quality spectral data for all significant chemiluminescent reactions will be available for future measurements.

3.4 Results and Summary

One of the significant results of this program has been the development of the techniques and procedures described in the preceding sections of this report. Although the basic principles of the proposed measurements were reasonably well defined prior to the inception of the program, a good deal of effort was required to reduce these concepts to practice. Clearly, even more work is required before the unwritten objective of finding a reaction that will serve as the basis for a whole new class of chemical lasers is satisfied. However, due to the accomplishments of the present program, most of the experimental measurements have been reduced to a routine level and future progress should be more rapid.

Although all of the measurements of the sequence are important,

it is apparent that the data acquired to date cannot be interpreted adequately until spectra of the chemiluminescent radiation from the various reactions are obtained. Measurements conducted under this program show that moderately high resolution spectra of the chemiluminescence can be obtained with the Optical Multichannel Analyzer system. Unfortunately, it was not received in time to be used on the present program. The measurement of spectra would receive high priority in a continuing effort.

The technique described in Appendix D for the measurement of the energy dependence of chemiluminescent reaction cross sections was also developed too late to be used routinely on all of the reactions studied. However, it is a relatively simple matter to perform the necessary experiments and data analysis at this point.

The principal findings of the present program are summarized in Table 5. Here the relative photon yields for the various reactions as obtained by the methods described in Section 3.3.2 are listed.

The radiative lifetimes of the chemiexcited molecules are also given. Since spectral information is lacking, the electronic states to which the lifetime measurements apply have not been identified. The experimental results are consistent with either a single state or with the combination of several states with nearly identical lifetimes. In view of the fact that a large number of these reactions have apparent lifetimes in the 10 to 100 microsecond range, the validity of the lifetime measurements has been questioned by other workers in the field. We can only state that the fundamental approach is scientifically sound and no experimental artifacts have as yet been found that would cause erroneous results. However, work is continuing to resolve this question.

TABLE 5. Summary of Chemiluminescent Reaction Data

Metal	Relative Photon Yield		Radiative Lifetime (μ sec)	Reaction Figure-of-Merit	
	N_2O	NO_2		N_2O	NO_2
Ba	1.02	1.13	-	-	-
Ce	.14	.14	107	15	15
Co	.11	.06	32	3	2
Cr	.09	.05	87	7	5
Fe	1.19	.82	20	24	16
Ge	.76	.39	55	42	21
Ho	1.23	.30	47	58	14
In	.61	-	17	10	-
Mn	∿ 0				
Mo	1.24	.54	34	42	18
Nd	.90	.60	43	39	25
Ni	∿ 0	-			
Si	.04	.04	-	-	-
Sm	.15	.01	48	7	<1
Sn	.07	.02	110	8	3
Ti	.57	.94	31	18	29

As discussed in Sections 3.3.2 and 3.3.3, determination of the total photon yield must take the radiative lifetime into account. This was done here by taking the product of the relative photon yield and the radiative lifetime to give "figures-of-merit" for the various reactions. These are listed in the last two columns of the table. On this basis, the reaction of Holmium with N_2O is the "best" of those studied, whereas some of the favorites such as Sn + N_2O fare rather poorly.

REFERENCES

1. J. M. Herbelin and N. Cohen, "The Chemical Production of Electronically Excited States in the H/NF_2 System", Chem. Phys. Lett. 20, 605 (1973).

2. M. Jeunehomme, "Oscillator Strength for the CN Red Band System", J. Chem. Phys. 42, 4086 (1965).

3. G. Palletto and M. Rigutte, "The $A^2\Pi$ and $X^2\Sigma$ States of the CN Molecule from the Berkeley Analysis of the CN Red System", Nuovo Cimento 39, 519 (1965).

4. R. G. Darwent and B. A. Thrush, "Excitation of Iodine by Singlet Molecular Oxygen", Chem. Soc. Faraday Disc. 53, 162 (1972).

5. N. V. Kondratiev, Rate Constants of Gas Phase Reactions, (National Bureau of Standards, COM-72-10014) January, 1972.

6. C. K. N. Patel, "Continuous-Wave Laser Action on Vibrational-Rotational Transitions of CO_2", Phys. Rev. 136, A1187 (1964).

7. A. K. McKnight and P. J. Modreski, "Chemical Production of Singlet Oxygen," Laser Digest, Fall 1974, AFWL-TR-74-344, 346.

8. J. A. Blauer and W. C. Solomon, "Catalytic Efficiencies of Atoms in the Vibrational Relaxation of HF and DF", 14th Symposium on Combustion 14, 189 (1972).

9. R. J. Donovan and D. Husain, Trans. Faraday Soc. 62, 1050 (1966).

10. K. Sakurai, G. Capelle and H. P. Broida, "Measurements of Lifetimes and Quenching Cross Sections of the B State of Iodine", J. Chem. Phys. 54, 1220 (1971).

11. G. Capelle, K. Sakurai and H. P. Broida, "Lifetimes and Self-Quenching Cross Sections of Vibrational Levels in the B State of Bromine", J. Chem. Phys. 54, 1728 (1971).

12. G. W. Holleman and J. I. Steinfeld, "Time-resolved Fluorescence of Iodine Monochloride", Chem. Phys. Lett. 12, 431 (1971).

13. N. H. Kiess and H. P. Broida, "Emission Spectra from Mixtures of Atomic Nitrogen and Organic Substances", Spectroscopy of Flames, 207 (1966).

14. D. W. Setser and B. A. Thrush, "Kinetics of Reactions Involving CN Emission I. General Features of Reactions with Active Nitrogen and Atomic Oxygen", Proc. Roy. Soc. A288, 256 (1965).

15. E. L. Tollefson and D. J. LeRoy, "The Reaction of Atomic Hydrogen with Acetylene", J. Chem. Phys. 16, 1057 (1948).

16. C. B. Colburn, et al, "Bond Strength of Tetrafluorohydrazine", Paper Presented at 140th Meeting of the American Chemical Society, Chicago, Illinois, September 6, 1961.

17. F. A. Johnson et al, "Quarterly Progress Report on Air Force High Energy Solid Propellant Program", Rohn and Haas Co., Rept. No. AF-7, November 1960.

18. B. A. Thrush, "Reactions of Hydrogen Atoms in the Gas Phase", Progress in Reaction Kinetics 3, 63 (1965).

19. M. A. A. Clyne and J. F. White, "Electronic Energy Transfer Processes in Fluorine-Containing Radicals: Singlet NF", Chem. Phys. Lett. 6, 465 (1970).

20. John V. White, "Long Optical Paths of Large Aperature", J. Op. Soc. Am. 32, 285 (1942).

21. J. C. Boden and B. A. Thrush, "Kinetics of Reactions Involving CN Emission IV. Study of the Reactions of CN by Electronic Absorption Spectroscopy", Proc. Roy. Soc. A305, 107 (1968).

22. A. C. G. Mitchell and M. W. Zemansky, Resonance Radiation and Excited Atoms, (Cambridge University Press, 1961) Appendix 4.

23. G. Herzberg, Spectra of Diatomic Molecules, (D. Van Nostrand Company, Inc., Princeton, New Jersey, 1950).

24. D. D. Davis and H. Okabe, "Determination of Bond Dissociation Energies in Hydrogen Cyanide, Cyanogen and Cyanogen Halides by the Photodissociation Method", J. Chem. Phys. 49, 5526 (1969).

25. R. F. C. Claridge, F. T. Greenaway and M. J. McEwan, "Reactions of Hydrogen Atoms with Hydrogen Cyanide", J. Phys. Chem. 74, 3293 (1970).

26. E. B. Turner, G. Emanuel and Roger Wilkens, The Nest Computer Program, Volume 1 , SAMSO-TR-70-311, July 1970.

27. S. E. Johnson and A. Fontijn, "150-230 nm Chemiluminescence from C, CN and CO and Observation of $C(^3P, ^1D)$ in the N/C_2F_4 and $N/O_2/C_2F_4$ Reactions", Chem. Phys. Lett. 23, 252 (1973).

28. E. A. Ogryzlo, J. P. Reilly and B. A. Thrush, "Vibrational Excitation of CO from the Reaction $C + O_2$", Chem. Phys. Lett. 23, 37 (1973).

29. J. A. Betts, Chemically Pumped Ultraviolet Laser Study , AFWL-TR-74-165, June 1974.

30. G. W. Taylor and D. W. Setser, "Quenching Rate Constants for $CO(a^3\Pi)$", J. Chem. Phys. 58, 4840 (1973).

31. S. N. Suchard, Spectroscopic Constants for Selected Heteronuclear Diatomic Molecules, Vol. II , Aerospace Report No. TR-0074 (4641)-6 p. N-34.

32. J. C. Stephenson, "Vibrational Energy Transfer in NO", J. Chem. Phys. 59, 1523 (1973).

33. a) W. Braun, A. M. Bass, D. D. Davies and J. D. Simmons, "Flash Photolysis of Carbon Suboxide: Absolute Rate Constants for Reactions of $C(^3P)$ and $C(^1D)$ with H_2, N_2, CO, NO, O_2 and CH_4", Proc. Roy. Soc. A312, 417 (1969).

b) D. Husain and L. J. Kirsch, "Reactions of Atomic Carbon by Kinetic Absorption Spectroscopy in the Vacuum Ultraviolet", Trans. Faraday Soc. 67, 2025 (1971).

34. T. G. Slanger and G. Black, "$CO(a^3\Pi)$, Its Production, Detection, Deactivation, and Radiative Lifetime", J. Chem. Phys. 55, 2164 (1971).

35. "New Gas Lasers Committee Report on Electronic Transition Chemical and Electrical Excited Lasers", 21-22 September 1972 meeting, Advanced Technology Branch, Laser Division, Air Force Weapons Laboratory, Kirtland Air Force Base, N. M.

36. J. F. Friichtenicht, "Laser-generated Pulsed Atomic Beams", Rev. Sci. Instrum. 45, 51 (1974).

37. N. G. Utterback, S. P. Tang and J. F. Friichtenicht, "Atomic and Ionic Beam Source Utilizing Pulsed Laser Blow Off", submitted to the Journal of the Physics of Fluids for publication.

38. B. deB. Darwent, Bond Dissociation Energies in Simple Molecules, U. S. Department of Commerce, National Bureau of Standards, NSR DS-NBS31, Issued January 1970.

39. T. L. Cottrell, The Strengths of Chemical Bonds, second edition (Butterworths Scientific Publications, London, 1958).

40. G. Hager, L. Wilson, and S. G. Hadley, "Reactions of Atomic Silicon and Germanium with Nitrous Oxide to Produce Electronically Excited Silicon Monoxide and Germanium Monoxide", Chem. Phys. Lett. 27, 439 (1974).

41. W. Felder and A. Fontijn, "High-Temperature Fast-Flow Reactor Study of Sn/N_2O Chemiluminescence", AeroChem Research Laboratories, Inc., Report No. TP-320, March 1975 (submitted to Chemical Physics Letters for publication).

42. M. J. Kinevsky and R. A. Carabetta, Chemical Laser Systems , Interim Technical Report, Contract No. DAAH01-73-C-0653 (1 September 1974 - 1 April 1975). General Electric Document No. 75 SDS 4219.

43. G. A. West and M. J. Berry, "CN Photodissociation and Predissociation Chemical Lasers: Molecular Electronic and Vibrational Laser Emissions", J. Chem. Phys. 61, 4700 (1974).

44. T. Fay, I. Marenin and W. Van Citters, "Perturbation Analysis and Constants for the Red System of the Cyanide Radical", J. Quant. Spectrosc. Radiat. Transfer 11, 1203 (1971).

45. S. P. Davis and J. G. Phillips, Red System ($A^2\Pi - X^2\Sigma$) of the CN Molecule, (University of California Press, Berkeley and Los Angeles.

46. J. M. Weinberg, E. S. Fishburne and K. N. Rao, "Infrared Bands of the CN Red System", J. Molec. Spectroscopy 22, 406 (1967).

47. L. Glatt, Synthetic Spectra for Diatomic Molecules $^2\Pi \rightarrow {}^2\Sigma$ and $^2\Sigma \rightarrow {}^2\Pi$ Band Sequences , TRW Report No. 06488-6363-RO-00, February, 1970.

48. E. E. Whiting, J. O. Arnold and G. C. Lyle, A Computer Program for a Line-by-Line Calculation of Spectra from Diatomic Molecules and Atoms Assuming a Voigt Line Profile , NASA TN D-5088, October, 1969.

49. J. F. Friichtenicht, "Laser-generated Pulsed Atomic Beams", Rev. Sci. Instrum. 45, 51 (1974).

50. H. S. W. Massey, Electronic and Ionic Impact Phenomena, 2nd Ed. Vol. 3, (Oxford Press, London, 1971).

51. P. L. Owen and C. K. Thornhill, Aeronautical Research Council (U.K.) R & M No. 2616 (1948).

52. F. S. Sherman, Lockheed MSC Tech. Rept., Fluid Mechanics 6-90-63-61, (1963).

53. H. Ashkenas and F. S. Sherman, Rarefied Gas Dynamics, J. H. DeLeeuw, Ed., (Academic Press, New York, 1966).

54. N. G. Utterback, S. P. Tang, and J. F. Friichtenicht, "Atomic and Ionic Beam Source Utilizing Pulsed Laser Blow Off", submitted to the Journal of the Physics of Fluids for publication.

APPENDIX A. Spectroscopy of the CN($A^2\Pi - X^2\Sigma$) System

The $X^2\Sigma$ ground state of the CN radical belongs strictly to Hund's coupling case (b) so that the quantum number K of the total angular momentum apart from spin is defined. The first excited electronic state, $A^2\Pi$, is intermediate between Hund's case (a) and case (b). The $A^2\Pi$ state is "inverted", with the $^2\Pi_{3/2}$ levels lying lower than the corresponding $^2\Pi_{1/2}$ levels. Since the coupling constant A is (-) 52.2 cm^{-1}, the separation of the lower $^2\Pi_{3/2}$ and upper $^2\Pi_{1/2}$ components is approximately 50 cm^{-1} for low J and slowly increases with J.

Herzberg[23] shows that for $^2\Pi \rightarrow {}^2\Sigma$ transitions, where the $^2\Pi$ state belongs to Hund's case (a), all transitions obeying the selection rules $\Delta J = 0, \neq 1$ are possible. This means that there are 12 allowed transitions arising from a given J'. A Fortrat diagram for the (9,3) CN red band is given in Herzberg,[23] page 260. From this it can be seen that four pairs of the twelve branches superimpose, leaving eight independent branches. A more detailed description of the CN energy levels is given by West and Berry[43] in Appendix A of their paper.

The vibration-rotation constants of Fay, Marenin and van Citters[44] were used to calculate the term values and transition energies for the 0, 1 and 0,2 bands. These constants yield a very good fit for the (0,0)[45] and (0,1)[46] bands where good experimental values were available.

In order to obtain a fit to our experimental spectrum, it was also desirable to determine the relative rotational line intensities of the various lines. Under conditions of rotational and vibrational equilibrium, the line intensities can be approximated by[47]:

$$I(v',v'';\ m,i,n) \simeq -\frac{\sigma''}{\sigma'} \frac{N'}{Q_{v',r'}} \frac{4\pi e^2 h}{m_e} \frac{f_{el}}{\nu_{v',v''}} \cdot I_{rel}$$

where

$$I_{rel} = \nu^4(v',v'';m,i,n)\ q(v',v'')\ S(m,i,n)\ \exp\{-c_2 T^{-1}[G'_o(v')+F'(m,i)]\}$$

In the above $Q_{v',r'}$ is the rotation-vibration partition function for the upper state; f_{el} is the electronic f-number, ν is the transition frequency, $q(v',v'')$ is the Franck-Condon factor and $S(m,i,n)$ is the line strength factor. The index i can be plus one or minus one while the index n runs from -1 to +2. The index m is related to the upper state J' by $2m = 2J' + 1$. Table 6 correlates the (i,n) indices to spectral branches and also gives the equations for the rotational line strengths for each set of indices.[47] Line positions and relative line intensities were computed on a CDC 6000 series computer. They are plotted as a function of wavelength in Figure 38 for a temperature of 3000°K. The wavelength scale on such plots can be adjusted to match the experimental scale so the plots can be laid directly over experimental data to aid in rotational line identification.

Table 6. Correlation of Spectral "Branches" to (i,n) - Indices Pairs and Equations for Rotational Line Strength Factors

i	n	Spectral Branches $m = J' + 1/2$	Rotational Line Strength Factors $S(m,i,n)$
-1	-1	$R_{11}(m)$	$S(m,i,-1) = \dfrac{m^2 - iU(m)}{8m - 4}$
+1	-1	$S_{R_{21}}(m)$	
-1	0	$Q_{11}(m) + {}^{Q}R_{12}(m)$	$S(m,i,0) = \dfrac{3m^2 + 2m - iU(m)}{8m + 4}$
+1	0	$R_{22}(m) + {}^{R}Q_{21}(m)$	
-1	1	$P_{11}(m) + {}^{P}Q_{12}(m)$	$S(m,i,1) = \dfrac{3m^2 - 2m + iU(m)}{8m - 4}$
+1	1	$Q_{22}(m) + {}^{Q}P_{21}(m)$	
-1	2	${}^{O}P_{12}(m)$	$S(m,i,2) = \dfrac{m^2 + iU(m)}{8m + 4}$
+1	2	$P_{22}(m)$	

where: $U(m) \equiv \dfrac{m(m^2 - Y/2)}{[m^2 + Y/2(Y/2-2)]^{1/2}} \equiv \dfrac{m(m^2 - Y/2)}{z(m)}$; $Y = A_v/B_v$

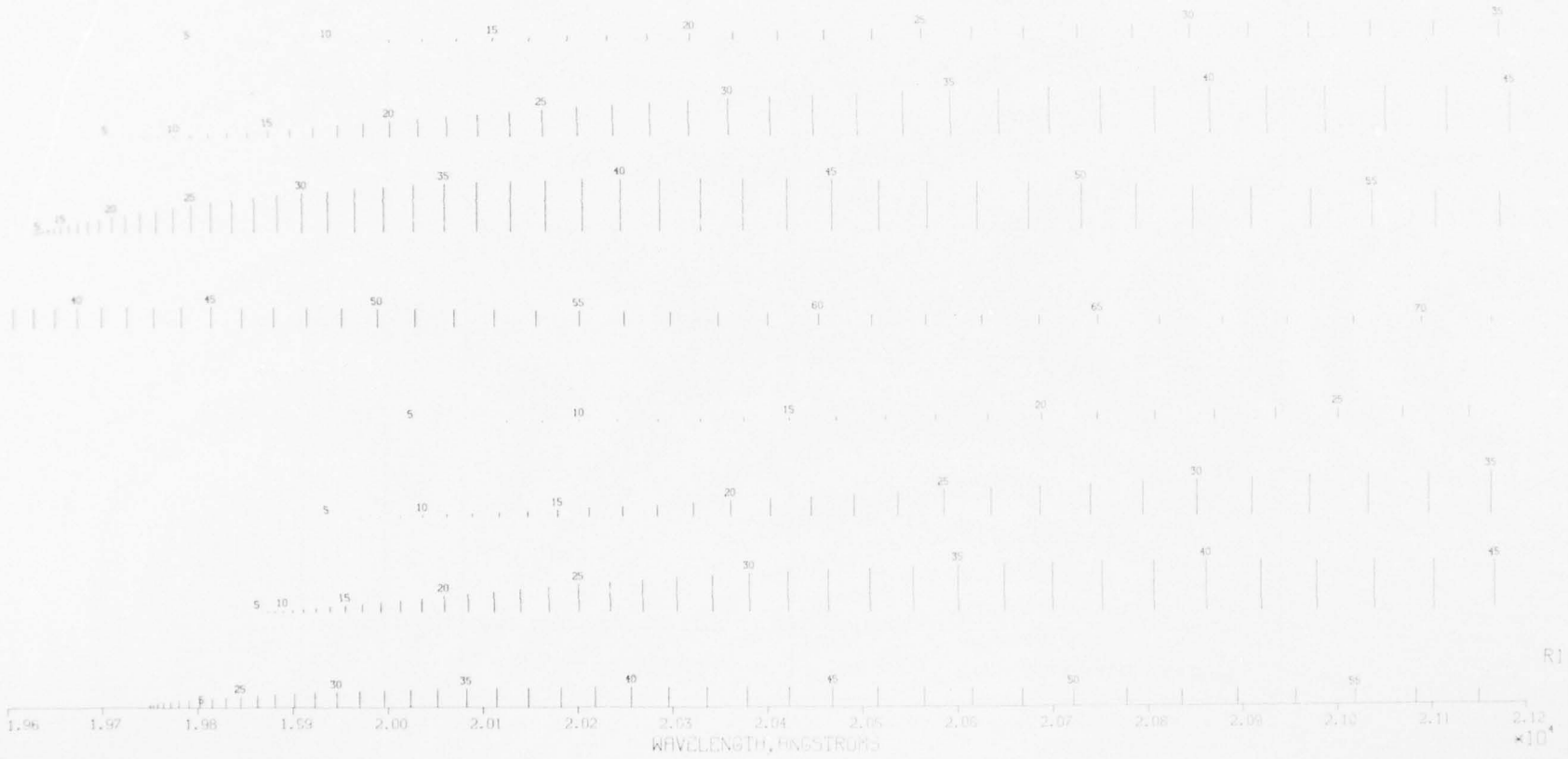

Figure 38. Plot of rotational line positions and line strengths for the (0,2) band of the CN(A-X) system.

APPENDIX B. Synthetic Spectra

Two computer programs for generating synthetic spectra were available. The one used most extensively was generated at TRW. It used the formulas in Appendix A to calculate relative line strengths of the various rotational ines in the bands in the spectral region of interest. These intensities were then normalized to 1 for the strongest line in the wavelength interval of interest. A slit function of the form

$$g(\lambda-\lambda_j) = \begin{cases} \frac{1}{\Delta\lambda}\left[\frac{\Delta\lambda - |\lambda - \lambda_j|}{\Delta\lambda}\right] & \text{for } |\lambda-\lambda_j| \leq \Delta\lambda \\ 0 & \text{for } |\lambda-\lambda_j| > \Delta\lambda \end{cases}$$

based on the experimental slit function was used. In the above, $\Delta\lambda$ is the slit width, λ is the independent variable and λ_j is the wavelength at which a rotational line exists. A set of discrete wavelenghts, λ_r, equally spaced between a minimum and maximum wavelength was then selected. The intensities resulting from all the discrete λ_j's were then computed from

$$I_T(\lambda_r) = \sum_j I_T(\lambda_j)\, g(\lambda_r - \lambda_j)$$

where $I_T(\lambda_j)$ is the computed relative intensity and the sum over j stands for a sum over n, i, m, v" and v'. These indices were described in Appendix A. The integrated intensity could then be plotted versus wavelength to produce a synthetic spectra. The spectra shown in Figure 18 of the report were generated in this manner with a 20Å slit width.

A second program created by Ames Research Center[48] was also available. Some attempts were made to use this program, but in general it was found to be easier to use the TRW generated program. The Ames

program contains more options and is more versatile for a variety of applications.

APPENDIX C. Selection of Lines for Gain Measurement

Considerable care was taken in chosing specific lines for use in a gain measurement. Careful spectroscopic measurements were first performed to identify the lines present in the experimental spectrum. An expanded spectrum of part of the (0,1) band is shown in Figure 39. Such spectra were used in conjunction with the calculated line positions and the synthetic spectra to choose a relatively "clean" line for gain measurements. The choice of lines considered was also limited to those in the Q_{11} and P_{11} branches as these are the lines where lasing occurred in a flash photolyses laser.[43] Several lines in the Q_{11} branch, specifically $Q_{11}(15)$ and $Q_{11}(17)$ of the (0,1) band were found to be most suitable for gain measurements. Identification of lines in the (0,2) band was more difficult due to lack of previous experimental data. This aspect of the gain measurement was the most time consuming as choice of overlapping lines could lead to erroneous measurements. A gain measurement using a pulsed CN laser such as has been built by Curt Wittig at University of California would be preferable in that only narrow, spectrally pure lines would be available.

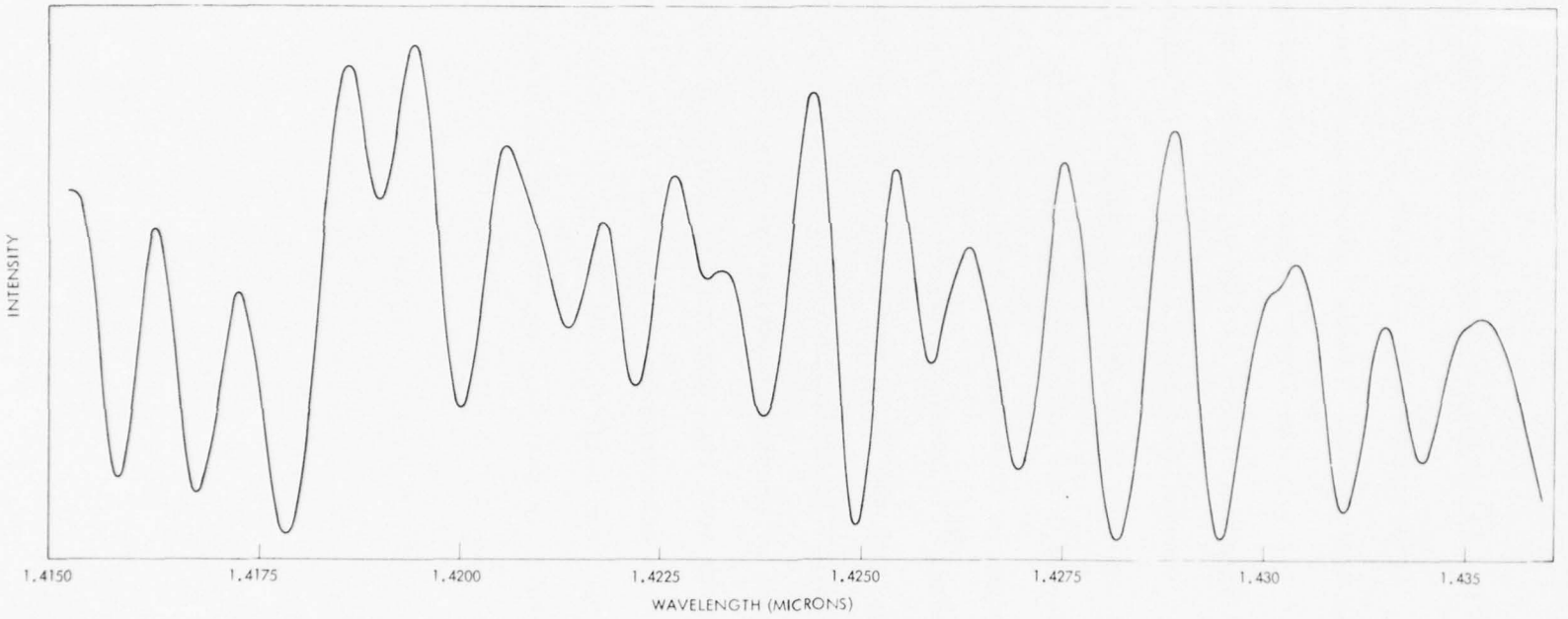

Figure 39. High resolution spectrum of a portion of the (0,1) band spectrum of the CN(A-X) system.

APPENDIX D

Measurement of Chemiluminescent Reaction Cross Sections for $B + N_2O \rightarrow BO^* + N_2$ and $Ho + N_2O \rightarrow HoO^* + N_2$

Prepared by

S. P. Tang, N. G. Utterback, and J. F. Friichtenicht

TRW Systems Group
Redondo Beach, California 91728

APPENDIX D

INTRODUCTION

Much of the current research on exothermic chemiluminescent reactions is motivated by the search for chemical systems compatible with the requirements of electronic transition chemical lasers. The reactions of metal atoms with various oxidizers to form chemiexcited metal-oxide molecules are included among those under study. A number of factors are involved in the ultimate applicability of these reactions, one of which is the reaction rate for formation of product molecules in the upper lasing state. In this Appendix, a new experimental technique for the measurement of reaction cross sections of chemiexcited states as a function of the kinetic energy of the reactants is described. Illustrative results for the $B + N_2O \rightarrow BO^* + N_2$ and $Ho + N_2O \rightarrow HoO^* + N_2$ reactions are presented. In principle, the reaction rate for a particular process can be determined from such cross section data.

The experiments utilize a crossed beam configuration where the metal atom beam is produced by the laser blow-off technique described by Friichtenicht.[49] This source delivers a high intensity pulse of metal atoms to the interaction region with a broad, but directly measureable, velocity distribution. The target gas beam is obtained from a room temperature nozzle source. The experiments are conducted by performing simultaneous measurements of the intensity of the chemiluminescent radiation from the reaction region and the intensity of the atom beam pulse downstream from the reaction region.

As presently constituted, the experiment yields the relative chemiluminescent reaction cross section as a function of atom energy and

the energy dependence of the total scattering cross section on a relative basis. A broad spectral response photomultiplier tube was used to detect the chemiluminescense in the initial experiments described here and, therefore, the chemiexcited state (or states) has not been identified.

EXPERIMENTAL APPARATUS AND PROCEDURES

A. Apparatus

The experimental apparatus shown schematically in Figure D1 utilizes a crossed atomic-molecular beam configuration. The metal atom beam is produced by the newly-developed technique of laser volatilization of solid material[49] and the target gas consists of a nozzle beam defined by supersonic free jet expansion. A Q-switched ruby laser is used to deliver a nominal 1 Joule pulse to the metal target in about 75 nanoseconds. The laser beam is directed through a quartz window and partially focused on the metal target by a 125 mm focal length lens. The lens-to-target distance is externally adjustable allowing variations in the laser beam energy density at the target surface. For the present experiments, this distance was empirically set at 100 mm for boron targets and 89 mm for holmium targets.

The laser beam targets (boron and holmium) in the form of ~1 micron thick vapor deposited films on glass microscope slides are mounted in an assembly that permits translation of the target along an axis normal to the laser beam and rotation of the target surface about this axis. The target is moved along the axis after each shot to expose fresh material for the succeeding shot. It was found that the velocity distribution of the atoms produced by laser bombardment is a function of the angle between the target normal and the laser beam axis. This angle was set arbitrarily at 45° for the present experiments. In all cases, the laser beam was directed through the glass slide and was incident on the side of the film in contact with the glass substrate.

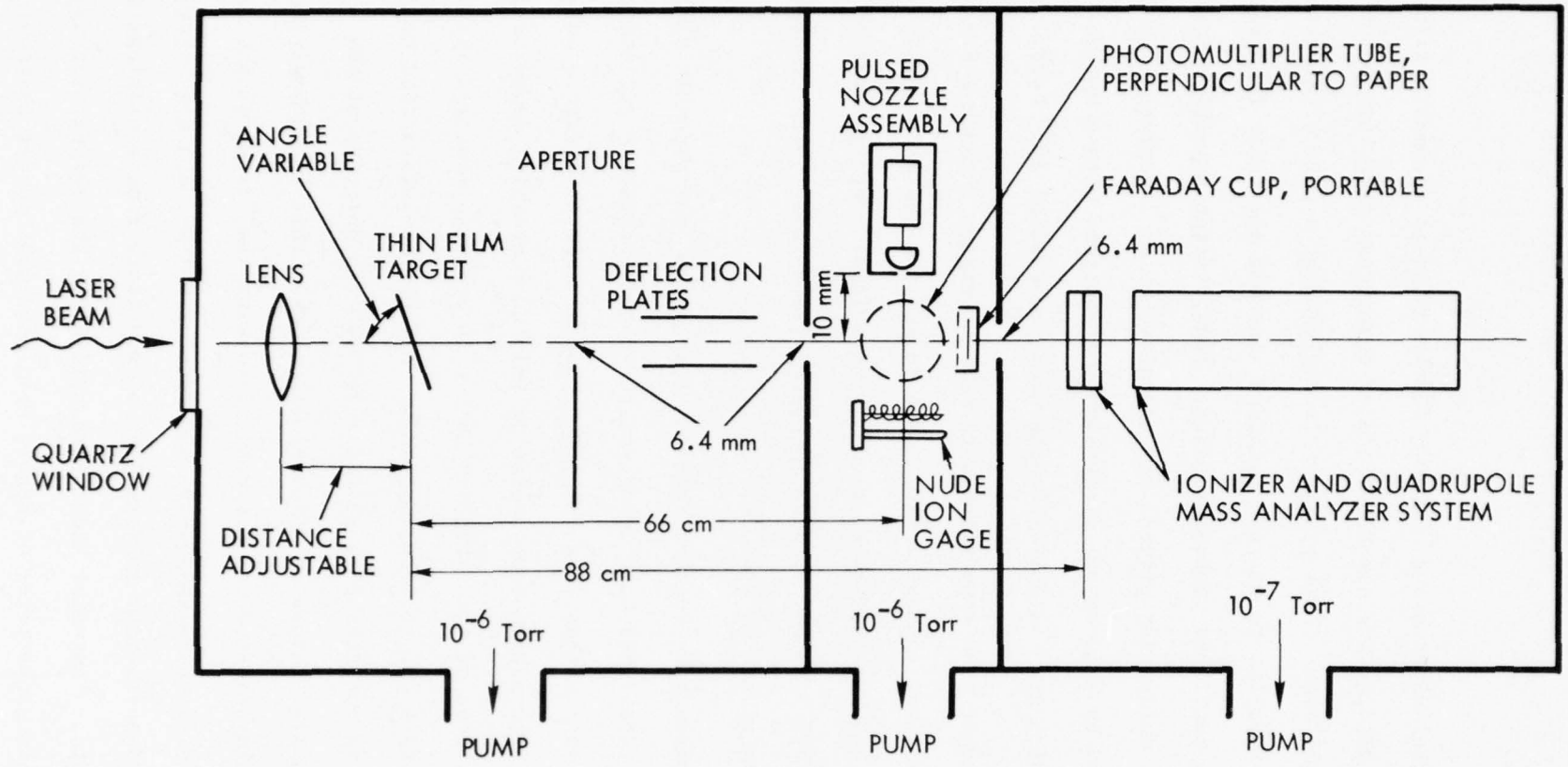

Figure D1. Schematic diagram of the experimental apparatus.

The metal vapor cloud expands freely until it becomes collisionless. A 6.4 mm collimating aperture located downstream from this point defines the atomic beam. This aperture is followed by a pair of electrostatic deflection plates to extract residual ions and electrons from the beam. The above mentioned components (i.e. lens, target assembly, collimating aperture and deflection plates) are contained in an integrated vacuum chamber evacuated by a 10-cm oil diffusion pump equipped with a water-cooled baffle which gives a nominal background pressure of 10^{-6} torr.

The atomic beam enters the interaction region through a 6.4 mm diameter by 30 mm long channel which serves to isolate the interaction region from the beam production section of the system. The interaction chamber is separately pumped by a 15-cm oil diffusion pump which maintains an ambient vacuum of better than 10^{-6} torr.

The interaction chamber contains the nozzle beam assembly and a photomultiplier tube (PMT) used to detect the chemiluminescent radiation. The axes of the nozzle beam, the PMT, and the metal atom beam form a mutually orthogonal set. The nozzle beam source is pointed vertically downward directly into the throat of the diffusion pump. In order to minimize system pumping requirements and to more accurately define the interaction region, the nozzle beam is operated in a pulsed mode with the duration of the molecular beam pulse limited to a few milliseconds. This is accomplished by a fast solenoid-actuated valve synchronized with the firing of the ruby laser. The valve opens in advance of the laser Q-switch by a time (between 1.0 and 2.5 msec) sufficient to establish steady state flow conditions in the molecular beam. The metal atom pulse arrives at the interaction region before appreciable backscatter of nozzle beam molecules occurs thereby

localizing the interaction region. Operation of the nozzle source is monitored by a nude ionization gauge of the Bayard-Alpert type located on the free jet axis downstream from the interaction zone. The collector of the gauge lies in a plane normal to the flow. The gauge is equipped with a buffered amplifier, and the signal is displayed on an oscilloscope to provide fast time response.

The nozzle orifice is formed by a 0.25 mm diameter hole drilled through 0.25 mm thick brass shim stock. The distance between the nozzle orifice and the axis of the atomic beam is 1.0 cm. The solenoid actuated valve assembly is immersed in the target gas reservoir which is maintained at room temperature. Stagnation pressures range between 5 and 50 torr as measured with a Baratron Pressure Meter (Type 77H-100, MKS Instruments, Inc.).

The center line of the nozzle beam source is located at a distance of 66 cm from the laser beam target. The field of view of the PMT used to detect the chemiluminescent radiation (RCA Type 8575) is restricted to the immediate vicinity of the interaction volume by a 6.4 mm diameter by 25 mm collimator. The photocathode of the PMT is located at a distance of 7.6 cm from the center of the interaction volume.

The interaction region also contains a Faraday cup that can be placed on the atom beam axis to verify that no ions remain in the atomic beam.

The third major section of the system contains the atom beam detection apparatus. This section is equipped with a combination ion-titanium sublimation pump (NRC Orb-Ion pump, Model 203) with a pumping

speed of approximately 100 liters sec^{-1}. Another 6.4 mm diameter by 30 mm channel isolates the detection section from the interaction region. Ambient pressure in this section is near 10^{-7} torr.

The beam detection system consists of an electron impact ionizer (Extranuclear Laboratories, Inc., Type II High Efficiency Ionizer), an rf quadrupole mass filter (Extranuclear Laboratories, Inc., Model 324-9 used with either the C or E high-Q head), and a 12-stage electron multipler tube (EMT) with Be-Cu dynodes (EMI venetian blind design).

A fixed fraction of the beam atoms that pass through the interaction zone without collision enter the ionizer. The entrance to the ionizer is located 88 cm from the laser target and 22 cm from the center of the interaction zone. Ionized beam atoms are focused to deliver maximum transmission through the quadrupole filter. Ions emerging from the quadrupole filter are deflected to the EMT by means of electrically biased planar grids. The ions impact the first dynode of the EMT with an energy of 4 keV. The resulting signal at the anode is amplified with a wide band operational amplifier and displayed on an oscilloscope.

B. Experimental Procedures

The information required to yield the cross section is obtained by the simultaneous measurement of the intensity of the chemiluminescent radiation from the reaction zone and the intensity of the atom beam pulse as measured with the quadrupole mass spectrometer located downstream from the interaction zone. Examples of photographic records of the signals are shown in Figure D2 for both holmium and boron atom beam pulses. The upper trace in each photograph is the signal from a photodiode used to monitor

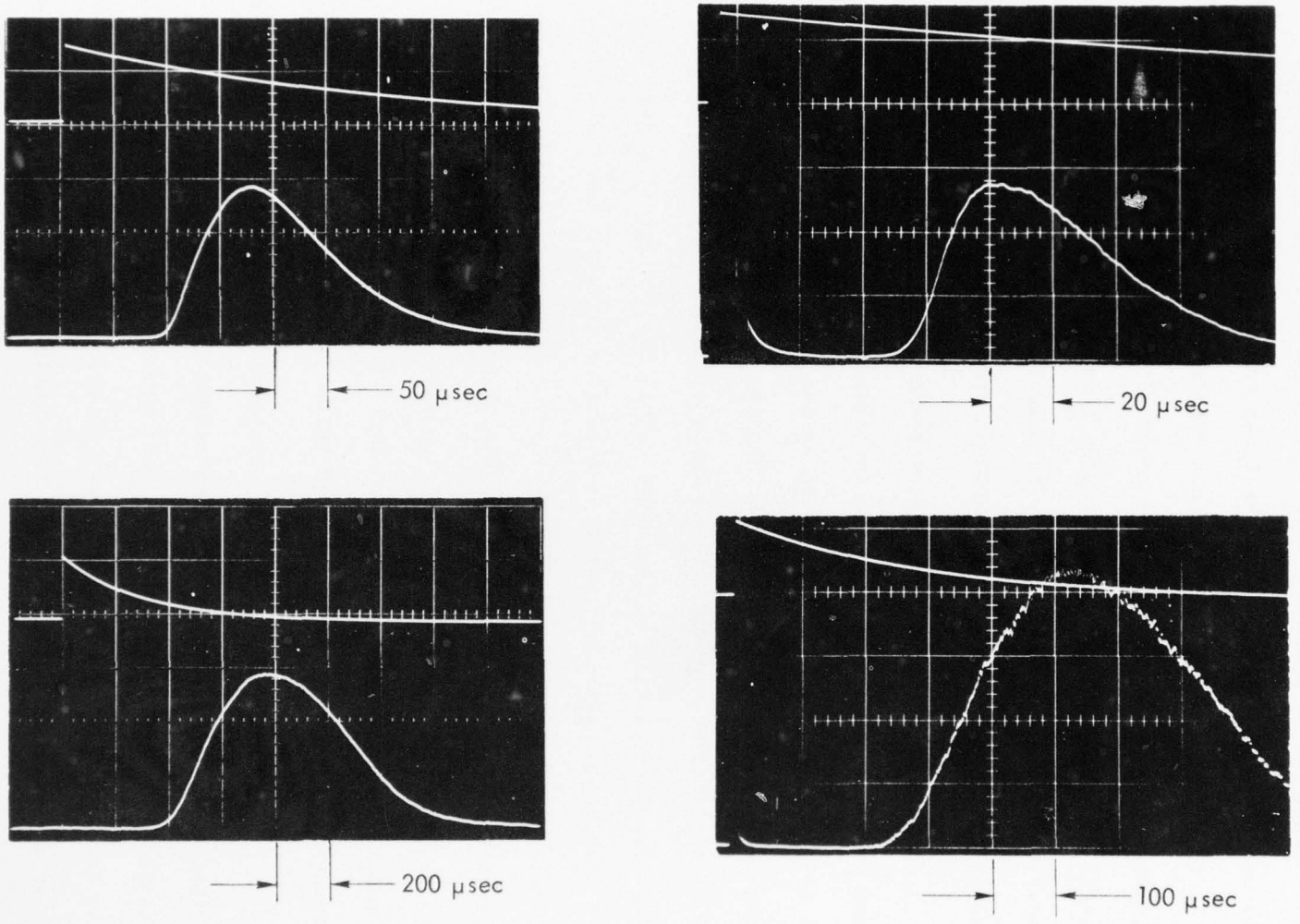

Figure D2. Typical oscillograms from the $B + N_2O \rightarrow BO^* + N_2$ (upper pair) and $Ho + N_2O \rightarrow HoO + N_2$ (Lower pair) tests.

the laser pulse and to provide a zero time reference. The signals from the mass spectrometer are displayed on the lower traces of the oscillograms on the left in the figure while the signals from the PMT are shown in the right hand photographs. These signals were recorded using two Tektronix 555 dual-beam oscilloscopes triggered from a common source. The sweep speeds of the lower beam were set independently to make the display as wide as reasonably possible to minimize measurement errors.

As discussed below, the instantaneous intensity of the chemiluminescent radiation is proportional to the flux of metal atoms impinging on the target gas. The signal recorded by the mass spectrometer system, however, is proportional to the number density of atoms within the ionizer volume at any instant of time. Since the atoms all originate at an essentially point source, the velocity of the atoms within the ionizer at a particular instant of time is specified by the elapsed time from the laser Q-switch. The transformation from number density to flux is accomplished by simply dividing the amplitude of the signal from the PMT by the arrival time on a point by point basis. Finally, the flux that would have been observed had the mass spectrometer been located at the crossed beam location is determined by multiplying the time base by the ratio of distances (66/88).

Prior to the taking of data, the mass spectrometer was calibrated and optimized using background gas as a source. Usually a number of shots were taken in order to establish the laser bombardment conditions to yield an atom beam pulse in the desired energy range. The possibility that the atom beam pulse contained other than the principal metal atoms was eliminated by checking the beam for the more obvious possible contaminants including dimers.

The experiments were conducted over a range of target gas pressures in order to determine the scattering cross section. The pressure in the target gas reservoir was monitored by the previously mentioned Baratron gauge.

C. Data Reduction and Analysis

The principles and fundamentals of atomic and molecular collision phenomena have been treated in an elegant account by Massey.[50] The following outline is presented to demonstrate the logic behind the data reduction method used. Several simplifying assumptions have been made: (1) gradients in the target gas density in the interaction volume are of secondary importance and can be ignored, (2) the velocity of the target gas molecules is small compared to the atom beam velocity and can be ignored, (3) the spectral distribution of the radiant energy is independent of velocity, and (4) the radiative lifetimes of the chemiexcited states are short compared to the residence time of the product molecules within the field of view of the PMT.

The change in atom beam intensity dJ(t) over a path length dx in the target gas is given by

$$dJ(t) = -\sigma_T n J(t) dx \qquad \text{Eq. (D1)}$$

where J(t) is the intensity of the atom beam pulse at time t, σ_T the total scattering cross section, and n the number density of target gas molecules. As used here σ_T represents the combined cross sections for reactive and inelastic collisions plus elastic scattering through angles greater than the acceptance angle of the mass spectrometer. The functional dependence on t simply implies that the energy of atoms within the

beam pulse is specified by their time of arrival at the detector. Integration of Eq.(D1) gives

$$J(t) = J_o(t) \exp(-\sigma_T n \ell) \qquad \text{Eq. (D2)}$$

where ℓ is the effective length of the target gas region, $J_o(t)$ is the incident beam intensity, and $J(t)$ is the intensity of the atom beam pulse as measured with the mass spectrometer.

Neither n nor ℓ in Eq.(D2) have been determined accurately which is the principal reason why the results are presented on a relative basis. However, it may be assumed that n is proportional to the stagnation pressure P in the reservoir[51,52,53] and that ℓ remains constant if the range in P is not large. Equation(D2) may be rewritten as

$$J(t) = J_o(t) \exp(-\sigma_T P) \qquad \text{Eq. (D3)}$$

where the implied constants have been set equal to unity which detracts nothing from the experiment.

The first step in the data reduction process is to determine σ_T from Eq.(D3). Since $J_o(t)$ is not directly measurable with the target gas system in operation, σ_T is determined by measuring $J(t)$ as a function of reservoir pressure. A graphical display of typical data is shown in Figure D3 for boron atoms and an N_2O target gas. For this example, $J(t)$ was measured at a time corresponding to the arrival of 1.75 eV boron atoms. The zero pressure intercept gives the value of $J_o(t)$ averaged over the several events and the slope of the line is proportional to σ_T. The deviations of individual points from the straight line are due principally to shot-to-shot variations in $J_o(t)$. The points shown are the averages of several events for each value of P. The best value of σ_T was determined

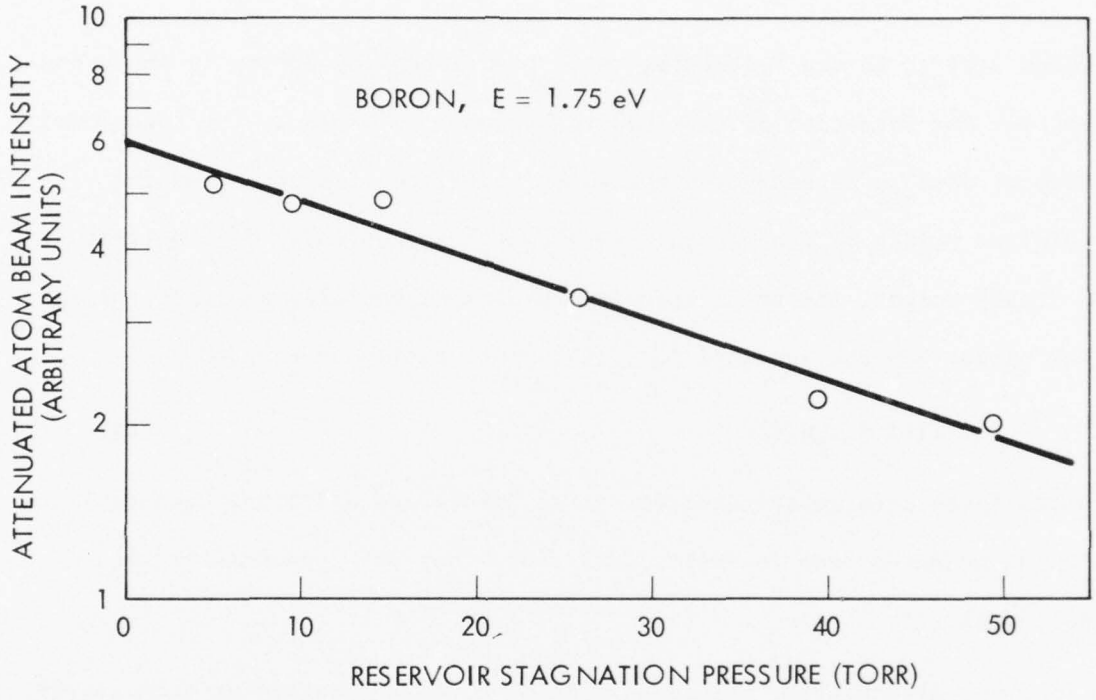

Figure D3. Typical plot of the intensity of boron atom pulses attenuated by collisions with an N_2O target gas as a function of the stagnation pressure in the target gas reservoir for a boron atom energy of 1.75 eV.

by a least-squares fit to the data points.

The increment of radiative intensity dS(t) from chemiexcited molecules produced in an element of length dx is given by

$$dS(t) = \sigma_r n J(t)_{eff} dx \qquad \text{Eq. (D4)}$$

where $J(t)_{eff}$ is the "effective" atom beam intensity and σ_r is the cross section for formation of chemiexcited product molecules. The functional form of $J(t)_{eff}$ depends upon the experimental configuration and the relative values of the several cross sections involved. In the limit of a "thin" target, the beam intensity remains essentially constant through the target gas and is equal to $J_o(t)$. Integration of Eq. (D4) yields

$$S(t) = \sigma_r J(t) P \qquad \text{Eq. (D5)}$$

where P has been substituted for $n\ell$ as before and $J_o(t)$ has been replaced by the measured beam intensity J(t) since they are approximately equal for small P.

Although the relative value of σ_r as a function of atom energy can be determined directly through the use of Eq. (D5), additional information can be obtained through the use of a thick target configuration. Let us consider two limiting cases in specifying the functional form of $J(t)_{eff}$. In the first case, assume that the change in intensity of the incident beam as measured with the mass spectrometer system is dominated by elastic collisions. Then for a thick target gas, elastically scattered atoms may have multiple collisions before exiting the interaction region, some of which may form chemiexcited molecules. But, since $\sigma_r \ll \sigma_T$ by our assumption, $J(t)_{eff} \approx J_o(t)$. Integration of Eq. (D4) with $J(t)_{eff} = J_o(t)$ yields

$$S(t) = \sigma_r P J(t) \exp(\sigma_T P) \qquad \text{Eq. (D6)}$$

where $J_o(t)$ has been replaced after integration by $J(t) \exp \sigma_T P$ as expressed in Eq. (D3).

In the other limiting case, it is assumed that collisions which reduce the intensity of the atom beam (as detected with the mass spectrometer) simultaneously remove atoms from further participation in reactive collisions. This condition would apply if, for example, $\sigma_T \approx \sigma_R$ where σ_R represents the total reactive cross section including both σ_r and the cross section for the formation of ground state molecules. This assumption leads to a functional form of $J(t)_{eff}$ given by

$$J(t)_{eff} = J_o(t) \exp(-\sigma_T n x) \qquad \text{Eq. (D7)}$$

which upon substitution into Eq. (4) and integration yields

$$S(t) = \frac{\sigma_r}{\sigma_T} J(t)[\exp(\sigma_T P) - 1] \qquad \text{Eq. (D8)}$$

where, again, $J_o(t)$ has been replaced by $J(t) \exp(\sigma_T P)$.

Values of σ_r were determined using all three formulations, i.e. through the use of Eqs. (D5), (D6), and (D8). In these equations $S(t)$, $J(t)$, and P are directly measurable quantities while the value of σ_T was determined by the method described above.

EXPERIMENTAL RESULTS

The experimental results are summarized graphically in Figure D4 for the B + N_2O reaction and in Figure D5 for the Ho + N_2O reaction.

Figure D4 shows that the total scattering cross section σ_T is essentially constant over the boron atom energy range covered by this experiment while σ_r increases by about an order of magnitude in the 1 to 4 eV range. The values of σ_r shown were determined by two of the three methods described above. In one case, σ_r was determined from the thin target formulation [Eq.(D5)] at P = 5 Torr. At P = 5 Torr, the ratio of J(t) to $J_o(t)$ was greater than 0.9 over the entire energy range indicating that the thin target approximation was justified. In the other case, σ_r was determined at several values of P between 5 and 50 Torr using the thick target formulation given in Eq.(D6), i.e. the case where $\sigma_T >> \sigma_r$. The data points plotted in Figure D4 for the thick target case are the averages for several values of pressure. The thin and thick target values have been arbitrarily set equal at 2.5 eV. It can be seen that the agreement between the two cases is excellent. The error bars shown represent approximately one standard deviation as determined by averaging several sets of data at each operating condition. Error bars have been omitted from most of the points for clarity of presentation.

Values of σ_r determined by the use of Eq.(D8) systematically increased with pressure which clearly contradicts the definition of a cross section. From this finding we are led to conclude that $\sigma_r << \sigma_T$ for B + N_2O collisions in the 1 to 4 eV energy range.

Data presented in Figure D5 shows that σ_T diminishes in magnitude

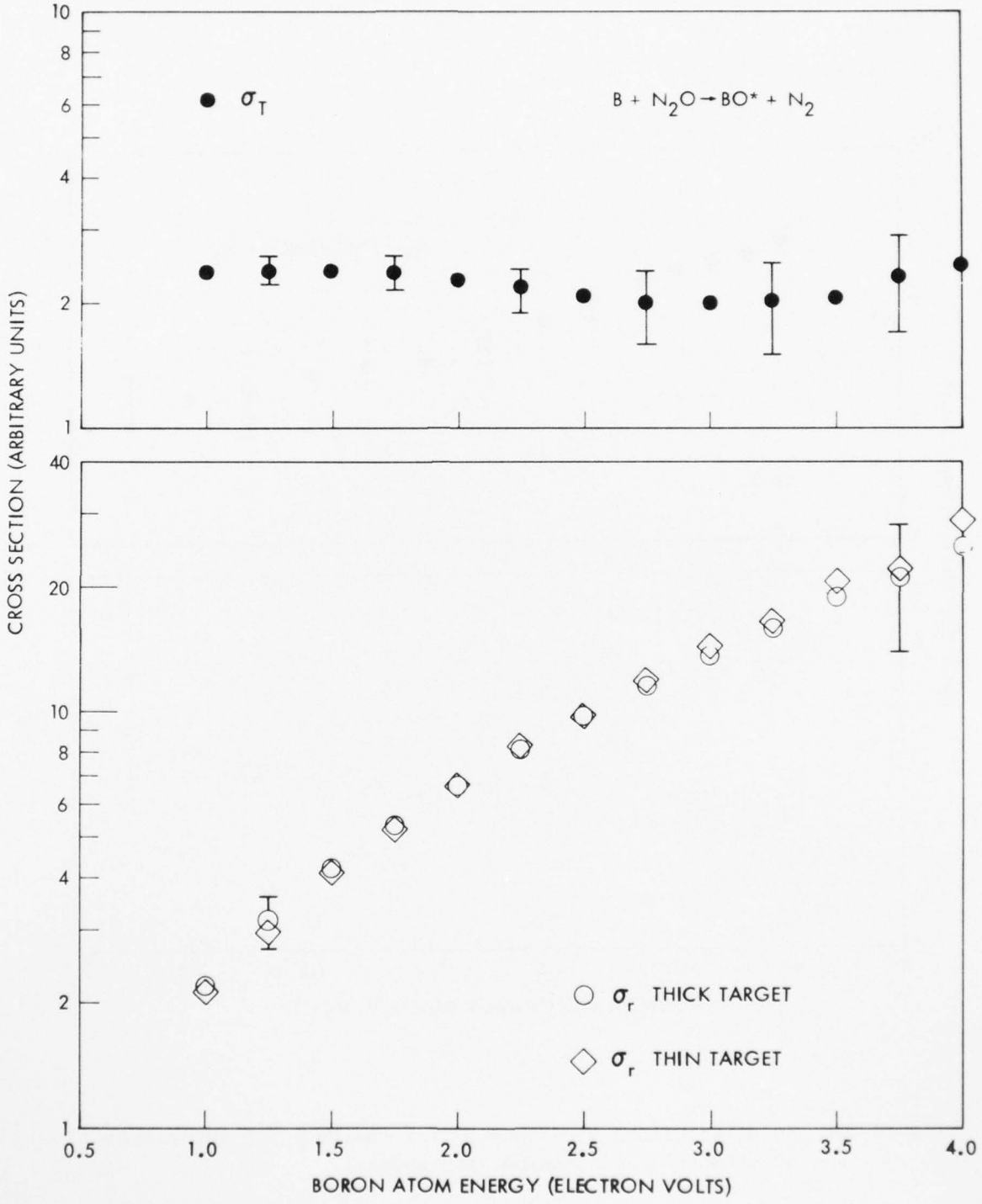

Figure D4. Relative values of σ_T and σ_r for the $B + N_2O$ interaction as a function of boron atom energy.

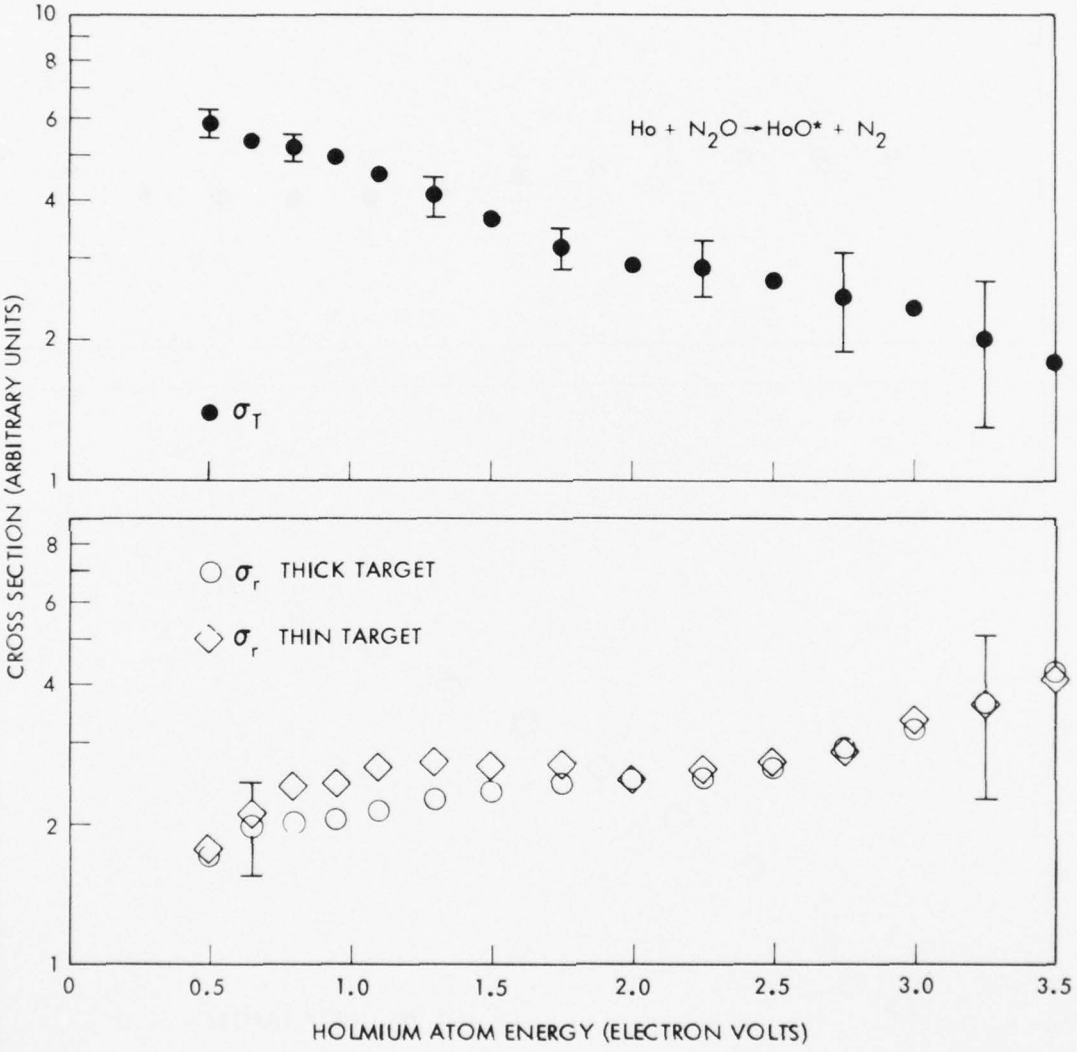

Figure D5. Relative values of σ_T and σ_r for the Ho + N_2O interaction as a function of holmium atom energy.

by about a factor of three in the holmium atom energy range from 0.5 to 3.5 eV for the Ho + N_2O interaction whereas σ_r increases by about a factor of two in the same energy range. Here, again, σ_r was determined by two of the three methods with essentially the same finding, i.e. good agreement was obtained between the thin and thick target experiments under the assumption that $\sigma_r << \sigma_T$. Treatment of the data was the same as for the B + N_2O interaction already discussed.

DISCUSSION

The experimental results presented here represent the first application of a new atomic beam technique to the measurement of the properties of chemical reactions on a molecular scale. The results have been presented on a relative basis because the target gas geometry cannot be specified with sufficient accuracy in the present configuration. Future work will utilize a differentially pumped static target gas system to rectify this situation.

Throughout this paper, the radiant energy detected has been characterized as chemiluminescence from excited electronic states of the metal monoxide. Although there has been no direct verification of this assertion, it is probably correct. The energy available for collisional excitation is insufficient to generate visible photons in the Ho + N_2O case. The possibility of collisional excitation cannot be ruled out in the B + N_2O case. However, in both cases, the exothermicity of the chemical reactions (6.3 eV for BO and 5.9 eV for HoO) significantly exceeds the available kinetic energy.

Another question concerns the internal energy state of the beam atoms which have been tacitly assumed to be in the ground state. A recent analysis[54] shows that the velocity distribution of the beam atoms is consistent with a Maxwellian distribution of velocities superimposed upon a directed velocity component. The analysis provides a model that can be used to specify the temperature of the Maxwellian distribution. This model, when applied to the present data, implies that the effective temperature of the gas cloud is on the order of

3000°K which argues against a significant population of excited state atoms in the beam. An experimental option which may be exercised in future measurements is that of varying the effective temperature of the metal atomic beam to see if systematic effects due to beam atom excitation are observed.

Finally, the lifetime of the emitting state (or states) can effect the measurements if it is comparable to or longer than the residence time of the product molecules within the field of view of the detector. For a given internal energy state, the velocity of the product molecules is proportional to the velocity of the incident atom. Hence, the observation time is inversely proportional to the atom velocity which would bias the detection efficiency in favor of the low velocity atoms if the lifetimes are indeed long.

Future experiments designed to answer these questions are planned.

ACKNOWLEDGEMENTS

This work was supported by the TRW Systems Group Independent Research and Development program. The authors wish to express their appreciation to M. E. Beverage for his assistance in data acquisition and J. L. Witte for his help in assembling the experimental apparatus.